NASA TN D-895

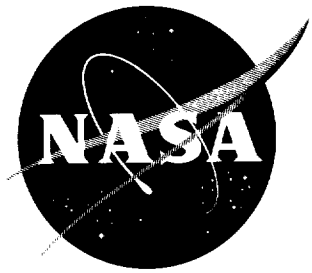

TECHNICAL NOTE

D-895

APPROXIMATE TEMPERATURE DISTRIBUTIONS AND STREAMWISE HEAT CONDUCTION EFFECTS IN THE TRANSIENT AERODYNAMIC HEATING OF THIN-SKINNED BODIES

By Raul J. Conti

Langley Research Center
Langley Field, Va.

NATIONAL AERONAUTICS AND SPACE ADMINISTRATION

WASHINGTON September 1961

P

NATIONAL AERONAUTICS AND SPACE ADMINISTRATION

TECHNICAL NOTE D-895

APPROXIMATE TEMPERATURE DISTRIBUTIONS AND STREAMWISE HEAT CONDUCTION EFFECTS IN THE TRANSIENT AERODYNAMIC HEATING OF THIN-SKINNED BODIES

By Raul J. Conti

SUMMARY

An approximate method is devised to determine temperature distributions during the transient aerodynamic heating of thin-skinned, heat-conducting bodies. This permits evaluation of the streamwise conduction errors arising in the measurement of heat-transfer coefficients based on the skin-temperature history.

The present method is valid for a large range of body shapes and thickness distributions, within the limitations of one-dimensional (streamwise) heat conduction, quasi-isothermal surface, constant adiabatic wall temperature, and negligible radiative heat transfer.

Numerical computations were carried out for flat plates, wedges, and conical, hemispherical, and hemicylindrical shells. The results are presented in the form of nondimensional charts that permit a rapid evaluation of a 10-percent error threshold in transient heat-transfer measurements.

INTRODUCTION

The transient heating of thin-skinned bodies subjected to an aerodynamic heat input has a wide practical interest in high-speed flight and model testing. This is, in general, a problem of three-dimensional time-dependent heat conduction where the heat input depends on the surface temperature distribution. This problem appears to be too complicated for generalized treatment and therefore several restrictive assumptions are necessary in order to make it amenable to computation.

One such assumption is the restriction to two-dimensional heat flow, which is realized under two-dimensional or axisymmetrical conditions. A second assumption is that the body be in a quasi-isothermal state. This allows the use of a constant-temperature heat-transfer

coefficient which is a function of longitudinal coordinate alone. The previous assumptions reduce the problem to that of two-dimensional transient heat conduction in the presence of a heat input represented by a time-independent heat-transfer coefficient, or constant heat-transfer coefficient and varying forcing function (adiabatic wall temperature).

The present investigation is concerned with the longitudinal conduction in the case where normal heating (across the skin) is assumed to be of a calorimetric type under a step forcing function. The thermal conductivity of the skin is assumed infinite in a direction perpendicular to the surface and the internal surface is assumed insulated, therefore the temperature is assumed constant across the skin. This is a good approximation in the case of thin-skinned bodies having a well insulated internal surface. Nevertheless, it must be kept in mind that normal conduction effects cannot be neglected at the very early times after time equal 0, when the temperature-time slopes of the outer and inner skin surfaces are substantially different. In any case, the problem of normal conduction in the absence of longitudinal conduction has been investigated in the past and solutions are available. (See, for instance, refs. 1 and 2.) When normal conduction proves to be significant, a first approximation to the complete picture may be obtained by writing the heat balance in an element of skin including both heat flows as obtained from the longitudinal and normal solutions.

Longitudinal conduction has the effect of relieving thermal concentration in the skin; it also distorts heat-transfer computations based on measured skin temperature history. The present investigation was initiated to obtain an approximate solution that would predict these effects, especially from the viewpoint of the error introduced in heat-transfer measurements. Under the assumptions previously mentioned, the solution obtained is applicable to bodies of arbitrary shape and thickness distribution, except for regions in the neighborhood of discontinuities in heat input, cross-sectional area, thickness distribution, or their derivatives. Numerical results are presented for simple shapes with heat inputs appropriate to laminar and turbulent boundary layers.

SYMBOLS

a	area of surface perpendicular to longitudinal (streamwise) direction
A_{ij}	$i = 1,2,3, \ldots$; $j = 1,2,3, \ldots$ functions given by equations (15)

c	specific heat of skin material
c_f	local skin-friction coefficient
C_L, C_T, C_Y	input parameters (table I)
F_L, F_T	input parameters (table I)
G	dimensionless temperature variable, $\frac{T - T_{t=0}}{T_{aw} - T_{t=0}}$
G_i	$i = 1,2,3, \ldots$ temperature components defined by equations (9), (10), and (11)
h	heat-transfer coefficient
h_i	indicated heat-transfer coefficient, defined by equation (17)
H_i	$i = 1,2,3,4,5,6$ constants representing heat-transfer level, $h\sqrt{X}$ or $hX^{1/5}$
k	thermal conductivity
K_1, K_2	arbitrary constants
l	skin thickness
L	characteristic length
m	mass of skin element
M	Mach number
n	arbitrary constant
Nu	Nusselt number based on coordinate x
p	pressure
$P(X)$	characteristic function defined by equation (6)
Pr	Prandtl number
q	total heat flow per unit time
$Q(X)$	characteristic function defined by equation (7)

R	outer radius of hemispherical or hemicylindrical shell
r	inner radius of hemispherical or hemicylindrical shell
Re	Reynolds number based on coordinate x
s	lateral area subjected to aerodynamic heating
S	input parameter (table I)
St	Stanton number
t	time
T	skin temperature
T'	reference temperature
U	velocity at edge of boundary layer
V	volume of skin element
v	speed of sound
W_L, W_T	input parameters (table I)
x	longitudinal coordinate
X	dimensionless longitudinal coordinate (table I)
α	thermal diffusivity of skin material
β	arbitrary constant
γ	ratio of specific heats for air
θ'_w	nondimensional solution for the heating of the yawed cylinder, from reference 3
Λ	yaw angle
μ	viscosity of air
ν	kinematic viscosity of air
ρ	density of skin material
τ	Fourier number, $\frac{\alpha}{L^2} t$

φ	wedge angle
ψ	cone semiapex angle
ω	temperature exponent in air viscosity law
$[\ ]_{10}$	refers to 10-percent-error point

Subscripts:

aw	adiabatic wall
b	pertaining to body
l	variable is referred to the skin thickness l
max	maximum value
R	variable is referred to the radius R
SL	stagnation line conditions
SN	conditions at the stagnation line derived from the normal flow component
SP	stagnation-point conditions
w	wall conditions
0	free-stream stagnation conditions
α	variable is referred to the diffusion distance per unit time $\sqrt{\alpha}$
∞	free-stream conditions

Superscripts:

*	applies to X_l, $X_l^* = \dfrac{l}{\tan \psi}$
'	first derivative with respect to X
"	second derivative with respect to X
'''	third derivative with respect to X
IV	fourth derivative with respect to X

THEORY

Heat-Conduction Equation

Consider one-dimensional heat conduction in a body of arbitrary shape, the outside surface of which is subjected to aerodynamic heating in the absence of radiation. Let an infinitesimal volume element be determined by two surfaces perpendicular to the longitudinal (x) direction, of area a and a + da and at a distance dx apart as represented in sketch (a):

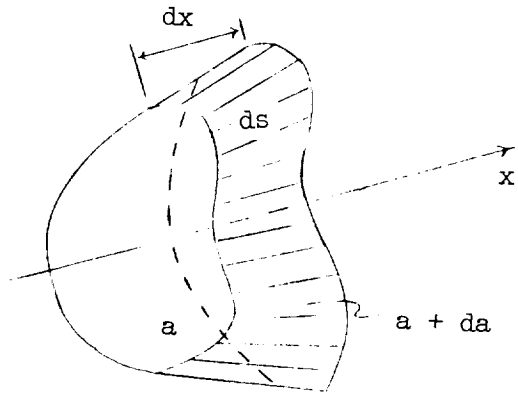

Sketch (a)

Let ds denote the element of lateral area subjected to aerodynamic heating. Since conduction is one-dimensional the temperature on the surfaces a and a + da is constant and equal to T and $T + \frac{\partial T}{\partial x} dx$, respectively. The mean temperature of the element is $T_m = T + \frac{\partial T}{\partial x} \frac{dx}{2}$. The heat balance in the element is

Heat stored = Aerodynamic heat in + Heat gained by conduction

The heat stored per unit time is

$$dq_s = c\ dm \frac{\partial T_m}{\partial t}$$

and if second-order differentials are neglected

$$dq_s = c\ dm \frac{\partial T}{\partial t} = \rho c\ dV \frac{\partial T}{\partial t} \tag{1}$$

The aerodynamic heat entering the element is

$$dq_{aero} = h\ ds(T_{aw} - T_m)$$

Again if second-order differentials are neglected

$$dq_{aero} = h\ ds(T_{aw} - T) \tag{2}$$

The heat gained by conduction through the surfaces a and a + da is

$$dq_{gc} = (q_{in})_a - (q_{out})_{a+da} = -ka\left(\frac{\partial T}{\partial x}\right)_x + k(a + da)\left(\frac{\partial T}{\partial x}\right)_{x+dx}$$

and if second-order differentials are neglected

$$dq_{gc} = ka \frac{\partial^2 T}{\partial x^2} dx + k\ da \frac{\partial T}{\partial x} \tag{3}$$

Therefore, the heat balance can be written as

$$\frac{\partial T}{\partial t} = \frac{h}{\rho c \frac{dV}{ds}}(T_{aw} - T) + \alpha \frac{\partial^2 T}{\partial x^2} + \alpha \frac{1}{a} \frac{da}{dx} \frac{\partial T}{\partial x} \tag{4}$$

since a dx = dV.

For the case of a timewise step heat input, constant adiabatic wall temperature, and initially isothermal body, the following dimensionless variables are defined:

$$G \equiv \frac{T - T_{t=0}}{T_{aw} - T_{t=0}}$$

$$\tau \equiv \frac{\alpha}{L^2} t$$

$$X \equiv \frac{x}{L}$$

where L is an appropriate reference length. Substitution into equation (4) leads to

$$\frac{\partial G}{\partial \tau} = P(X)(1 - G) + \frac{\partial^2 G}{\partial X^2} + Q(X)\frac{\partial G}{\partial X} \tag{5}$$

where

$$P(X) \equiv \frac{L^2}{\alpha} \frac{h(X)}{\rho c \frac{dV}{ds}(X)} \tag{6}$$

and

$$Q(X) \equiv \frac{1}{a(X)} \frac{da}{dX} \tag{7}$$

The functions P(X) and Q(X) describe the conditions (heat input and geometry) that characterize a particular problem and therefore they may be called the characteristic functions of the problem. It may be noticed that P and Q are assumed to be functions of X alone. For a given geometry this is always the case for Q but, in general, this is not true of P, which includes the aerodynamic heat-transfer coefficient h. In a strict sense, h depends upon the wall-temperature level and its distribution shape, and therefore it is, in general, a function of time as the body exchanges heat with the surroundings. However, there are many cases where the time dependency of h can be neglected. The following restriction is therefore imposed: the present solution is applicable to those cases where the aerodynamic heat-transfer coefficient can be considered to be a function of the longitudinal coordinate alone, and this will be referred to as a quasi-isothermal state of the body.

The restrictions on equation (5) may then be summarized as:

1. One-dimensional longitudinal (streamwise) heat conduction

2. Negligible radiation compared with aerodynamic heat input

3. Value of T_{aw} constant with time after $t = 0$, independent of X

4. Quasi-isothermal state of the body as defined previously

A further limitation concerns the behavior of the characteristic functions $P(X)$ and $Q(X)$. These functions may have singularities at the leading edge of sharp bodies, or where discontinuities of cross-sectional area or thickness distribution occur. The present approximate solution yields finite results only where $P(X)$, $Q(X)$, and their derivatives are continuous functions of X. (See eqs. (15).) Where discontinuities such as multivalued derivatives of $P(X)$ or $Q(X)$ are present, interference between the regions on both sides of the discontinuity will occur, and eventually will spread out to the neighboring regions. Accordingly, care should be exercised in applying the present results to bodies having such discontinuities.

Approximate Solution of the Heat Conduction Equation

An approximate solution of equation (5) has been obtained in the form of a series $G = G_1 + G_2 + G_3 + \ldots$ of which the first three terms have been computed. This series was determined by writing equation (5) as

$$\frac{\partial G_1}{\partial \tau} + \frac{\partial G_2}{\partial \tau} + \frac{\partial G_3}{\partial \tau} + \ldots = P(X)\left[1 - (G_1 + G_2 + G_3 + \ldots)\right] + \frac{\partial^2}{\partial X^2}(G_1 + G_2 + G_3 + \ldots) + Q(X)\frac{\partial}{\partial X}(G_1 + G_2 + G_3 + \ldots) \tag{8}$$

and letting the temperature components G_1, G_2, and G_3, respectively, be defined by the differential equations

$$\frac{\partial G_1}{\partial \tau} = P(X)(1 - G_1) \tag{9}$$

$$\frac{\partial G_2}{\partial \tau} = -P(X)G_2 + \frac{\partial^2 G_1}{\partial X^2} + Q(X)\frac{\partial G_1}{\partial X} \tag{10}$$

$$\frac{\partial G_3}{\partial \tau} = -P(X)G_3 + \frac{\partial^2 G_2}{\partial X^2} + Q(X)\frac{\partial G_2}{\partial X} \qquad (11)$$

Succeeding terms may be obtained similarly.

Such a separation of equation (5) is partly granted by the linearity of the equation, and the results are validated a posteriori by comparison with numerical integrations of equation (5) to be discussed later.

The physical interpretation of the temperature components G_1, G_2, G_3, and so forth, is the following: G_1 is the calorimetric temperature, that is, the temperature that would exist in the absence of conduction; G_2 is the temperature introduced by conduction arising from the $G_1(X)$ distribution, and it includes the "interference" term $-P(X)G_2$, that is, the perturbation in aerodynamic input due to the presence of G_2; G_3 is due to the conduction arising from G_2 plus its own "interference"; and successive terms can be similarly interpreted.

In this way, an infinite series is obtained as a solution to equation (5). If a finite number of components is used the last one should include its own conduction for equation (5) to be satisfied exactly. For instance, if three components are used, the terms $\frac{\partial^2 G_3}{\partial X^2} + Q(X)\frac{\partial G_3}{\partial X}$ should be added to the right-hand side of equation (11). Since this would complicate the equation to the same degree as the original equation (eq. (5)), the conduction terms of G_3 are neglected in equation (11) and they therefore represent the error introduced in the solution.

The temperature $G = G_1 + G_2 + G_3$ should not be expected to satisfy exactly the boundary conditions since it is not a complete solution. It was found that, as the leading edge of sharp bodies is approached, the first terms of the series become divergent and therefore no solution is presented at or near the leading edge of sharp bodies.

The procedure for solving equations (9), (10), and (11) is the following: the solution of equation (9) is

$$G_1 = 1 - e^{-P\tau}$$

This temperature may be used to compute G_2 from equation (10), which in turn allows the solution of equation (11) for G_3, and so on.

When such a procedure is followed, the results for the first three terms are

$$G_1 = 1 - e^{-P\tau} \tag{12}$$

$$G_2 = \left(A_{11}\tau^2 - A_{12}\tau^3\right)e^{-P\tau} \tag{13}$$

$$G_3 = \left(A_{21}\tau^3 - A_{22}\tau^4 + A_{23}\tau^5 - A_{24}\tau^6\right)e^{-P\tau} \tag{14}$$

where

$$\left.\begin{aligned}
A_{11} &= \frac{1}{2}(P'' + QP') \\
A_{12} &= \frac{1}{3}(P')^2 \\
A_{21} &= \frac{1}{6}\left(P^{IV} + 2P''Q' + P'Q'' + 2P'''Q + P'QQ' + P''Q^2\right) \\
A_{22} &= \frac{1}{24}\left[7(P'')^2 + 10P'P''' + 16P'P''Q + 6(P')^2Q' + 3(P')^2Q^2\right] \\
A_{23} &= \frac{1}{30}\left[13(P')^2P'' + 5(P')^3Q\right] \\
A_{24} &= \frac{1}{18}(P')^4
\end{aligned}\right\} \tag{15}$$

In the preceding equations the functional dependency of P and Q (defined in eqs. (6) and (7)) is omitted for brevity.

According to equation (5) the heat-transfer coefficient with conduction is

$$h = \frac{\alpha}{L^2}\rho c\,\frac{dV}{ds}\left(\frac{\frac{\partial G}{\partial \tau}}{1 - G} - \frac{\frac{\partial^2 G}{\partial X^2} + Q\frac{\partial G}{\partial X}}{1 - G}\right) \tag{16}$$

The quantity

$$h_i \equiv \frac{\alpha}{L^2}\rho c\,\frac{dV}{ds}\,\frac{\frac{\partial G}{\partial \tau}}{1 - G} = \rho c\,\frac{dV}{ds}\,\frac{\frac{\partial T}{\partial t}}{T_{aw} - T} \tag{17}$$

is readily obtained from temperature-time measurements and may be termed the indicated heat-transfer coefficient, which would be obtained from a calorimetric (no conduction) analysis. Then from equation (16), the ratio of h_i/h may be expressed as

$$\frac{h_i}{h} = 1 + \frac{1}{P}\frac{\frac{\partial^2 G}{\partial X^2} + Q\frac{\partial G}{\partial X}}{1 - G}$$

According to the present solution this quantity is

$$\frac{h_i}{h} = 1 + \frac{\frac{1}{P}\left[2A_{11}\tau - 3(A_{12} - A_{21})\tau^2 - 4A_{22}\tau^3 + 5A_{23}\tau^4 - 6A_{24}\tau^5\right]e^{-P\tau}}{1 - (G_1 + G_2 + G_3)} \tag{18}$$

Equation (18) may be used as a correction for measured values of the heat-transfer coefficient, that is

$$h_{corrected} = h_{i(measured)}\left(\frac{1}{h_i/h}\right) \tag{19}$$

Numerical Integration

The approximate solution previously described was checked by comparison with direct integration of equation (5) in several particular cases. Numerical integrations of equation (5) were carried out for a flat plate and solid wedge, under specified heat inputs. Equation (5) may be written in terms of finite differences as

$$G_{X,\tau+\Delta\tau} = G_{X,\tau} + P\left(1 - G_{X,\tau}\right)\Delta\tau + \left(G_{X+\Delta X,\tau} - 2G_{X,\tau} + G_{X-\Delta X,\tau}\right)\frac{\Delta\tau}{(\Delta X)^2}$$

$$+ Q\left(G_{X+\Delta X,\tau} - G_{X,\tau}\right)\frac{\Delta\tau}{\Delta X} \tag{20}$$

This equation, with the boundary conditions

$$G_{X,0} = 0$$

$$G_{0,\tau} = G_{\Delta X,\tau}$$ [1]

was integrated by steps with the aid of an IBM card-programed digital computer.

This type of solution introduces an error due to the finite step size; therefore small step sizes are desirable. Furthermore, in order to obtain a solution, it was found that $\frac{\Delta\tau}{(\Delta X)^{\beta}}$ must be less than some function of P.[2] Hence, as ΔX is decreased $\Delta\tau$ must be decreased too. This taxes the storage capabilities of the computer and, therefore, solutions of this type may be expected to be restricted to short times. Comparison between these numerical solutions for short times and the approximate solutions of the present paper are discussed later in the section entitled "Presentation of Results."

APPLICATION OF THE SOLUTION

The application of the present solution to a particular case consists essentially in determining the functions $A_{ij}(X)$ given by equation (15) as functions of P and Q, with which equations (12), (13), (14), and (18) may be computed, yielding $G(X,\tau)$ and $\frac{h_i}{h}(X,\tau)$.

A detailed discussion of the functions $A_{ij}(X)$ is included in appendix A for the flat plate, the wedge, and the conical shell with laminar and turbulent boundary layers and for the hemispherical and the hemicylindrical shells with laminar boundary layers. For each of these cases computations were carried out by combining the heat-transfer level and certain body properties in a free parameter called the input parameter (see definitions in table I). The characteristic length L was

---

[1]For bodies having finite leading edges this boundary condition follows directly from the condition of no heat conduction at the leading edge $\left[\left(\frac{\partial G}{\partial X}\right)_{0,\tau} = 0\right]$. For sharp bodies this is not necessarily so, but apparently the present boundary condition still holds, as pointed out in reference 4.

[2]For instance, for the case of a flat plate of constant thickness a necessary condition for the step size is

$$\frac{\Delta\tau}{(\Delta X)^2} < \frac{P(\Delta X)\left[1 - P(\Delta X)\Delta\tau\right] - P(2\,\Delta X)\left[1 - P(2\,\Delta X)\Delta\tau\right]}{\left[P(3\,\Delta X) - 2P(2\,\Delta X) + P(\Delta X)\right] - \left[P(2\,\Delta X) - P(\Delta X)\right]}$$

particularized for each configuration in appendix A and is also shown in table I. In this way, a set of curves $G(X,\tau)$; $\frac{h_i}{h}(X,\tau)$ was obtained for each of the body shapes mentioned, for a range of values of the corresponding input parameter. Thus, for any particular set of free-stream conditions and body properties, once the input parameter is calculated, the present solution provides the temperature and heat-transfer correction as functions of time and the coordinate of the point.

A collection of methods for the estimation of the input parameter from free-stream conditions is included in appendix B for ready reference.

PRESENTATION OF RESULTS

Results of the numerical computations, as compared with the approximate solutions, are presented in figures 1, 2, and 3 for particular bodies and heat inputs. It may be seen that a good agreement is obtained for the temperature variable G and reasonable agreement is shown in h_i/h.

Results of the approximate solution, described in the previous section, are too bulky for a complete presentation. Therefore, only one plot for a typical value of the input parameter is presented for each body shape in figures 4 to 11. In the particular case of the stagnation point of blunt bodies complete results including the effects of the input parameters are presented in figures 12 and 13. For other than this particular case the effects of the input parameters are illustrated by means of partial results presented in figures 14 to 18 in the form of charts that provide a rapid means of calculating a 10-percent error threshold in heat-transfer measurements. These charts give the location and temperature of the point where the error in indicated heat-transfer coefficient is 10 percent. This fictitious point has a coordinate $[X]_{10}$ that varies with time. At any given instant, points at $X > [X]_{10}$ or $X < [X]_{10}$ will have errors in indicated heat-transfer coefficient larger or smaller than 10 percent, as the case may be.

LIMITING SOLUTIONS

Limiting solutions for h_i/h for small values of P_τ may be obtained by using the temperature

$$G_1 = 1 - e^{-P\tau}$$

in equation (16) and letting $P_\tau \ll 1$. For the flat plate, wedge, and conical shell the heat-transfer coefficient is assumed to be proportional to $x^{-1/2}$ and $x^{-1/5}$ for laminar and turbulent boundary layers, respectively. When the condition $P_\tau \ll 1$ is imposed, equations are obtained for h_i/h that are independent of the heat input. The coordinate $[X]_{10}$ of the point having a 10-percent conduction error may be obtained by setting $h_i/h = 1.1$, and it proves to be proportional to the square root of the Fourier number τ for all cases, as shown by equations for the

flat plate with laminar boundary layer:

$$\frac{h_i}{h} = 1 + \frac{3}{4}\tau_l X_l^{-2} \tag{21a}$$

$$\left[X_l\right]_{10} = 2.74\tau_l^{1/2} \tag{21b}$$

flat plate with turbulent boundary layer:

$$\frac{h_i}{h} = 1 + \frac{6}{25}\tau_l X_l^{-2} \tag{22a}$$

$$\left[X_l\right]_{10} = 1.55\tau_l^{1/2} \tag{22b}$$

wedge with laminar boundary layer:

$$\frac{h_i}{h} = 1 + \frac{9}{4}\tau_\alpha X_\alpha^{-2} \tag{23a}$$

$$\left[X_\alpha\right]_{10} = 4.74\tau_\alpha^{1/2} \tag{23b}$$

wedge with turbulent boundary layer:

$$\frac{h_i}{h} = 1 + \frac{36}{25}\tau_\alpha X_\alpha^{-2} \tag{24a}$$

$$\left[X_\alpha\right]_{10} = 3.79\tau_\alpha^{1/2} \tag{24b}$$

conical shell with laminar boundary layer:

$$\frac{h_i}{h} = 1 + \frac{1}{4}\tau_l X_l^{-2} \tag{25a}$$

$$\left[X_l\right]_{10} = 1.58\tau_l^{1/2} \tag{25b}$$

conical shell with turbulent boundary layer:

$$\frac{h_i}{h} = 1 + \frac{1}{25}\tau_l X_l^{-2} \tag{26a}$$

$$\left[X_l\right]_{10} = 0.63\tau_l^{1/2} \tag{26b}$$

For the hemispherical and hemicylindrical shells in laminar flow (heat-transfer coefficient assumed proportional to $\cos X_R$), the corresponding equations are

for the hemispherical shell:

$$\frac{h_i}{h} = 1 - 2\tau_R\left(1 + \frac{1}{2}P\tau_R \tan^2 X_R\right) \tag{27a}$$

$$\tan^2\left[X_R\right]_{10} = \frac{0.1 - 2\tau_R}{P\tau_R^2} \tag{27b}$$

and for the hemicylindrical shell:

$$\frac{h_i}{h} = 1 - \tau_R\left(1 + P\tau_R \tan^2 X_R\right) \tag{28a}$$

$$\tan^2\left[X_R\right]_{10} = \frac{0.1 - \tau_R}{P\tau_R^2} \tag{28b}$$

At the stagnation point equations (27a) and (23a) yield, respectively,

$$\frac{h_i}{h} = 1 - 2\tau_R \qquad \text{(10-percent error at } \tau_R = 0.05\text{)}$$

and

$$\frac{h_i}{h} = 1 - \tau_R \qquad \text{(10-percent error at } \tau_R = 0.10\text{)}$$

As would be expected, the conduction error is larger in the hemispherical shell due to the three-dimensional effect. As indicated by equations (27) and (28) the limiting solutions for the hemispherical and hemicylindrical shell are not independent of the heat input everywhere, since $\tan^2 X_R$ appears as a factor of $P\tau$. The limiting solutions are included in the charts of figures 14 to 18 and it may be seen that they indicate the correct trend.

DISCUSSION OF RESULTS

General Results

Figures 4 to 11 show plots of $G(X,\tau)$ $(G = G_1 + G_2 + G_3)$ and $\frac{h_i}{h}(X,\tau)$ for typical values of the corresponding input parameter. (See definitions in table I.) Solid lines correspond to regions where $|G_1| > |G_2| > |G_3|$.

Flat plate, wedge, and conical shell.- For these bodies the results are qualitatively similar. The temperature variable G, which is maximum at the leading edge or tip, decreases asymptotically to zero at infinity. During the transient heating the ratio h_i/h has to be zero at the leading edge since h is assumed to be proportional to $x^{-1/2}$ or $x^{-1/5}$ and h_i remains finite. (See, for instance, refs. 5 and 4.) This ratio is equal to one at infinity, where conduction effects are not felt at finite times. Points removed from the leading-edge region but at finite distances have positive errors $\left(\frac{h_i}{h} > 1\right)$; that is, these points show a net gain of heat due to conduction. Consequently, at any time (except $t = 0$) during the transient heating the curves $\frac{h_i}{h}(X)$ must go through a maximum. At early times these maximums are very near the leading edge, in the region where the first three temperature components of the present solution do not converge. At later times the maximums shift progressively downstream (into the region of convergence of the first three components) and become increasingly smaller, as illustrated schematically in the following sketch, based on figures 4(b), 5(b), 6(b), 7(b), and 8(b):

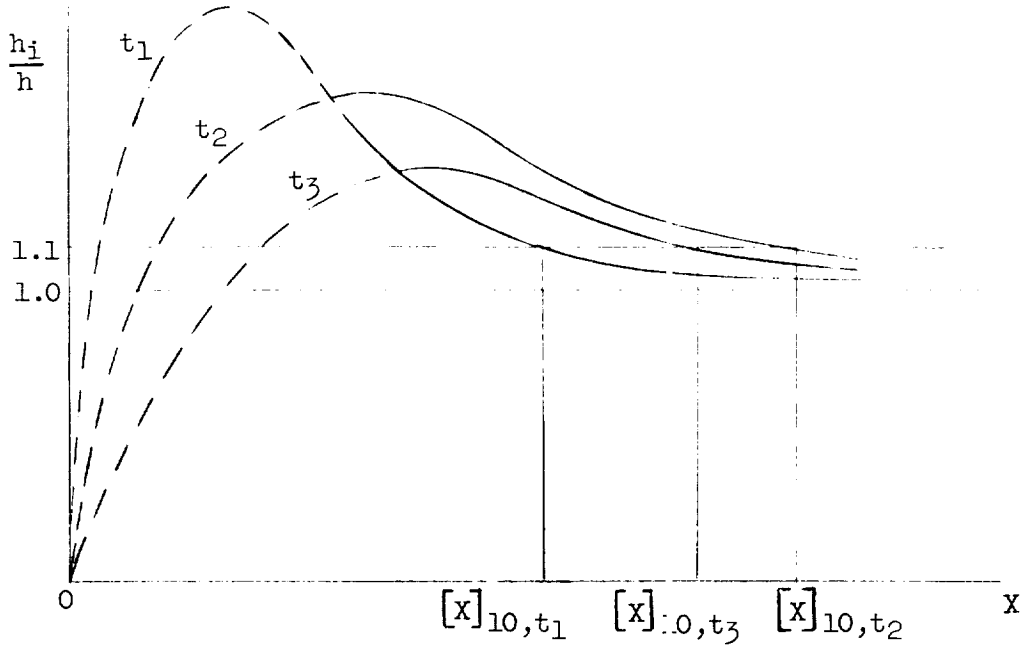

Sketch (b)

Hemispherical and hemicylindrical shells.- For these bodies the heat input has been assumed to be of the form $h = (\text{Constant})(\cos X_R)$. This distribution closely represents the actual heat input near the stagnation region, and approximates it for values of X_R up to about 60°. The cosinusoidal distribution becomes unsuitable downstream of boundary-layer transition regions or close to $X_R = \frac{\pi}{2}$, but the assumption that T_{aw} is independent of X_R in any case restricts the use of the present solution to regions nearer the stagnation point. The solution is presented for values of X_R up to 60° to show trends. Within these limitations the solutions show an X-wise monotonic decrease of both G and h_i/h. Values of h_i/h are always less than unity, which means a net loss of heat due to conduction and increasing negative errors in a downstream direction.

For stagnation regions plots of h_i/h as a function of G are presented in figures 12 and 13. For the hemispherical shell (fig. 12) a fourth temperature component G_4 has been included, as described in appendix A.

A plot of the calorimetric temperature G_1 is also included (solid lines, figs. 12 and 13). Points on the G_1 curves correspond to points on the G curves lying on the same line of τ_R = Constant. If only G_1 and τ_R are available, values of h_i/h are obtained by reading the ordinate of the corresponding point in the G curve (broken line). Figures 12 and 13 allow evaluation of the relieving effects of conduction in the heating of stagnation regions by direct comparison of G and G_1. It may be noticed that the input parameters S and C_Y play a dominant role. For approximate values of $S < 10$ or $C_Y < 5$, large conduction (compared to the aerodynamic input) is present even for small temperature rises, whereas for approximate values of $S > 50$ or $C_Y > 20$, conduction is small even for large temperature rises.

Ten-Percent Error Charts

In figures 14, 15, 16, 17, and 18 results are presented for the point having a 10-percent conduction error, over a range of values of the input parameters. This point has been chosen since it is believed that the determination of a 10-percent conduction error threshold would be useful in evaluating heat-transfer measurements and for purposes of model design. Furthermore, it is believed that, while the first three temperature components considered in the present numerical calculations grant enough accuracy for the determination of errors of this order, the computation of substantially larger errors should include more temperature components.

Flat plate, wedge, and conical shell[3].- (Figs. 14, 15, and 16.) From the previous discussion of these bodies it follows that the location of the point having a 10-percent conduction error moves downstream with time while the corresponding temperature increases. Except for the immediate neighborhood of the leading edge, all points upstream of this location gain heat by conduction at a rate of more than 10 percent of the aerodynamic heat input whereas all points downstream gain heat at a rate of less than 10 percent of the aerodynamic heat input.

During the early part of the temperature rise ($G < 0.1$) the downstream motion of the 10-percent-error point is very nearly proportional

---

[3]It was found that for the conical shell having a turbulent boundary layer the curves of G plotted against X are very steep near the tip and rapidly level off downstream (see fig. 9(a)). This places the 10-percent-error point in a relatively forward location, where the first three temperature components do not converge satisfactorily (see fig. 9(b)). Therefore, the 10-percent-error chart (fig. 16(b)) was obtained by extrapolation of 1-percent, 2-percent, and 3-percent errors, located well within the region of convergence.

to $\sqrt{\tau}$ independently of the input parameter, as predicted by the limiting solutions. This downstream motion continues at a decreasing speed until it stops and reverses, as illustrated in sketch (b) and figures 4(b) and 5(b). Reversal points correspond to maximums in the solid lines of figures 14, 15, and 16. These maximums were observed to occur at a given value of $[G]_{10}$ for each body and boundary-layer combination considered. Shortly after $[X]_{10,max}$ is attained the curves terminate, the termination corresponding to the time when the maximum error becomes less than 10 percent.

It was found that under different conditions (such as heat input and body properties) for a given temperature rise $[G]_{10}$, the location of the 10-percent error point $[X]_{10}$ is inversely proportional to some power of the input parameter. This relationship may be obtained from the limiting solutions for small temperature rises. For instance, for a flat plate in laminar flow the temperature variable in the limiting solution is

$$G_1 = 1 - e^{-P\tau} \approx P\tau$$

and since

$$P = F_L X_l^{-1/2}$$

the result is approximately

$$G_1 = F_L X_l^{-1/2} \tau$$

therefore, the time at which the 10-percent-error point will attain a given position at a given temperature is

$$\tau = \frac{[G_1]_{10}}{F_L} [X_l]_{10}^{1/2}$$

Replacing τ in the corresponding limiting solution (eq. (21b) yields for a flat plate with laminar boundary layer:

$$[X_l]_{10} = (2.74)^{4/3} [G_1]_{10}^{2/3} F_L^{-2/3} \qquad (29a)$$

Similarly, equations for the other bodies considered are obtained

for a flat plate with turbulent boundary layer:

$$\left[X_l\right]_{10} = (1.55)^{10/9}\left[G_1\right]_{10}^{5/9}F_T^{-5/9} \tag{29b}$$

for a wedge with laminar boundary layer:

$$\left[X_\alpha\right]_{10} = (4.74)^4\left[G_1\right]_{10}^2\left(\frac{W_L}{\tan\varphi}\right)^{-2} \tag{29c}$$

for a wedge with turbulent boundary layer:

$$\left[X_\alpha\right]_{10} = (3.79)^{5/2}\left[G_1\right]_{10}^{5/4}\left(\frac{W_T}{\tan\varphi}\right)^{-5/4} \tag{29d}$$

for a conical shell with laminar boundary layer:

$$\left[X_l\right]_{10} = (1.58)^{4/3}\left[G_1\right]_{10}^{2/3}C_L^{-2/3} \tag{29e}$$

for a conical shell with turbulent boundary layer:

$$\left[X_l\right]_{10} = (0.63)^{10/9}\left[G_1\right]_{10}^{5/9}C_T^{-5/9} \tag{29f}$$

Equations (29) were checked for large values of G by using the results of the present solution presented in figures 14, 15, and 16. It was found that although the proportionality constants are not the same, the functional relation between $[X]_{10}$ and the input parameters holds true for large values of G.

The values of $[X]_{10,max}$ previously discussed follow the same pattern since they occur at given values of $[G]_{10}$. The corresponding equations were obtained from the present solution by means of plots similar to that shown in figure 19, and they are

for a flat plate with laminar boundary layer:

$$\left[X_l\right]_{10,max} = 4.2F_L^{-2/3} \tag{30a}$$

for a flat plate with turbulent boundary layer:

$$\left[X_l\right]_{10,max} = 3.2F_T^{-5/9} \tag{30b}$$

for a wedge with laminar boundary layer:

$$\left[X_\alpha\right]_{10,max} = 40\left(\frac{W_L}{\tan \varphi}\right)^{-2} \tag{30c}$$

for a wedge with turbulent boundary layer:

$$\left[X_\alpha\right]_{10,max} = 6.3\left(\frac{W_T}{\tan \varphi}\right)^{-5/4} \tag{30d}$$

for a conical shell with laminar boundary layer:

$$\left[X_l\right]_{10,max} = 1.2C_L^{-2/3} \tag{30e}$$

for a conical shell with turbulent boundary layer:

$$\left[X_l\right]_{10,max} = 0.62C_T^{-5/9} \tag{30f}$$

It must be noticed that large values of the input parameter (that is, small values of $\left[X\right]_{10}$ for a given temperature rise, and small values of $\left[X\right]_{10,max}$) do not necessarily correspond to forward physical locations of the 10-percent point $\left[x\right]_{10}$ or the reversal point $\left[x\right]_{10,max}$, since the input parameters include some power of the reference length in the numerator. The effect of the different parameters involved in determining the relative physical position of the 10-percent error point and of the reversal point is better expressed by the following equations that follow directly from equations (29) and (30): (subscripts 1 and 2 represent two arbitrary sets of conditions having the same temperature rise $\left[G\right]_{10}$)

flat plate and conical shell with laminar boundary layer:

$$\frac{\left(\left[x\right]_{10}\right)_2}{\left(\left[x\right]_{10}\right)_1} = \frac{\left(\left[x\right]_{10,max}\right)_2}{\left(\left[x\right]_{10,max}\right)_1} = \left\{\frac{l_2}{l_1}\frac{(k_b)_2}{(k_b)_1}\frac{\left[h(x)\sqrt{x}\right]_1}{\left[h(x)\sqrt{x}\right]_2}\right\}^{2/3} \tag{31a}$$

flat plate and conical shell with turbulent boundary layer:

$$\frac{\left([x]_{10}\right)_2}{\left([x]_{10}\right)_1} = \frac{\left([x]_{10,max}\right)_2}{\left([x]_{10,max}\right)_1} = \left\{\frac{l_2}{l_1}\frac{(k_b)_2}{(k_b)_1}\frac{\left[h(x)x^{1/5}\right]_1}{\left[h(x)x^{1/5}\right]_2}\right\}^{5/9} \tag{31b}$$

wedge with laminar boundary layer:

$$\frac{\left([x]_{10}\right)_2}{\left([x]_{10}\right)_1} = \frac{\left([x]_{10,max}\right)_2}{\left([x]_{10,max}\right)_1} = \left\{\frac{\tan\varphi_2}{\tan\varphi_1}\frac{(k_b)_2}{(k_b)_1}\frac{\left[h(x)\sqrt{x}\right]_1}{\left[h(x)\sqrt{x}\right]_2}\right\}^{2} \tag{31c}$$

wedge with turbulent boundary layer:

$$\frac{\left([x]_{10}\right)_2}{\left([x]_{10}\right)_1} = \frac{\left([x]_{10,max}\right)_2}{\left([x]_{10,max}\right)_1} = \left\{\frac{\tan\varphi_2}{\tan\varphi_1}\frac{(k_b)_2}{(k_b)_1}\frac{\left[h(x)x^{1/5}\right]_1}{\left[h(x)x^{1/5}\right]_2}\right\}^{5/4} \tag{31d}$$

Notice the different effect of the parameters indicated by the different exponents: if, for instance, the thermal conductivity of a flat plate with laminar boundary layer is doubled, $[x]_{10,max}$ is increased by about 60 percent whereas the same variation in a wedge results in a 400-percent increase in $[x]_{10,max}$.

Hemispherical and hemicylindrical shells.- (Figs. 17 and 18.) In these cases the 10-percent-error point moves with time toward the stagnation region. Points upstream of its location ($0.9 < h_i/h < 1.0$) lose heat by conduction at a rate of less than 10 percent of the aerodynamic input, and points downstream ($h_i/h < 0.9$) lose heat at an increasing rate, always larger than 10 percent of the aerodynamic heat input.

It was found that for the 10-percent-error point, for a given temperature rise $[G]_{10}$, an increase of the input parameters S or C_Y always results in an increase of $[X_R]_{10}$. This relationship may be obtained directly from the results of figures 17 and 18, as shown in figure 20 for three values of $[G]_{10}$. For small temperature rises the same results may be obtained by making use of the limiting solutions. For the case of a hemispherical shell, the temperature variable in the limiting solution is

$$G_1 = 1 - e^{-P\tau_R} \approx P\tau_R$$

and

$$P = S \cos X_R$$

therefore

$$\tau_R = \frac{G_1}{S \cos X_R}$$

Replacing P and τ_R in the limiting solution (eq. (27a)) and letting $h_i/h = 0.9$ (for the 10-percent-error point) gives

$$S = 20\left[G_1\right]_{10} \frac{1 + \frac{1}{2}\left[G_1\right]_{10} \tan^2\left[X_R\right]_{10}}{\cos\left[X_R\right]_{10}}$$

and for constant $\left[G_1\right]_{10}$ it follows that

$$\frac{dS}{d\left[X_R\right]_{10}} = 20\left[G_1\right]_{10} \frac{\sin\left[X_R\right]_{10}}{\cos^2\left[X_R\right]_{10}}\left[1 + \left[G_1\right]_{10}\left(\frac{1}{\cos^2\left[X_R\right]_{10}} + \frac{1}{2}\tan^2\left[X_R\right]_{10}\right)\right]$$

This is an essentially positive quantity, which means that an increase in S at constant $\left[G_1\right]_{10}$ results in an increase in $\left[X_R\right]_{10}$. The same conclusions are applicable to the case of the hemicylindrical shell.

It is also generally true that for any given point X_R, for a given temperature rise G, an increase of the input parameter results in smaller conduction errors, as illustrated for the stagnation point in figures 12 and 13.

From the previous considerations it is then concluded that, in order to decrease conduction errors for a given temperature rise, large values of the input parameters are desirable. Inspection of the definitions of the input parameters (table I) then leads to the conclusion that small skin thickness and thermal conductivity, and large body radius

and stagnation heat-transfer coefficient (with body radius predominating) are desirable in order to minimize conduction effects.

Typical Examples of Application of Solutions

Flat plate with laminar boundary layer.- (Fig. 14(a).) The following conditions, which may be typical of a wind-tunnel test, are assumed:

L
1
2
2
7

M	5
T_o, °F	600
T_w, °F	100
p_o, lb/sq in. gage	800
l, in.	0.030
α, sq ft/sec	46.3×10^{-6}
Material	Stainless steel

The input parameter is calculated according to appendix B, and for this case it is approximately $F_L = 0.03$. From figure 14(a) the successive locations and temperatures of the 10-percent-error point may be obtained for this value of F_L. For instance, at $t = 3$ seconds $(\tau_l = 22.2)$ the 10-percent-error point is located 15 thicknesses aft of the leading edge $\left([X_l]_{10} = 15\right)$ and its temperature corresponds to $G_{10} = 0.165$, that is, a 16.5-percent (of the potential) increase above the initial temperature. Under the conditions assumed the maximum downstream position of the 10-percent-error point would be at 42 thicknesses aft of the leading edge and would occur at $t = 44.6$ seconds $(\tau_l = 330)$. All stations beyond that point will have conduction errors never in excess of 10 percent of the aerodynamic heat input.

Hemispherical shell with laminar boundary layer.- A $\frac{1}{2}$- inch-radius hemispherical shell is considered under the same free-stream conditions as those for the flat plate in the preceding section. With $h_{SP} = 0.0815 \frac{\text{Btu}}{(\text{sq ft})(\text{sec})(^\circ\text{R})}$, $k_b = 10 \frac{\text{Btu}}{(\text{ft})(\text{hr})(^\circ\text{R})}$, and $l = 0.030$ inch the input parameter is $S \approx 21.6$. The progress of the 10-percent-error point may be approximately followed in figures 12 and 17 for $S = 20$. When the stagnation point has experienced a temperature rise of $G = 0.525$ (at $\tau_R = 0.04$, fig. 12) it has a conduction error of

7.8 percent; the 10-percent-error point is at 46° (fig. 17) and has a temperature rise of 41 percent. The forward motion of the 10-percent-error point continues until it reaches the stagnation point at $\tau_R = 0.0506$ ($t \approx 1.9$ seconds) with $G \approx 0.6$. After this time the conduction error is larger than 10 percent of the aerodynamic input throughout the body.

CONCLUDING REMARKS

An approximate method has been devised to compute transient temperature distributions and streamwise conduction errors in heat-transfer measurements. This method can be applied to a large range of body shapes and thickness distributions, within the limitations of one-dimensional heat conduction, time-independent heat-transfer coefficient, constant adiabatic wall temperature, and negligible radiation effects.

The method consists in evaluating the temperature as the summation of temperature components, of which the first three (and in one case, four) components have been calculated. The method is suitable for computation by means of an ordinary desk computing machine.

Numerical computations were carried out for semi-infinite flat plates, wedges, and conical shells, and for hemispherical and hemicylindrical shells. Free-stream conditions and body properties were included in a free parameter, called input parameter. Complete results are presented for specific values of the input parameter, and charts showing the location and temperature of the point having a 10-percent conduction error in measured heat-transfer coefficient are presented for a range of values of the input parameter. This presentation permits a rapid determination of a 10-percent-error threshold in heat-transfer measurements.

In the cases of the semi-infinite flat plate, the wedge, and the conical shell all points except those in the immediate neighborhood of the leading edge or tip show a net gain of heat due to conduction. The fictitious 10-percent-error point moves downstream with time with decreasing speed until it stops and reverses its motion, thereby achieving a maximum downstream position. Since all points downstream of the 10-percent-error point have conduction errors smaller than 10 percent, it follows that points downstream of the maximum never sustain errors larger than 10 percent. The coordinate of this maximum position increases with increasing thermal conductivity of the skin and skin thickness or wedge angle, and decreasing heat-transfer level.

In the cases of hemispherical and hemicylindrical shells there is a net loss of heat due to conduction, which increases in a downstream

direction. The 10-percent-error point moves upstream with increasing time until it reaches the stagnation point, after which it loses significance since the errors are larger than 10 percent throughout the body. This occurs at values of the Fourier number, based on the radius, of approximately 0.05 and 0.10 for the hemisphere and hemicylinder, respectively. For a given temperature rise, minimum conduction is achieved with small skin thickness and thermal conductivity and large body radius and stagnation heat transfer, body radius being the dominant factor. Conversely, if large thermal relieving effects are sought near the stagnation region, a thick, highly conductive skin with small nose radius is desirable.

Langley Research Center,
National Aeronautics and Space Administration,
Langley Field, Va., March 27, 1961.

APPENDIX A

APPLICATION OF THE SOLUTION TO SIMPLE BODIES

This appendix is concerned with the application of the present solution to the following bodies, exposed to aerodynamic heat transfer through laminar and turbulent boundary layers:

1. Flat plate
2. Solid wedge
3. Conical shell
4. Hemispherical shell
5. Hemicylindrical shell

All bodies except the solid wedge were assumed to have constant skin thickness.

The heat-transfer coefficient was assumed to be of the form

$$h = (\text{Constant})\left(X^{-1/2}\right) \quad \text{and} \quad h = (\text{Constant})\left(X^{-1/5}\right)$$

for the first three bodies, and

$$h = (\text{Constant})(\cos X)$$

for the last two. A compilation of commonly used methods for estimating the constants is included in appendix B.

When the heat-transfer coefficient is proportional to X^{-n}, equations (15) reduce to a simpler form. Two examples of particular interest are:

For

$$P(X) = K_1 X^{-n}$$

$$Q(X) = 0$$

equations (15) become

$$
\left.
\begin{aligned}
A_{11} &= \tfrac{1}{2} K_1 n(n+1)X^{-(n+2)} \\
A_{12} &= \tfrac{1}{3} K_1^2 n^2 X^{-(2n+2)} \\
A_{21} &= \tfrac{1}{6} K_1 n(n+1)(n+2)(n+3)X^{-(n+4)} \\
A_{22} &= \tfrac{1}{24} K_1^2 n^2 (n+1)(17n+27)X^{-(2n+4)} \\
A_{23} &= \tfrac{13}{30} K_1^3 n^3 (n+1)X^{-(3n+4)} \\
A_{24} &= \tfrac{1}{18} K_1^4 n^4 X^{-(4n+4)}
\end{aligned}
\right\} \qquad \text{(A1)}
$$

L
1
2
2
7

For

$$P(X) = K_2 X^{-n}$$

$$Q(X) = \frac{1}{X}$$

equations (15) become

$$
\left.
\begin{aligned}
A_{11} &= \tfrac{1}{2} K_2 n^2 X^{-(n+2)} \\
A_{12} &= \tfrac{1}{3} K_2^2 n^2 X^{-(2n+2)} \\
A_{21} &= \tfrac{1}{6} K_2 n^2 (n+2)^2 X^{-(n+4)} \\
A_{22} &= \tfrac{1}{24} K_2^2 n^2 (17n^2 + 28n + 8)X^{-(2n+4)} \\
A_{23} &= \tfrac{1}{30} K_2^3 n^3 (13n+8)X^{-(3n+4)} \\
A_{24} &= \tfrac{1}{18} K_2^4 n^4 X^{-(4n+4)}
\end{aligned}
\right\} \qquad \text{(A2)}
$$

where K_1, K_2, and n are arbitrary constants.

Flat Plate

This is the case of a semi-infinite flat plate of constant thickness l exposed to a two-dimensional fluid flow on one side. In this case

$$\frac{dV}{ds} = l \quad \text{and} \quad a(X) = \text{Constant}$$

Let the characteristic length L be equal to l; then the nondimensional variables are

$$X_l = \frac{x}{l} \quad \text{and} \quad \tau_l = \frac{\alpha}{l^2} t$$

L
1
2
2
7

and the characteristic functions $P(X)$ and $Q(X)$ become

$$P(X_l) = \frac{lh(X_l)}{k_b} \quad \text{and} \quad Q(X_l) = 0$$

Laminar boundary layer.- The heat-transfer coefficient is of the form

$$h(X_l) = H_l X_l^{-1/2}$$

therefore

$$P(X_l) = F_L X_l^{-1/2}$$

$$Q(X_l) = 0$$

where $F_L \equiv \frac{lH_l}{k_b}$. Now the functions $A_{ij}(X_l)$ may be obtained from equations (A1)

$$\left.\begin{aligned} A_{11} &= \frac{3}{8} F_L X_l^{-5/2} \\ A_{12} &= \frac{1}{12} F_L^2 X_l^{-3} \end{aligned}\right\} \qquad (A3)$$

(Equations continued on next page)

$$\left.\begin{aligned} A_{21} &= \frac{35}{32} F_L X_l^{-9/2} \\ A_{22} &= \frac{71}{128} F_L^2 X_l^{-5} \\ A_{23} &= \frac{13}{160} F_L^3 X_l^{-11/2} \\ A_{24} &= \frac{1}{288} F_L^4 X_l^{-6} \end{aligned}\right\} \tag{A3}$$

Turbulent boundary layer.- In this case

$$h(X_l) = H_2 X_l^{-1/5}$$

therefore

$$P(X_l) = F_T X_l^{-1/5}$$

$$Q(X_l) = 0$$

where

$$F_T \equiv \frac{lH_2}{k_b}$$

From equations (A1), the following equations may be obtained:

$$\left.\begin{aligned} A_{11} &= \frac{6}{50} F_T X_l^{-11/5} \\ A_{12} &= \frac{1}{75} F_T^2 X_l^{-12/5} \\ A_{21} &= \frac{528}{1,875} F_T X_l^{-21/5} \\ A_{22} &= \frac{38}{625} F_T^2 X_l^{-22/5} \\ A_{23} &= \frac{13}{3,125} F_T^3 X_l^{-23/5} \\ A_{24} &= \frac{1}{11,250} F_T^4 X_l^{-24/5} \end{aligned}\right\} \tag{A4}$$

Solid Wedge

Consider a semi-infinite solid wedge having a wedge angle φ and with aerodynamic heat transfer on one side only. The restriction of one-dimensional heat conduction reduces the applicability of the present solution to the front section where the thickness is small.

In this case there is no satisfactory physical reference length. The variables were made nondimensional with reference to the diffusion distance per unit time:

$$L \equiv \sqrt{\alpha}$$

Therefore

$$X_\alpha = \frac{x}{\sqrt{\alpha}} \quad \text{and} \quad \tau_\alpha = t$$

It may be noticed that, with this particular arrangement where the unit time is implicit, the choice of the unit time determines the units to be used for t and α. For instance, if the unit time is one second, then $\tau = t$ seconds and α must be expressed in $(\text{length})^2/\text{sec}$.

If an element of unit width is considered, such as that indicated in the following sketch:

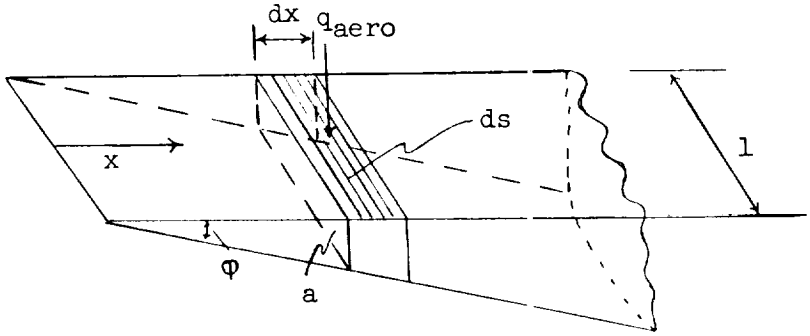

then

$$dV(X_\alpha) = \alpha X_\alpha \tan \varphi \, dX_\alpha$$

$$ds(X_\alpha) = \sqrt{\alpha} \, dX_\alpha$$

$$a(X_\alpha) = \sqrt{\alpha} \, X_\alpha \tan \varphi$$

Therefore the characteristic functions are

$$P(X_\alpha) = \frac{h(X_\alpha)}{\rho c\sqrt{\alpha} X_\alpha \tan \varphi}$$

$$Q(X_\alpha) = \frac{1}{X_\alpha}$$

Laminar boundary layer.- The heat-transfer coefficient is

$$h(X_\alpha) = H_3 X_\alpha^{-1/2}$$

where

$$H_3 = H_1\left(\frac{1}{\sqrt{\alpha}}\right)^{1/2}$$

Therefore

$$P(X_\alpha) = \frac{W_L}{\tan \varphi} X_\alpha^{-3/2}$$

$$Q(X_\alpha) = \frac{1}{X_\alpha}$$

where

$$W_L \equiv \frac{H_3}{\rho c\sqrt{\alpha}}$$

Then, equations (A2) yield

$$\left.\begin{aligned} A_{11} &= \frac{9}{8}\left(\frac{W_L}{\tan \varphi}\right) X_\alpha^{-3.5} \\ A_{12} &= \frac{3}{4}\left(\frac{W_L}{\tan \varphi}\right)^2 X_\alpha^{-5} \\ A_{21} &= \frac{147}{32}\left(\frac{W_L}{\tan \varphi}\right) X_\alpha^{-5.5} \\ A_{22} &= \frac{1,059}{128}\left(\frac{W_L}{\tan \varphi}\right)^2 X_\alpha^{-7} \end{aligned}\right\} \quad (A5)$$

(Equations continued on next page)

$$\left.\begin{aligned} A_{23} &= \frac{99}{32}\left(\frac{W_L}{\tan\varphi}\right)^3 X_\alpha^{-8.5} \\ A_{24} &= \frac{9}{32}\left(\frac{W_L}{\tan\varphi}\right)^4 X_\alpha^{-10} \end{aligned}\right\} \qquad (A5)$$

Turbulent boundary layer.- Here the heat-transfer coefficient is

$$h(X_\alpha) = H_4 X_\alpha^{-1/5}$$

and

$$H_4 = H_2\left(\frac{l}{\sqrt{\alpha}}\right)^{1/5}$$

then

$$P(X_\alpha) = \frac{W_T}{\tan\varphi} X_\alpha^{-6/5}$$

$$Q(X_\alpha) = \frac{1}{X_\alpha}$$

where

$$W_T \equiv \frac{H_4}{\rho c\sqrt{\alpha}}$$

From equations (A2) are obtained

$$\left.\begin{aligned} A_{11} &= \frac{18}{25}\left(\frac{W_T}{\tan\varphi}\right) X_\alpha^{-3.2} \\ A_{12} &= \frac{12}{25}\left(\frac{W_T}{\tan\varphi}\right)^2 X_\alpha^{-4.4} \\ A_{21} &= \frac{1,536}{625}\left(\frac{W_T}{\tan\varphi}\right) X_\alpha^{-5.2} \\ A_{22} &= \frac{2,478}{625}\left(\frac{W_T}{\tan\varphi}\right)^2 X_\alpha^{-6.4} \end{aligned}\right\} \qquad (A6)$$

(Equations continued on next page)

$$\left.\begin{aligned} A_{23} &= \frac{4,248}{3,125}\left(\frac{W_T}{\tan\varphi}\right)^3 X_\alpha^{-7.6} \\ A_{24} &= \frac{72}{625}\left(\frac{W_T}{\tan\varphi}\right)^4 X_\alpha^{-8.8} \end{aligned}\right\} \qquad (A6)$$

Conical Shell

Consider the case of a conical shell of constant thickness l and included angle 2ψ as shown in the following sketch:

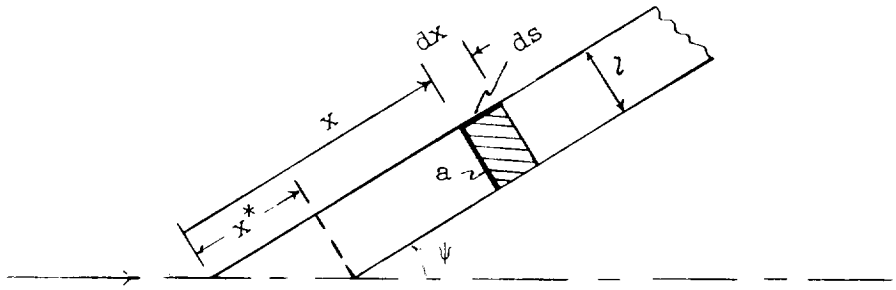

Let the nondimensional variables be

$$X_l = \frac{x}{l} \quad \text{and} \quad \tau_l = \frac{\alpha}{l^2}\,t$$

In the annular element of volume shown, for $X_l \geqq X_l^*$

$$a(X_l) = \pi l^2\left[\cos\psi + 2\left(X_l - X_l^*\right)\sin\psi\right]$$

$$dV = l\,a(X_l)\,dX_l$$

$$ds = 2\pi l^2 \sin\psi\; X_l\, dX_l$$

It may be noticed that for the conical shell the "effective" thickness $\frac{dV}{ds} = l\left(1 - \frac{1}{2}\frac{X_l^*}{X_l}\right)$ is smaller than the physical thickness, which it approaches asymptotically with x. Now the characteristic equations are

$$P(X_l) = \frac{lh(X_l)}{k_b} \frac{1}{1 - \frac{1}{2}\frac{X_l^*}{X_l}}$$

$$Q(X_l) = \frac{1}{X_l - \frac{1}{2} X_l^*}$$

where

$$X_l^* = \frac{1}{\tan \psi}$$

Similarly, for $X_l \leqq X_l^*$

$$a(X_l) = \pi l^2 \sin \psi \tan \psi X_l^2$$

$$dV = \pi l^3 \sin \psi \tan \psi X_l^2 \, dX_l$$

from which it follows that

$$P(X_l) = 2 \frac{lh(X_l)}{k_b} \frac{X_l^*}{X_l}$$

$$Q(X_l) = \frac{2}{X_l}$$

It may be noted that the derivatives of the characteristic functions have discontinuities at $X_l = X_l^*$; therefore, interference effects are to be expected between the tip and the shell. Further study of the tip effect was not undertaken; however, this problem is treated in reference 4. Consequently, only the characteristic equations for $X_l >> X_l^*$ are considered, that is:

$$P(X_l) = \frac{lh(X_l)}{k_b}$$

$$Q(X_l) = \frac{1}{X_l}$$

L
1
2
2
7

These equations must be used with the understanding that they do not hold true for regions in the neighborhood of the tip.

Laminar boundary layer.- The heat-transfer coefficient may be written as

$$h(X_l) = H_5 X_l^{-1/2}$$

then

$$P(X_l) = C_L X_l^{-1/2}$$

$$Q(X_l) = \frac{1}{X_l}$$

where

$$C_L \equiv \frac{lH_5}{k_b}$$

Equations (A2) may again be used here, and they yield

$$\left.\begin{aligned} A_{11} &= \frac{1}{8} C_L X_l^{-5/2} \\ A_{12} &= \frac{1}{12} C_L^2 X_l^{-6/2} \\ A_{21} &= \frac{25}{96} C_L X_l^{-9/2} \\ A_{22} &= \frac{35}{128} C_L^2 X_l^{-10/2} \\ A_{23} &= \frac{29}{480} C_L^3 X_l^{-11/2} \\ A_{24} &= \frac{1}{288} C_L^4 X_l^{-12/2} \end{aligned}\right\} \quad (A7)$$

Turbulent boundary layer.- The heat-transfer coefficient may be expressed as

$$h(X_l) = H_6 X_l^{-1/5}$$

The corresponding characteristic equations are then

$$P(X_l) = C_T X_l^{-1/5}$$

$$Q(X_l) = \frac{1}{X_l}$$

where

$$C_T \equiv \frac{lH_6}{k_b}$$

Further use of equations (A2) gives

$$\left.\begin{aligned}
A_{11} &= \frac{1}{50} C_T X_l^{-11/5} \\
A_{12} &= \frac{1}{75} C_T^2 X_l^{-12/5} \\
A_{21} &= \frac{121}{3,750} C_T X_l^{-21/5} \\
A_{22} &= \frac{119}{5,000} C_T^2 X_l^{-22/5} \\
A_{23} &= \frac{53}{18,750} C_T^3 X_l^{-23/5} \\
A_{24} &= \frac{1}{11,250} C_T^4 X_l^{-24/5}
\end{aligned}\right\} \qquad \text{(A8)}$$

L
1
2
2
7

Hemispherical Shell

Consider the case of a thin shell of variable thickness having a hemispherical outer shape, shown in the following sketch:

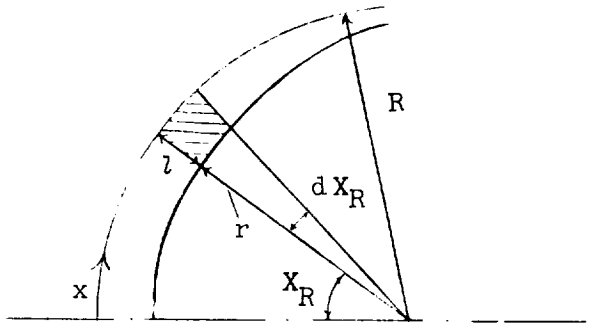

The nondimensional variables are defined as follows:

$$X_R = \frac{x}{R} \quad \text{and} \quad \tau_R = \frac{\alpha}{R^2} t$$

In the annular volume element of which the upper cross section is indicated in the sketch

$$a(X_R) = 2\pi\left(Rl - \frac{l^2}{2}\right)\sin X_R$$

$$dV = a(X_R)\left(R - \frac{l}{2}\right)dX_R$$

$$ds = 2\pi R^2 \sin X_R \, dX_R$$

L
1
2
2
7

therefore

$$\frac{dV}{ds} = l\left(1 - \frac{1}{2}\frac{l}{R}\right)^2$$

$$P(X_R) = \frac{R^2}{\alpha}\frac{h(X_R)}{\rho c l\left(1 - \frac{1}{2}\frac{l}{R}\right)^2}$$

$$Q(X_R) = \frac{1}{\tan X_R} + \frac{R - l}{R - \frac{l}{2}}\frac{d}{dX_R}(\log l)$$

If the shell has a constant thickness

$$P(X_R) = \frac{R^2}{\alpha}\frac{h(X_R)}{\rho c l\left(1 - \frac{1}{2}\frac{l}{R}\right)^2}$$

$$Q(X_R) = \frac{1}{\tan X_R}$$

If the boundary layer is laminar the heat-transfer coefficient may be approximately represented by $h(X_R) = h_{SP} \cos X_R$ for X_R up to about 70°. When this heat-transfer distribution is used the characteristic functions for constant thickness may be written as

$$P(X_R) = S \cos X_R$$

$$Q(X_R) = \frac{1}{\tan X_R}$$

where

$$S \equiv \frac{1}{k_b} \frac{R^2}{l\left(1 - \frac{1}{2}\frac{l}{R}\right)^2} h_{SP}$$

and h_{SP} denotes the heat-transfer coefficient at the stagnation point. The functions $A_{ij}(X_R)$ are obtained by replacing the characteristic functions and their derivatives in equations (15) which yield

$$\left.\begin{aligned} A_{11} &= -S \cos X_R \\ A_{12} &= \frac{1}{3} S^2 \sin^2 X_R \\ A_{21} &= \frac{2}{3} S \cos X_R \\ A_{22} &= S^2\left(\frac{3}{2}\cos^2 X_R - \frac{2}{3}\right) \\ A_{23} &= -\frac{3}{5} S^3 \sin^2 X_R \cos X_R \\ A_{24} &= \frac{1}{18} S^4 \sin^4 X_R \end{aligned}\right\} \qquad (A9)$$

L
1
2
2
7

Stagnation Point for the Hemispherical Shell

The stagnation region of a hemispherical shell is of particular interest since most blunt bodies may be very well represented by a spherical shape in the neighborhood of the nose, and this is a critical area with respect to aerodynamic heat transfer. Furthermore, for axisymmetrical flow the boundary layer may be expected to be always laminar in the stagnation area, and the cosinusoidal distribution of heat-transfer coefficient that was assumed closely represents the actual conditions. Consequently, in an effort to obtain a more accurate solution for the stagnation point, a fourth temperature component term G_4 was computed for this particular case. By following the same general procedure described in the text, the following results were obtained:

$$G_1(\tau_R) = 1 - e^{-S\tau_R}$$

$$G_2(\tau_R) = -S\tau_R^2 e^{-S\tau_R}$$

$$G_3(\tau_R) = \left(\frac{2}{3} S\tau_R^3 - \frac{5}{6} S^2\tau_R^4\right)e^{-S\tau_R}$$

$$G_4(\tau_R) = \left(-\frac{1}{3} S\tau_R^4 + \frac{22}{15} S^2\tau_R^5 - \frac{61}{90} S^3\tau_R^6\right)e^{-S\tau_R}$$

$$\frac{h_i}{h}(\tau_R) = 1 + \frac{\left[-2\tau_R + 2\tau_R^2 - \left(\frac{10}{3} S + \frac{4}{3}\right)\tau_R^3 + \frac{22}{3} S\tau_R^4 - \frac{61}{15} S^2\tau_R^5\right]e^{-S\tau_R}}{1 - G}$$

L
1
2
2
7

where

$$G = G_1 + G_2 + G_3 + G_4$$

$$P(X_R) = S \cos X_R$$

$$Q(X_R) = \frac{1}{\tan X_R}$$

$$S \equiv \frac{1}{k_b} \frac{R^2}{l\left(1 - \frac{1}{2}\frac{l}{R}\right)^2} h_{SP}$$

Hemicylindrical Shell

In this case the thin shell has a hemicylindrical outer shape and variable thickness l. A sketch showing a cross section of the shell perpendicular to the cylinder axis would be the same as the sketch shown for the hemispherical shell. The outer radius is used as the reference length; therefore,

$$X_R = \frac{x}{R} \quad \text{and} \quad \tau_R = \frac{\alpha}{R^2} t$$

In the volume element indicated in the sketch, having unit depth,

$$a(X_R) = l(X_R)$$

$$dV = l\left(R - \frac{l}{2}\right)dX_R$$

$$ds = R\, dX_R$$

The "effective thickness" in this case is, then

$$\frac{dV}{ds} = l\left(1 - \frac{1}{2}\frac{l}{R}\right)$$

and the characteristic functions are

$$P(X_R) = \frac{1}{k_b}\frac{R^2}{l\left(1 - \frac{1}{2}\frac{l}{R}\right)} h(X_R)$$

$$Q(X_R) = \frac{d}{dX_R}(\log l)$$

If the thickness l is constant, these last two equations become

$$P(X_R) = \frac{1}{k_b}\frac{R^2}{l\left(1 - \frac{1}{2}\frac{l}{R}\right)} h(X_R)$$

$$Q(X_R) = 0$$

If the boundary layer is laminar the heat-transfer coefficient may be approximated by

$$h(X_R) = h_{SL} \cos X_R$$

Therefore, the characteristic equations for constant skin thickness may be written

$$P(X_R) = C_Y \cos X_R$$

$$Q(X_R) = 0$$

where

$$C_Y \equiv \frac{1}{k_b}\frac{R^2}{l\left(1 - \frac{1}{2}\frac{l}{R}\right)} h_{SI}$$

and h_{SL} is the heat-transfer coefficient at the stagnation line.

Substitution of these equations and their derivatives into equations (15) yields

$$\left.\begin{aligned} A_{11} &= -\frac{1}{2} C_Y \cos X_R \\ A_{12} &= \frac{1}{3} C_Y^2 \sin^2 X_R \\ A_{21} &= \frac{1}{6} C_Y \cos X_R \\ A_{22} &= \frac{1}{24} C_Y^2 \left(17 \cos^2 X_R - 10\right) \\ A_{23} &= -\frac{13}{30} C_Y^3 \sin^2 X_R \cos X_R \\ A_{24} &= \frac{1}{18} C_Y^4 \sin^4 X_R \end{aligned}\right\} \qquad \text{(A10)}$$

APPENDIX B

ESTIMATION OF THE HEAT-TRANSFER COEFFICIENT

Applications of the present solution to the particular cases of flat plate, wedge, conical shell, hemispherical shell, and hemicylindrical shell are presented in appendix A. In these applications only the functional dependence of the heat-transfer coefficient upon the longitudinal coordinate has been fixed. The input parameters F_L, F_T, W_L, W_T, C_L, C_T, S, and C_Y were left arbitrary and may be theoretically or experimentally determined for each particular case. As a matter of convenience, in this appendix are compiled a few commonly used methods that may serve as a guide for the estimation of the input parameters.

Flat Plate With Laminar Boundary Layer

The input parameter is

$$F_L = \frac{lH_l}{k_b}$$

where H_l is defined by

$$h(X_l) = H_l X_l^{-1/2}$$

Making use of the identity

$$h(X_l) = Pr_\infty \left(St \sqrt{Re}\right)_\infty k_\infty \frac{\sqrt{Re_\infty / ft}}{\sqrt{l}} X_l^{-1/2}$$

F_L may be written as

$$F_L = Pr_\infty \left(St \sqrt{Re}\right)_\infty \frac{k_\infty}{k_b} \sqrt{Re_{\infty,l}} \qquad (B1)$$

The heat-transfer parameter $\left(St\sqrt{Re}\right)_\infty$ may be obtained, for instance, from reference 6. Figure 21, reproduced from reference 6, shows a plot of $\left(St\sqrt{Re}\right)_\infty$ as a function of Mach number and wall-temperature level.

Flat Plate With Turbulent Boundary Layer

In this case the skin-friction coefficient may be obtained by using a solution of the Blasius type for incompressible flow, in conjunction with a T' reference-temperature method. Thus,

$$c_f = 0.059\left(Re_\infty\right)^{-1/5}\left(\frac{T'}{T_\infty}\right)^{(\omega-4)/5}$$

where the viscosity has been assumed to be proportional to T^ω. The reference temperature T' may be obtained from reference 7 as

$$\frac{T'}{T_\infty} = 1 + 0.035M_\infty^2 + 0.45\left(\frac{T_w}{T_\infty} - 1\right) \qquad (B2)$$

The heat-transfer coefficient is then obtained by means of the modified Reynolds analogy

$$St = (Pr)^{-2/3}\,\frac{c_f}{2}$$

$$h\left(X_l\right) = 0.0295k_\infty\left(Pr_\infty\right)^{1/3}\left(Re_\infty/ft\right)^{4/5}\left(\frac{T'}{T_\infty}\right)^{-0.648} l^{-1/5}X_l^{-1/5} \equiv H_2X_l^{-1/5}$$

where the value $\omega = 0.76$ has been used. In this case the input parameter is

$$F_T = \frac{lH_2}{k_b}$$

therefore

$$F_T = 0.0295 \frac{k_\infty}{k_b}(Pr_\infty)^{1/3}\left(Re_{\infty,l}\right)^{4/5}\left(\frac{T'}{T_\infty}\right)^{-0.648} \qquad (B3)$$

where T'/T_∞ is a function of Mach number and wall-temperature ratio given by equation (B2).

L
1
2
2
7

Wedge With Laminar Boundary Layer

The heat-transfer coefficient is the same as that for the flat plate and, expressed in terms of the wedge variable X_α, is

$$h(X_\alpha) = H_1\left(\frac{l}{\sqrt{\alpha}}\right)^{1/2} X_\alpha^{-1/2}$$

H_1 was given for the flat plate as

$$H_1 = Pr_\infty\left(St\sqrt{Re}\right)_\infty k_\infty \frac{\sqrt{Re_\infty/ft}}{\sqrt{l}}$$

therefore

$$h(X_\alpha) = Pr_\infty\left(St\sqrt{Re}\right)_\infty k_\infty \frac{\sqrt{Re_\infty/ft}}{\alpha^{1/4}} X_\alpha^{-1/2} \equiv H_3 X_\alpha^{-1/2}$$

and the input parameter $W_L = \dfrac{H_3}{\rho c\sqrt{\alpha}}$ becomes

$$W_L = Pr_\infty\left(St\sqrt{Re}\right)_\infty \frac{k_\infty}{k_b}\sqrt{Re_\infty/ft}\,\alpha^{1/4} \qquad (B4)$$

The heat-transfer parameter $St\sqrt{Re}$ may be obtained from figure 21, where local flow conditions outside the boundary layer are to be used for the quantity $(\ )_\infty$.

Wedge With Turbulent Boundary Layer

The input parameter is

$$W_T = \frac{H_4}{\rho c \sqrt{\alpha}}$$

where H_4 is defined by

$$h(X_\alpha) = H_4 X_\alpha^{-1/5}$$

and is related to the flat-plate value H_2 through

$$H_4 = H_2 \left(\frac{l}{\sqrt{\alpha}}\right)^{1/5}$$

therefore

$$h(X_\alpha) = 0.0295 k_\infty (Pr_\infty)^{1/3} (Re_\infty/ft)^{4/5} \left(\frac{T'}{T_\infty}\right)^{-0.648} \alpha^{-1/10} X_\alpha^{-1/5} = H_4 X_\alpha^{-1/5}$$

and

$$W_T = 0.0295 \frac{k_\infty}{k_b} (Pr_\infty)^{1/3} (Re_\infty/ft)^{4/5} \alpha^{2/5} \left(\frac{T'}{T_\infty}\right)^{-0.648} \qquad (B5)$$

where T'/T_∞ may be computed from equation (B2). For an inclined surface, the local flow conditions just outside the boundary layer are to be used as the effective free-stream conditions.

Cone With Laminar Boundary Layer

The input parameter is

$$C_L = \frac{lH_5}{k_b}$$

where H_5 is defined by

$$h(X_l) = H_5 X_l^{-1/2}$$

H_5 may be calculated with the aid of Mangler's transformation from a flat-plate solution where the free-stream conditions are replaced by the inviscid-flow conditions at the surface of the cone. This gives

$$H_5 = \sqrt{3}\left[\Pr\left(St\sqrt{Re}\right)_\infty k_\infty \frac{\sqrt{Re_\infty/ft}}{\sqrt{l}}\right]_{\text{cone surface}}$$

therefore

$$C_L = \sqrt{3}\left[\Pr\left(St\sqrt{Re}\right)_\infty \frac{k_\infty}{k_b}\sqrt{Re_l}\right]_{\text{cone surface}} \tag{B6}$$

The heat-transfer parameter $\left(St\sqrt{Re}\right)_\infty$ may be obtained from figure 21 by using the values of Mach number and static temperature that the inviscid flow would have at the surface of the cone.

Cone With Turbulent Boundary Layer

A cone with a turbulent boundary layer has the same skin-friction coefficient as an equivalent flat plate having a Reynolds number equal to one-half that of the cone (ref. 8). The equivalent flat plate is one having free-stream conditions equal to the inviscid-flow conditions at the surface of the cone. Therefore, by means of equation (B3) there is obtained

$$C_T = (2)^{1/5}\left[0.0295\,\frac{k_\infty}{k_b}\,(Pr_\infty)^{1/3}\,(Re_{\infty,l})^{4/5}\left(\frac{T'}{T_\infty}\right)^{-0.648}\right]_{\text{cone surface}} \tag{B7}$$

The value of T'/T_∞ may be obtained from equation (B2) by using the Mach number and static temperature of the inviscid flow at the surface of the cone.

Hemispherical Shell

The input parameter for the hemispherical shell was defined in appendix A as

$$S = \frac{1}{k_b}\,\frac{R^2}{l\left(1 - \frac{1}{2}\,\frac{l}{R}\right)^2}\,h_{SP}$$

where h_{SP} is the heat-transfer coefficient at the stagnation point, and may be written as

$$h_{SP} = \left(\frac{Nu}{\sqrt{Re}}\right)_w \left(\frac{k}{\sqrt{\nu}}\right)_w \left(\frac{dU}{dx}\right)_{SP}^{1/2}$$

where w denotes wall conditions and SP denotes stagnation point. The heat-transfer parameter $\left(\frac{Nu}{\sqrt{Re}}\right)_w$ has been obtained by several investigators. One solution, due to Reshotko and Cohen, is presented in figure 22 reproduced from reference 9. For free-stream Mach numbers larger than about 2 a good approximation for the velocity gradient $\left(\frac{dU}{dx}\right)_{SP}$ is obtained by means of a modified Newtonian flow, namely

$$\left(\frac{dU}{dx}\right)_{SP} = \frac{v_0}{R}\left[\frac{2}{\gamma}\left(1 - \frac{p_\infty}{p_{SP}}\right)\right]^{1/2}$$

where v denotes speed of sound and γ is the ratio of specific heats. By using this velocity gradient, h_{SP} may be expressed in terms of free-stream conditions as

$$h_{SP} = \frac{(2\gamma)^{1/4}}{\sqrt{R}}\left(v_0 p_\infty\right)^{1/2}\left(\frac{1}{v}\frac{k}{\sqrt{\mu}}\frac{Nu}{\sqrt{Re}}\right)_w\left(\frac{p_{SP}}{p_\infty}\right)^{1/2}\left(1 - \frac{p_\infty}{p_{SP}}\right)^{1/4}$$

Therefore

$$S = \frac{1}{k_b}(2\gamma)^{1/4}\frac{R^{3/2}}{l\left(1 - \frac{1}{2}\frac{l}{R}\right)^2}\left(v_0 p_\infty\right)^{1/2}\left(\frac{1}{v}\frac{k}{\sqrt{\mu}}\frac{Nu}{\sqrt{Re}}\right)_w\left(\frac{p_{SP}}{p_\infty}\right)^{1/2}\left(1 - \frac{p_\infty}{p_{SP}}\right)^{1/4} \quad (B8)$$

The heat-transfer parameter $\left(\frac{Nu}{\sqrt{Re}}\right)_w$ is given in figure 22; $\frac{p_{SP}}{p_\infty}$ is the Rayleigh pitot pressure ratio.

Hemicylindrical Shell

In appendix A the heat-transfer-coefficient distribution for the hemicylindrical shell was assumed to be of the form

$$h\left(X_R\right) = h_{SL}\cos X_R$$

where X_R is measured in a plane perpendicular to the cylinder axis. This is a good approximation to the actual distribution for values of X_R of less than about 60°, for both yawed and unyawed cylinders.

The heat-transfer coefficient on the stagnation line of a cylinder at a yaw angle Λ may be written

$$h_{SL} = \frac{(2\gamma)^{1/4}}{\sqrt{R}}\left(v_{O,N}p_\infty\right)^{1/2}\left(\frac{1}{v}\frac{k}{\sqrt{\mu}}\frac{Nu}{\sqrt{Re}}\right)_w\left(\frac{p_{SN}}{p_\infty}\right)^{1/2}\left(1 - \frac{p_\infty}{p_{SN}}\right)^{1/4} \qquad (B9)$$

The heat-transfer parameter $\left(\frac{Nu}{\sqrt{Re}}\right)_w$ may be obtained from the solution of reference 3 by Reshotko and Beckwith. At the stagnation line

L
1
2
2
7

$$\left(\frac{Nu}{\sqrt{Re}}\right)_w = \theta'_w(Pr)^{0.46}$$

where θ'_w is the solution mentioned, and is presented in figure 23, reproduced from reference 3.

In equation (B9) the subscript N indicates that the quantity is derived from the normal component of the free-stream Mach number $M_N = M_\infty \cos \Lambda$. Accordingly

$$v_{O,N} = v_\infty\left(1 + \frac{\gamma - 1}{2} M_N^2\right)^{1/2}$$

and $\frac{p_{SN}}{p_\infty}$ is the pitot pressure ratio in a plane perpendicular to the cylinder axis.

Equation (B9) was obtained by use of a modified Newtonian velocity gradient at the stagnation line, which applies only for $M_N > 1.5$. For the velocity gradient at $M_N < 1.5$ see figure 9 of reference 3.

REFERENCES

1. Trimpi, Robert L., and Jones, Robert A.: Transient Temperature Distribution in a Two-Component Semi-Infinite Composite Slab of Arbitrary Materials Subjected to Aerodynamic Heating With a Discontinuous Change in Equilibrium Temperature or Heat-Transfer Coefficient. NACA TN 4308, 1958.

2. Cooper, Morton, and Mayo, Edward E.: Normal Conduction Effects on Heat-Transfer Data During Transient Heating of Thin-Skin Models. Jour. Aero. Sci. (Readers' Forum), vol. 24, no. 6, June 1957, pp. 461-462.

3. Reshotko, Eli, and Beckwith, Ivan E.: Compressible Laminar Boundary Layer Over a Yawed Infinite Cylinder With Heat Transfer and Arbitrary Prandtl Number. NACA Rep. 1379, 1958. (Supersedes NACA TN 3986.)

4. Parker, Hermon M.: Transient Temperature Distributions in Simple Conducting Bodies Steadily Heated Through a Laminar Boundary Layer. NACA TN 3058, 1953.

5. Bryson, A. E., Budiansky, Bernard, and Carrier, George F.: Leading-Edge Temperature of a Flat Plate Subjected to Aerodynamic Heating. Jour. Aero. Sci. (Readers' Forum), vol. 24, no. 4, Apr. 1957, pp. 311-312.

6. Van Driest, E. R.: Investigation of Laminar Boundary Layer in Compressible Fluids Using the Crocco Method. NACA TN 2597, 1952.

7. Sommer, Simon C., and Short, Barbara J.: Free-Flight Measurements of Turbulent-Boundary-Layer Skin Friction in the Presence of Severe Aerodynamic Heating at Mach Numbers From 2.8 to 7.0. NACA TN 3391, 1955.

8. Van Driest, E. R.: Turbulent Boundary Layer on a Cone in a Supersonic Flow at Zero Angle of Attack. Jour. Aero. Sci., vol. 19, no. 1, Jan. 1952, pp. 55-57, 72.

9. Reshotko, Eli, and Cohen, Clarence B.: Heat Transfer at the Forward Stagnation Point of Blunt Bodies. NACA TN 3513, 1955.

TABLE I.- DEFINITIONS OF VARIABLES AND INPUT PARAMETERS

Body	Boundary layer	Input parameter		Nondimensional variables
		Symbol	Definition	
Flat plate	Laminar	F_L	$\frac{l}{k_b}\left[h\left(X_l\right)\sqrt{X_l}\right]$ or $\frac{\sqrt{l}}{k_b}\left[h(x)\sqrt{x}\right]$	$X_l = \frac{x}{l}$ $\tau_l = \frac{\alpha}{l^2}t$
	Turbulent	F_T	$\frac{l}{k_b}\left[h\left(X_l\right)X_l^{1/5}\right]$ or $\frac{l^{4/5}}{k_b}\left[h(x)x^{1/5}\right]$	
Wedge	Laminar	W_L	$\frac{\sqrt{\alpha}}{k_b}\left[h\left(X_\alpha\right)\sqrt{X_\alpha}\right]$ or $\frac{\alpha^{1/4}}{k_b}\left[h(x)\sqrt{x}\right]$	$X_\alpha = \frac{x}{\sqrt{\alpha}}$ $\tau_\alpha = t$
	Turbulent	W_T	$\frac{\sqrt{\alpha}}{k_b}\left[h\left(X_\alpha\right)X_\alpha^{1/5}\right]$ or $\frac{\alpha^{2/5}}{k_b}\left[h(x)x^{1/5}\right]$	
Conical shell	Laminar	C_L	$\frac{l}{k_b}\left[h\left(X_l\right)\sqrt{X_l}\right]$ or $\frac{\sqrt{l}}{k_b}\left[h(x)\sqrt{x}\right]$	$X_l = \frac{x}{l}$ $\tau_l = \frac{\alpha}{l^2}t$
	Turbulent	C_T	$\frac{l}{k_b}\left[h\left(X_l\right)X_l^{1/5}\right]$ or $\frac{l^{4/5}}{k_b}\left[h(x)x^{1/5}\right]$	
Hemispherical shell	Laminar	S	$\frac{1}{k_b}\frac{R^2}{l\left(1-\frac{1}{2}\frac{l}{R}\right)^2}h_{SP}$	$X_R = \frac{x}{R}$ $\tau_R = \frac{\alpha}{R^2}t$
Hemicylindrical shell	Laminar	C_Y	$\frac{1}{k_b}\frac{R^2}{l\left(1-\frac{1}{2}\frac{l}{R}\right)}h_{SL}$	

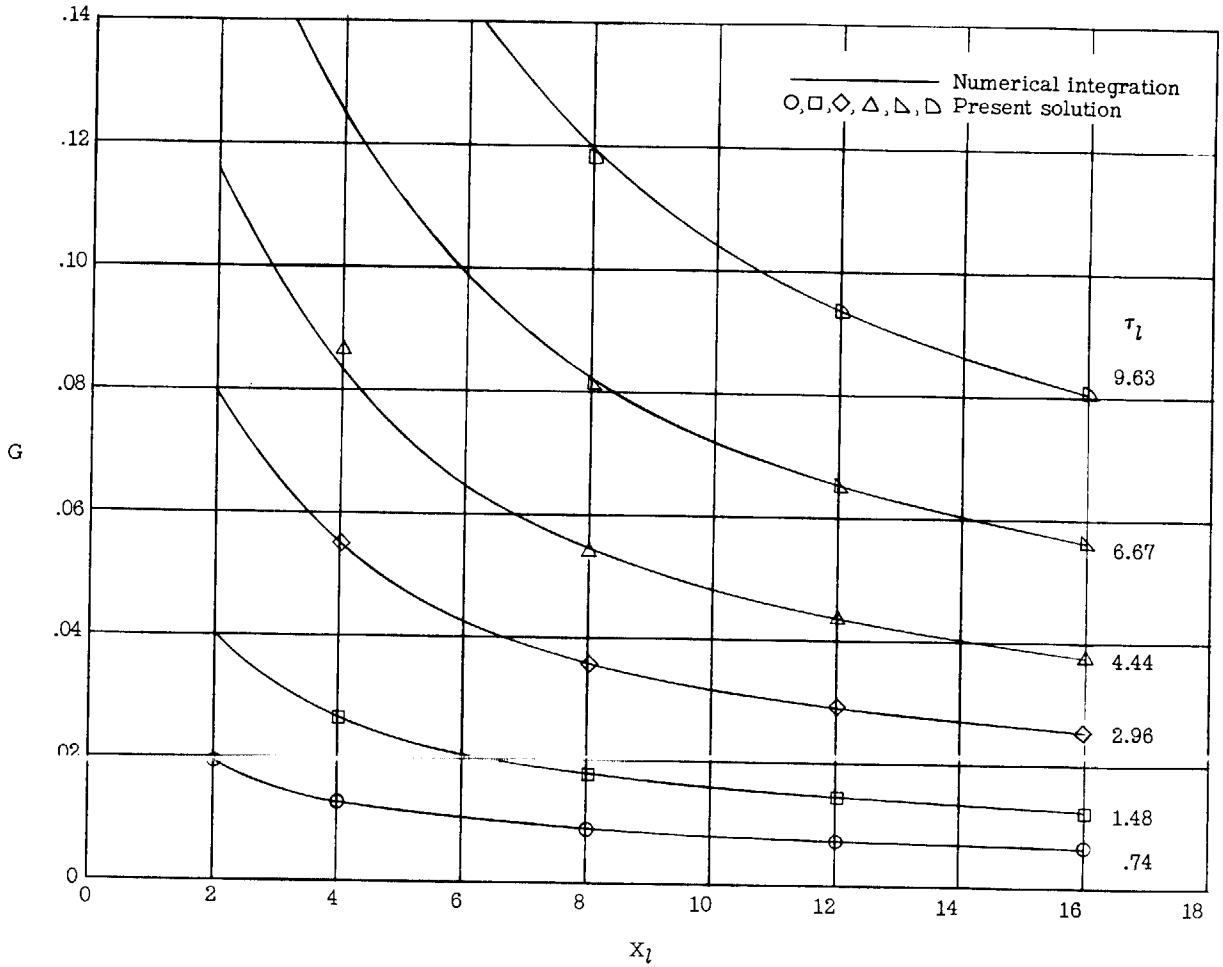

(a) Temperature distribution.

Figure 1.- Comparison of numerical integration with present solution for flat plate with laminar boundary layer. $F_L = 0.0343$.

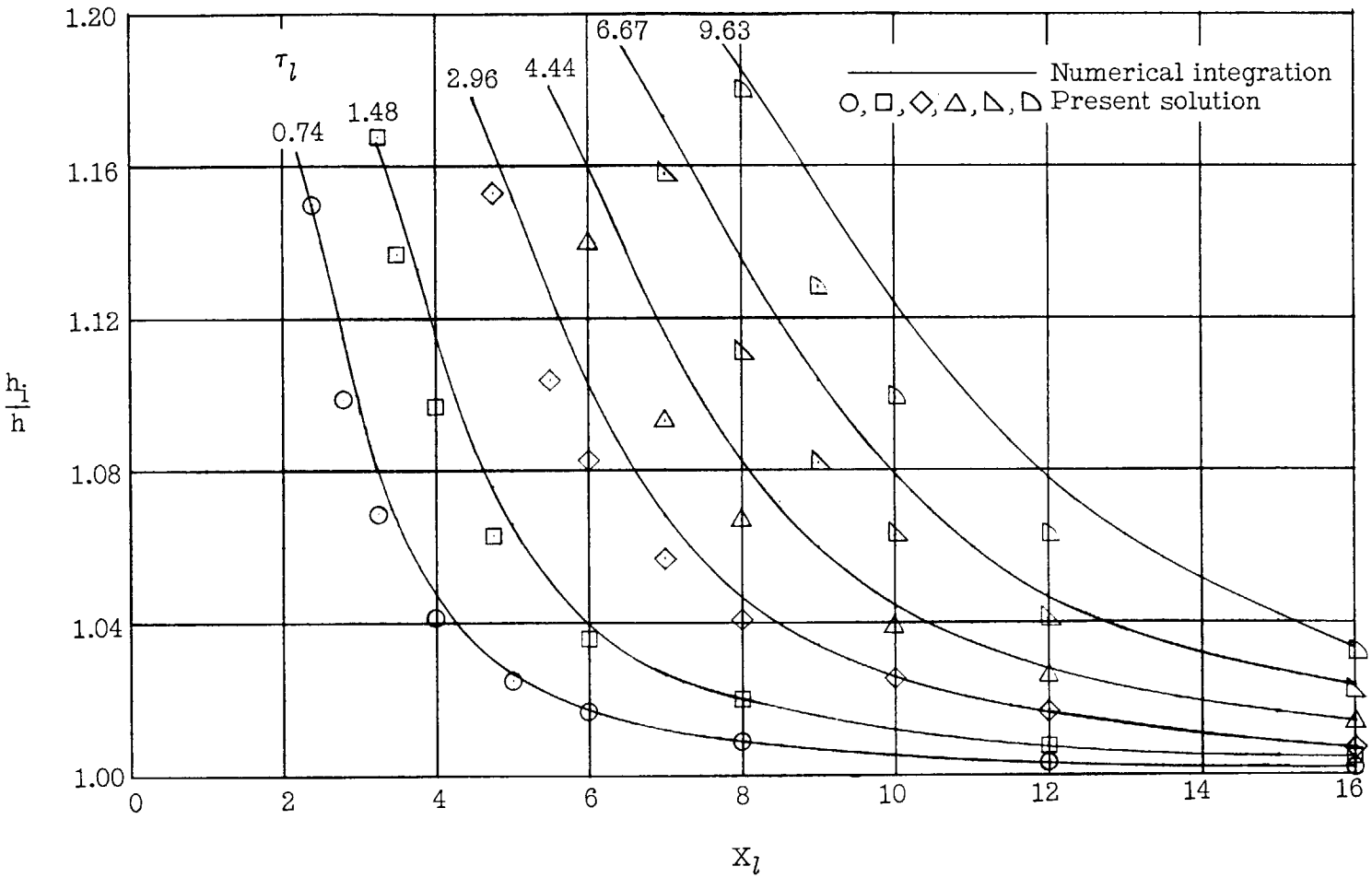

(b) Error distribution.

Figure 1.- Concluded.

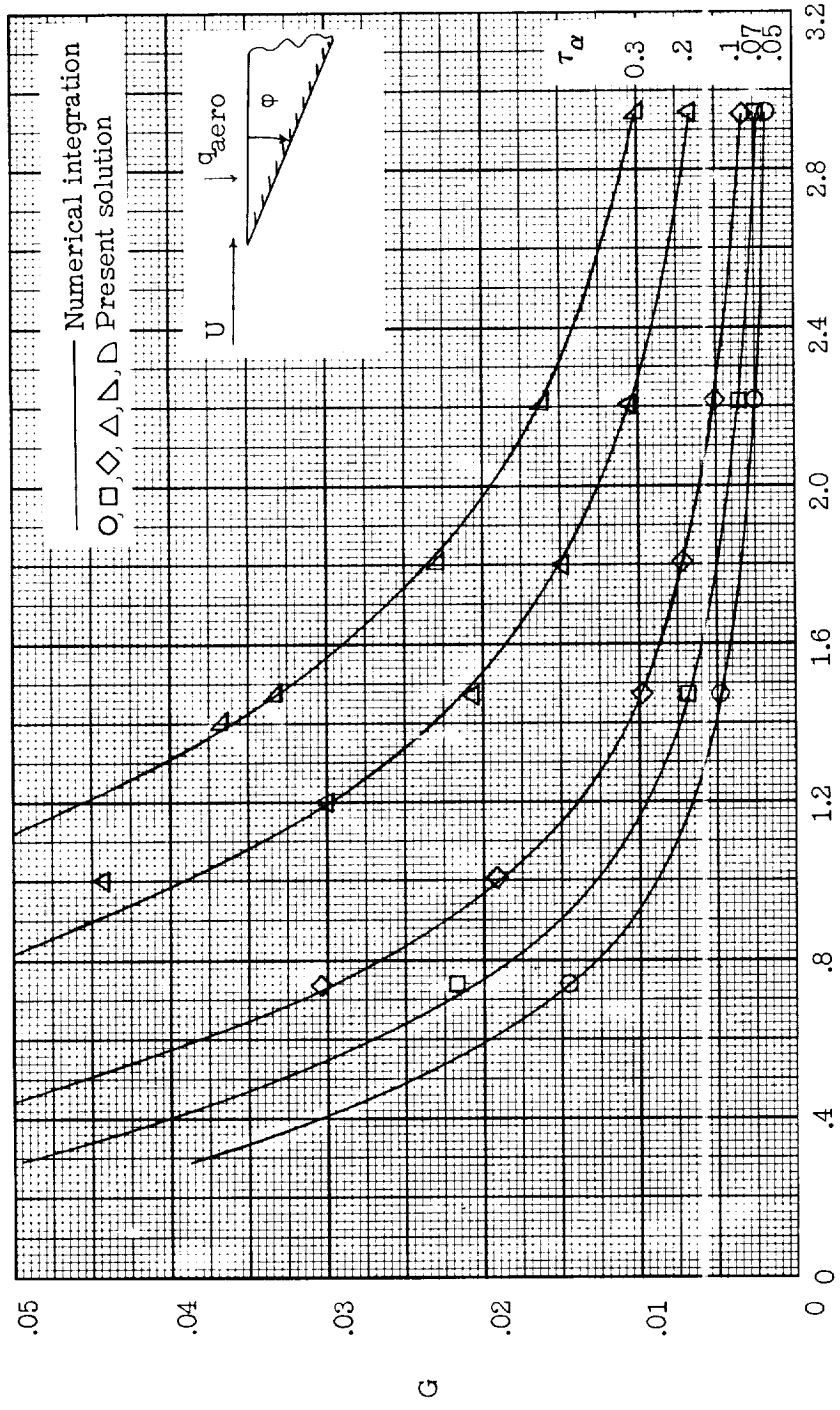

(a) Temperature distribution.

Figure 2.- Comparison of numerical integration with present solution for wedge with laminar boundary layer. $\frac{W_L}{\tan \varphi} = 0.1624$.

L-1227

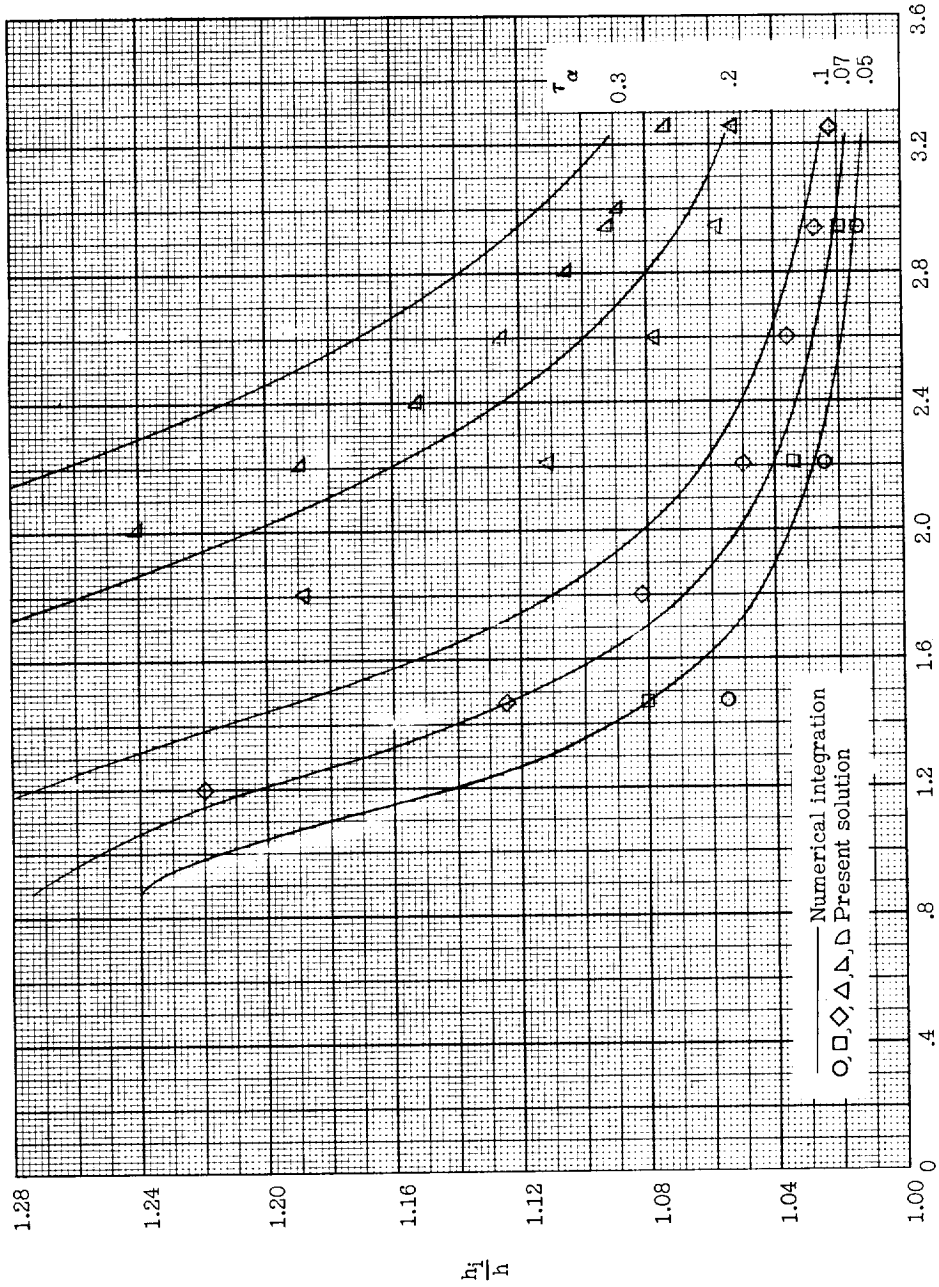

(b) Error distribution.

Figure 2.- Concluded.

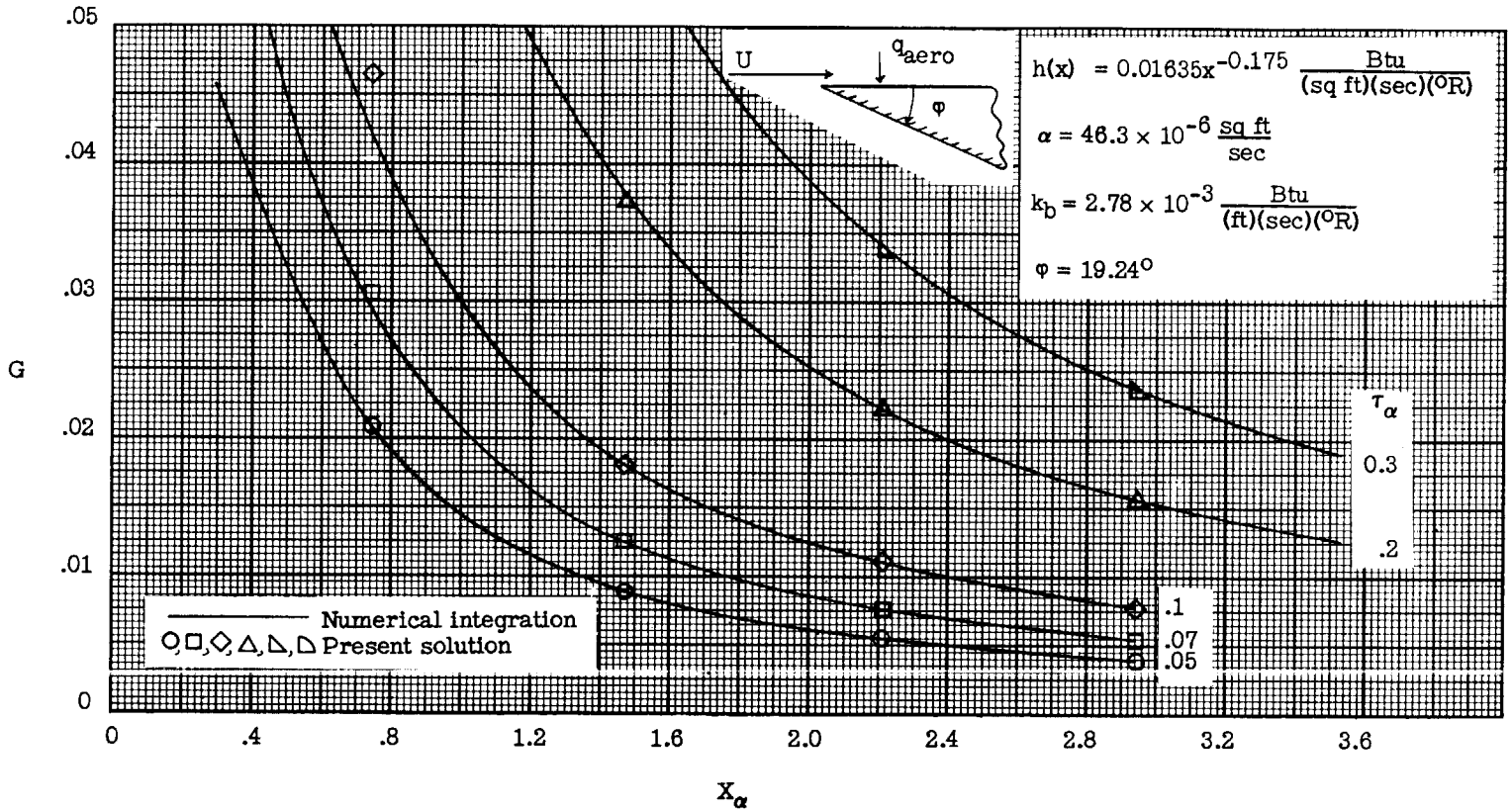

(a) Temperature distribution.

Figure 3.- Comparison of numerical integration with present solution for wedge with turbulent boundary layer.

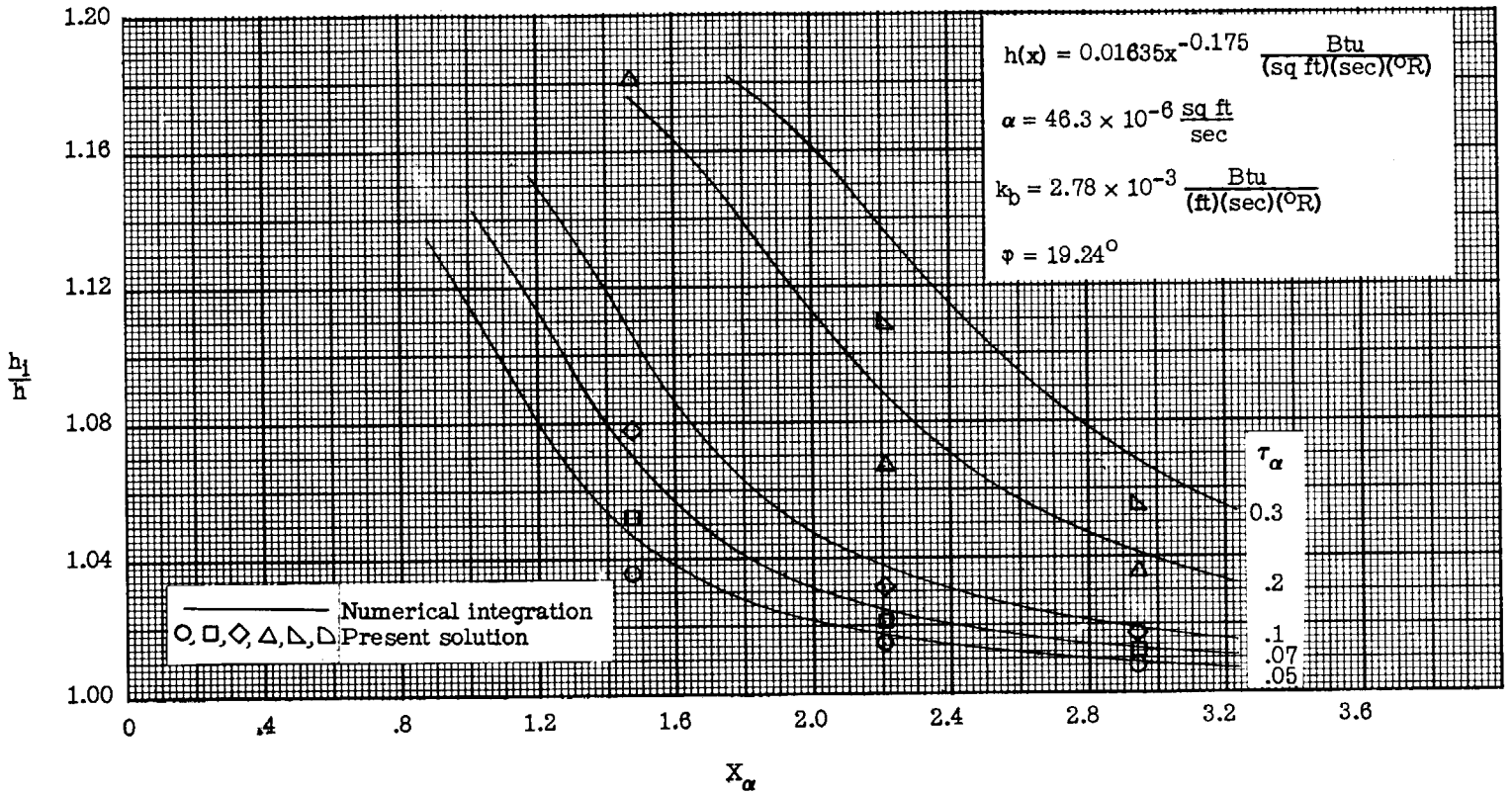

(b) Error distribution.

Figure 3.- Concluded.

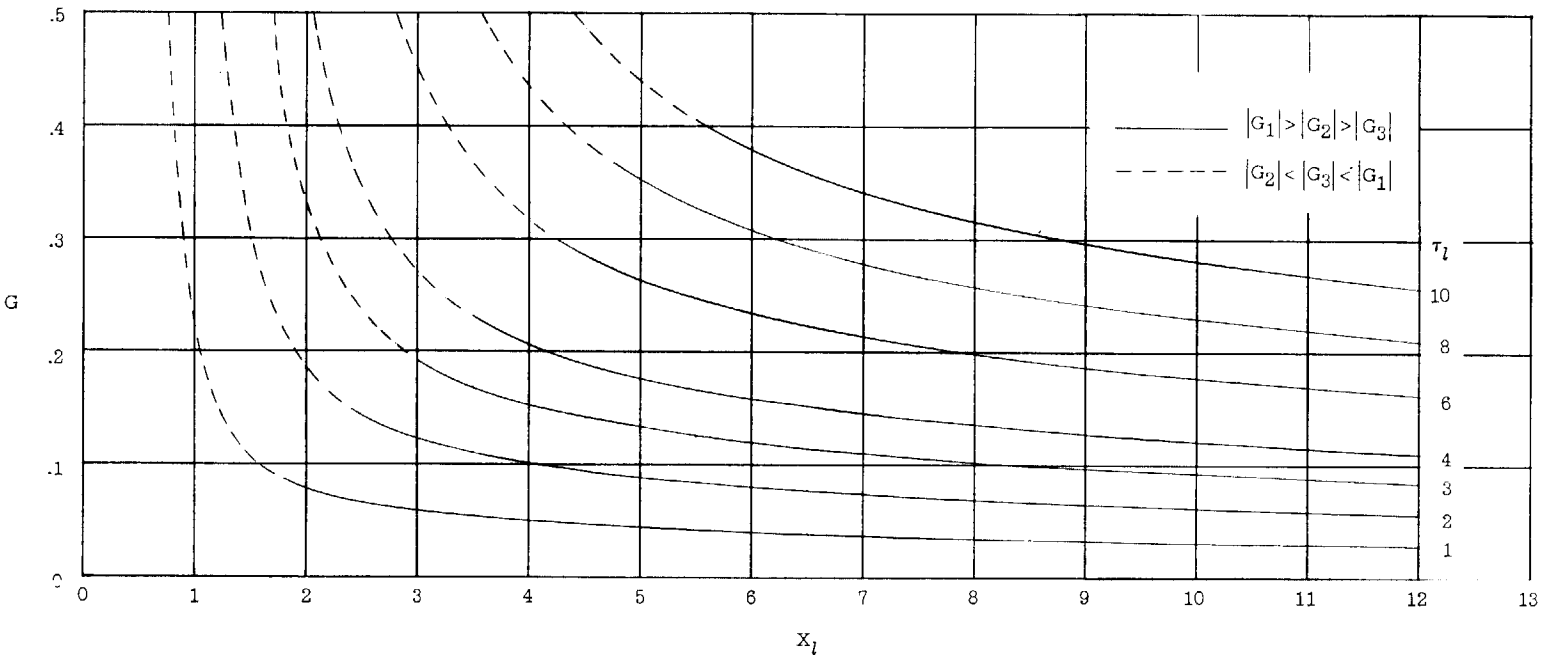

(a) Temperature distribution.

Figure 4.- Typical temperature and error distributions for flat plate of constant thickness with laminar boundary layer. $F_L = 0.1$.

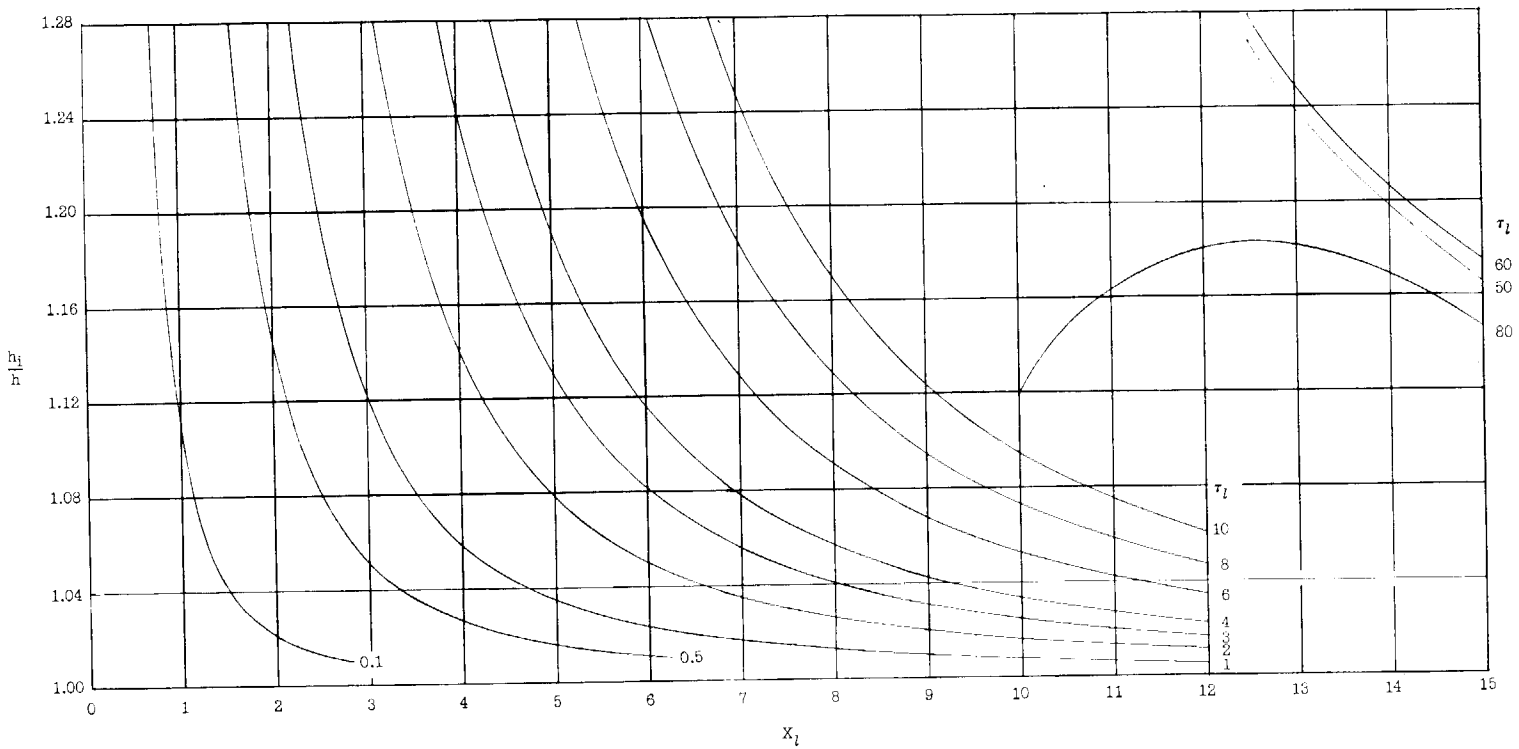

(b) Error distribution.

Figure 4.- Concluded.

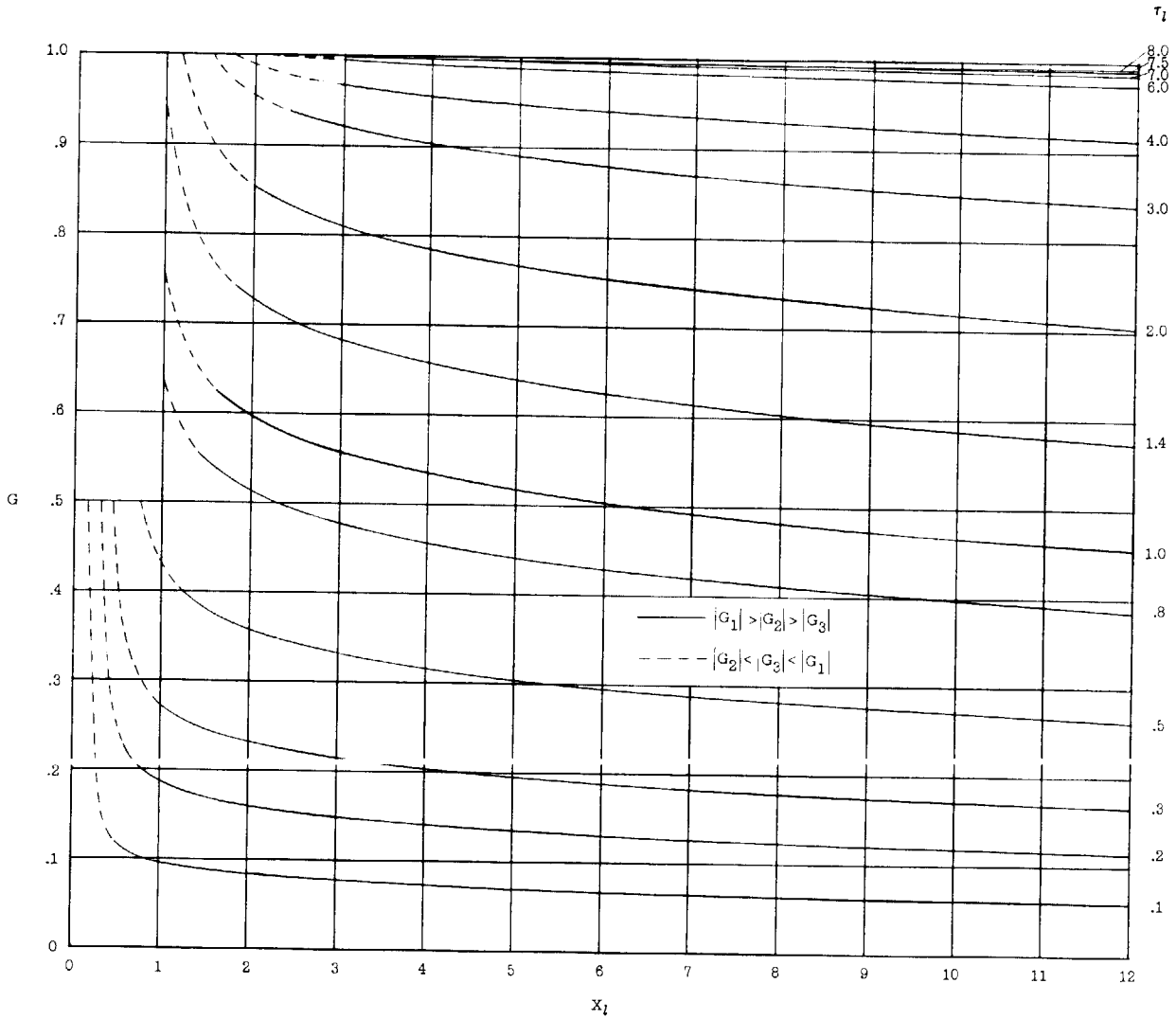

(a) Temperature distribution.

Figure 5.- Typical temperature and error distributions for flat plate of constant thickness with turbulent boundary layer. $F_T = 1.0$.

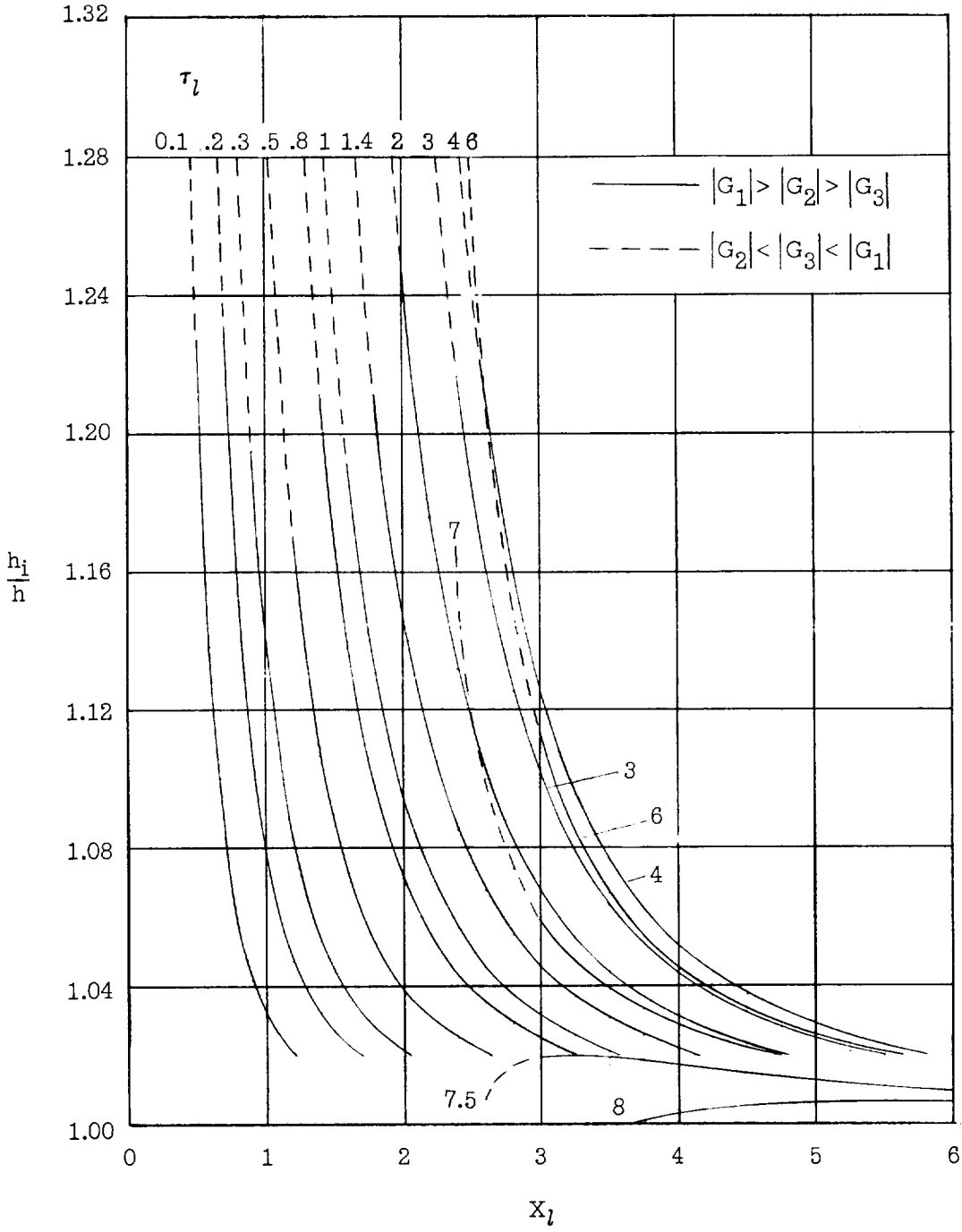

(b) Error distribution.

Figure 5.- Concluded.

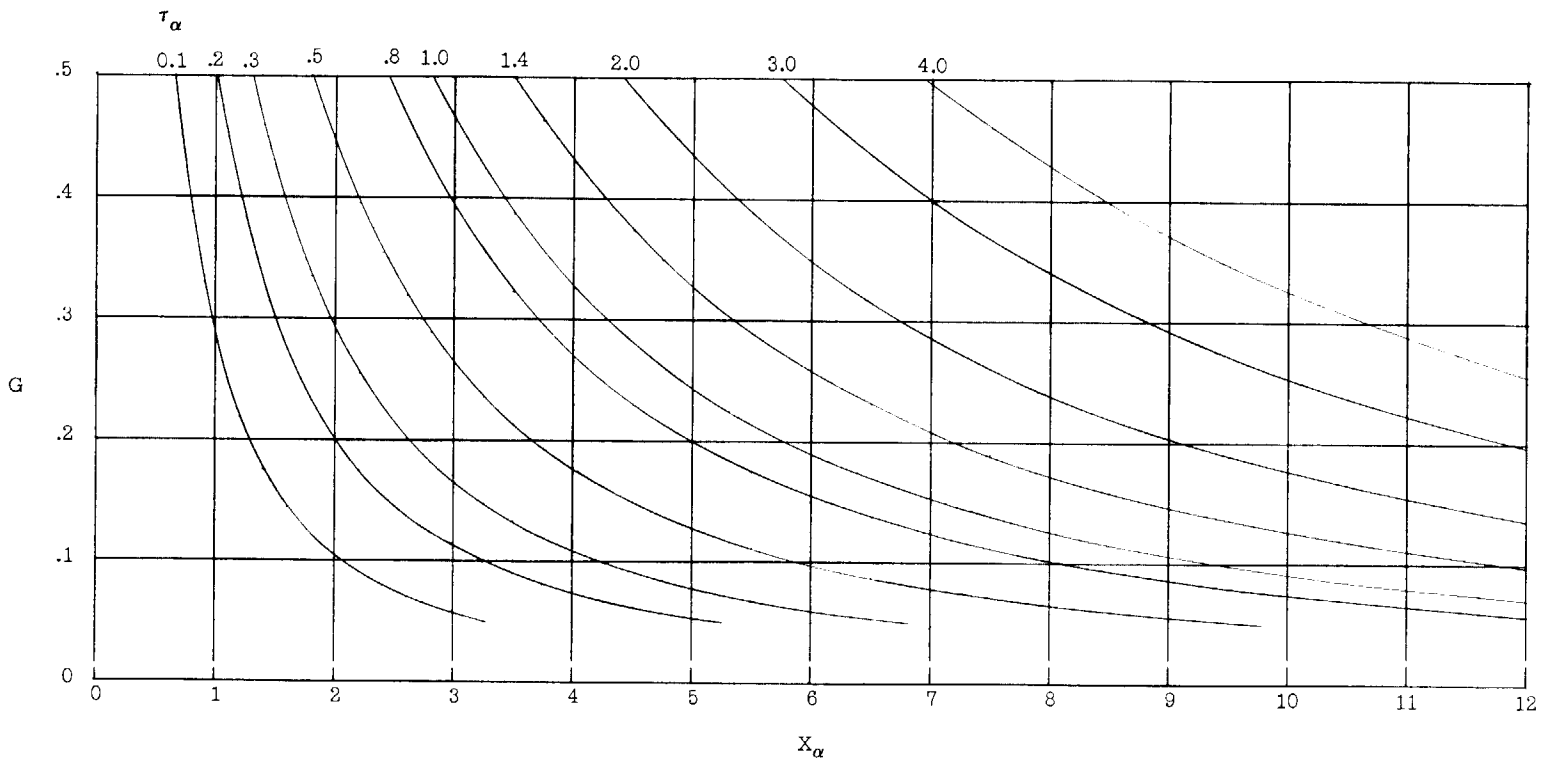

(a) Temperature distribution.

Figure 6.- Typical temperature and error distributions for wedge with laminar boundary layer. $\frac{W_L}{\tan \varphi} = 3.0$.

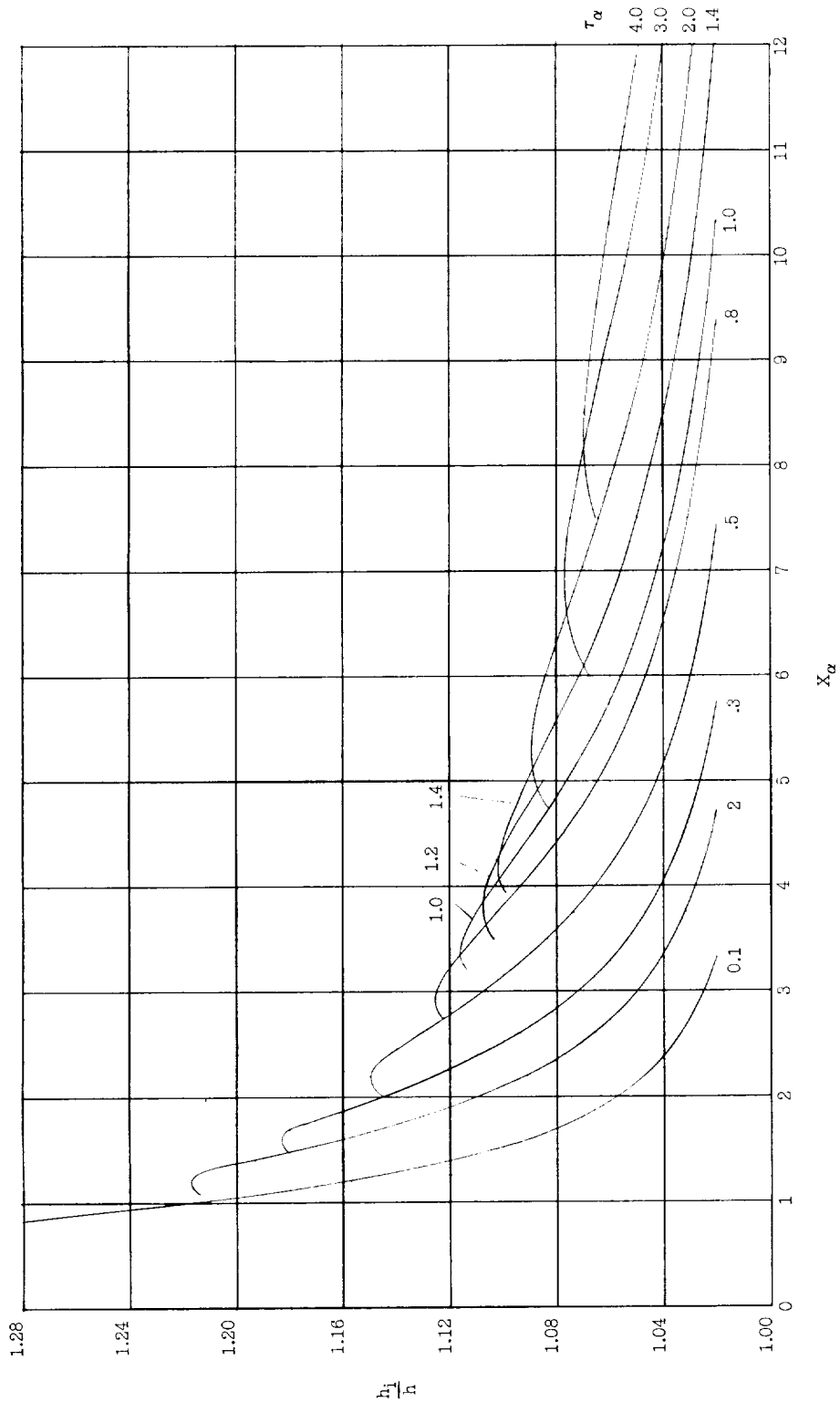

(b) Error distribution.

Figure 6.- Concluded.

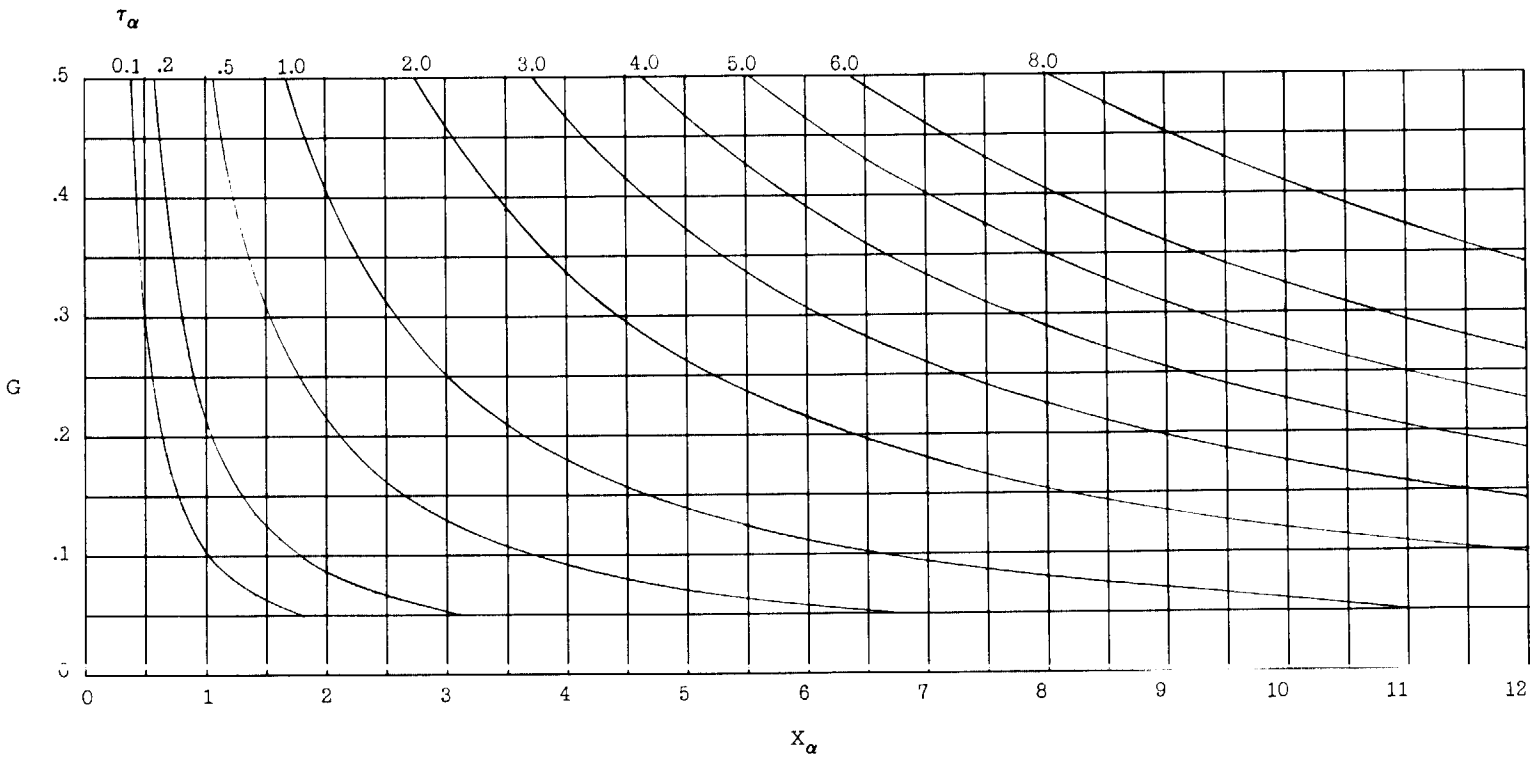

(a) Temperature distribution.

Figure 7.- Typical temperature and error distributions for wedge with turbulent boundary layer.

$$\frac{W_T}{\tan \varphi} = 1.0.$$

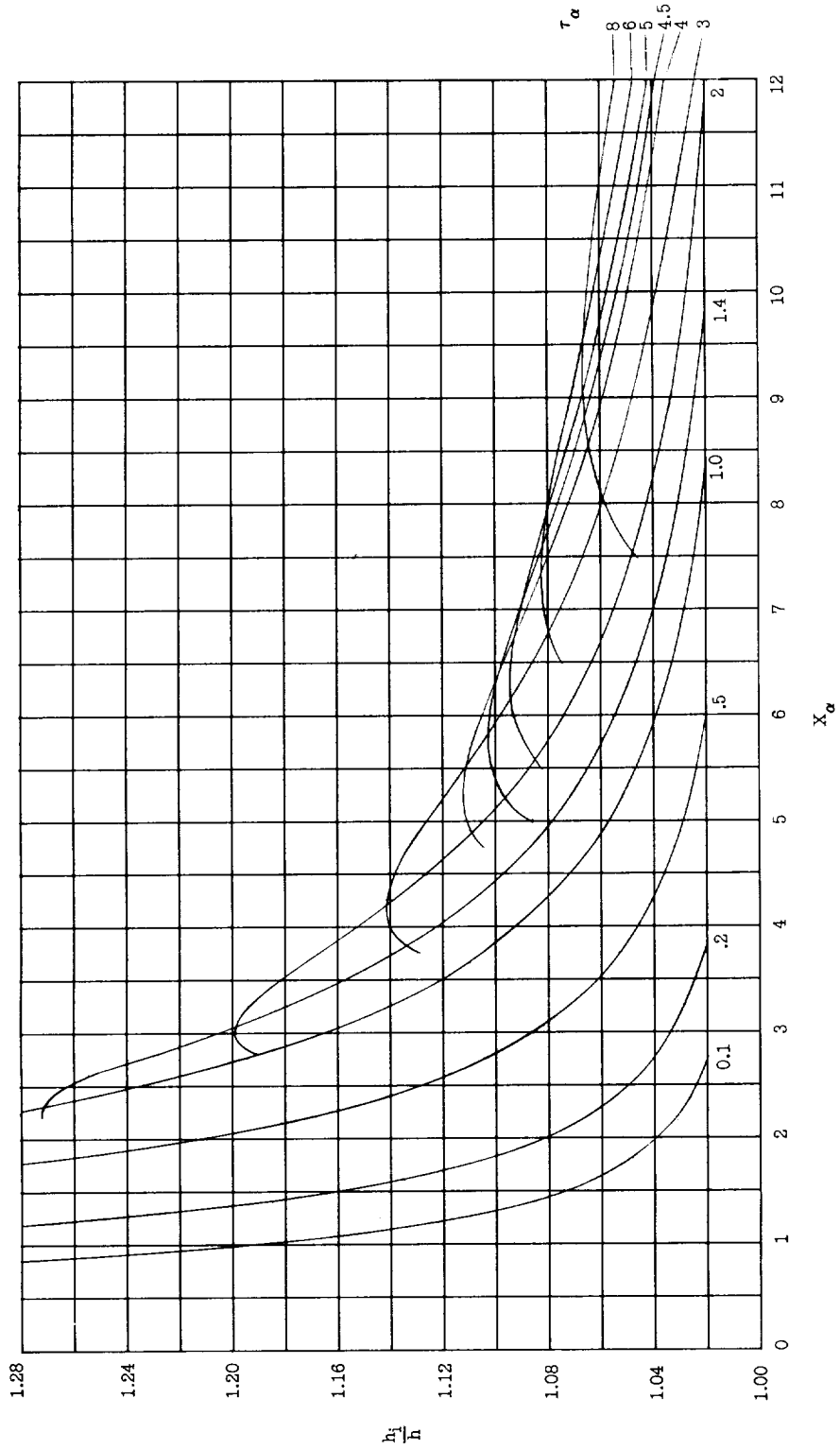

(b) Error distribution.

Figure 7.- Concluded.

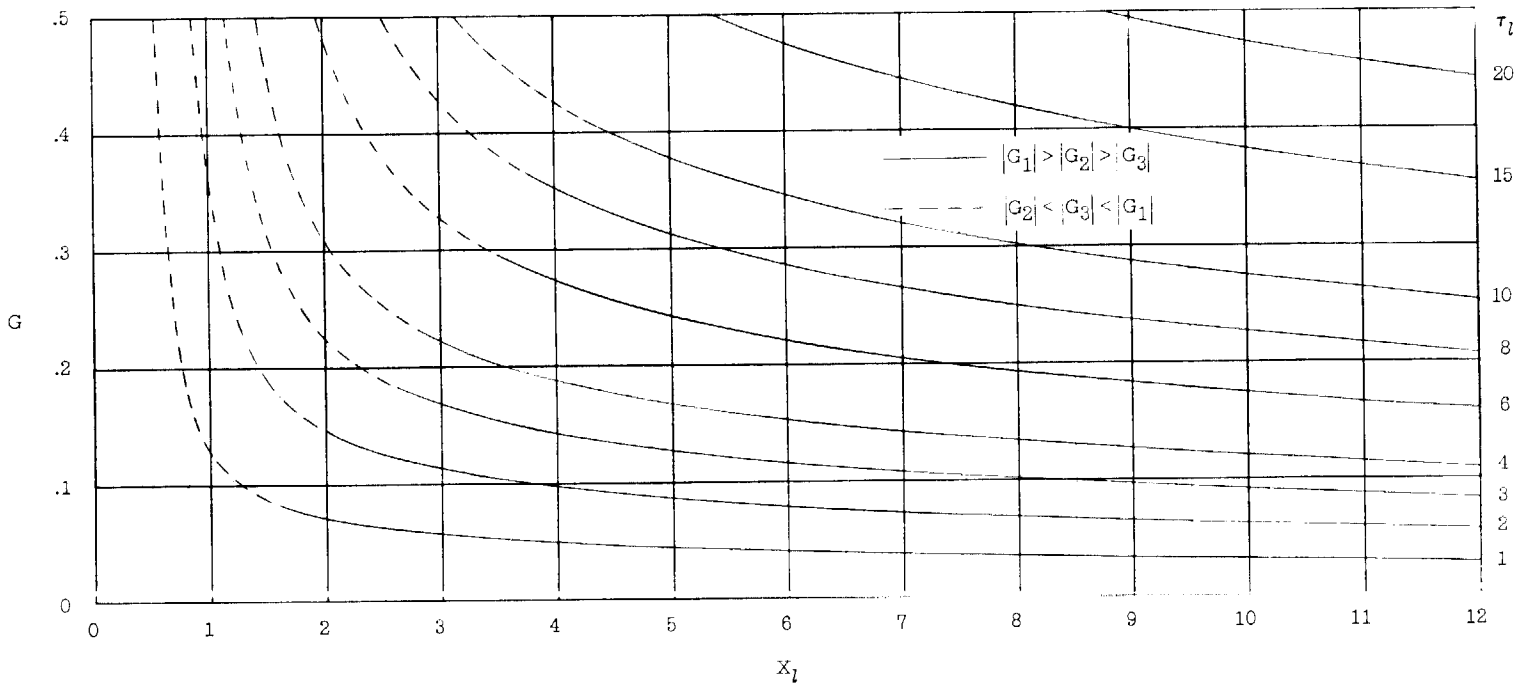

(a) Temperature distribution.

Figure 8.- Typical temperature and error distributions for conical shell of constant thickness with laminar boundary layer. $C_L = 0.1$.

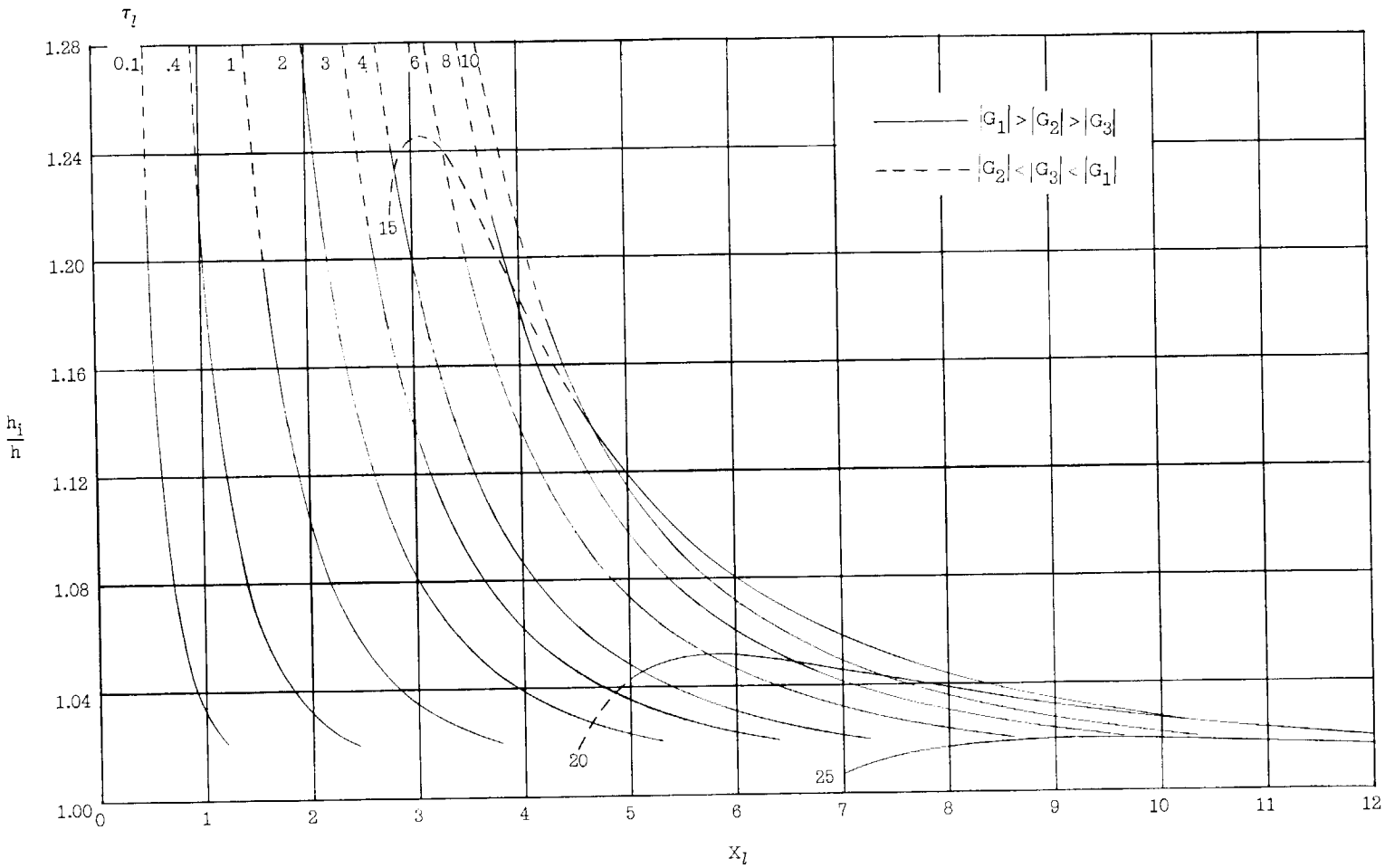

(b) Error distribution

Figure 8.- Concluded.

(a) Temperature distribution.

Figure 9.- Typical temperature and error distributions for conical shell of constant thickness with turbulent boundary layer. $C_T = 0.01$.

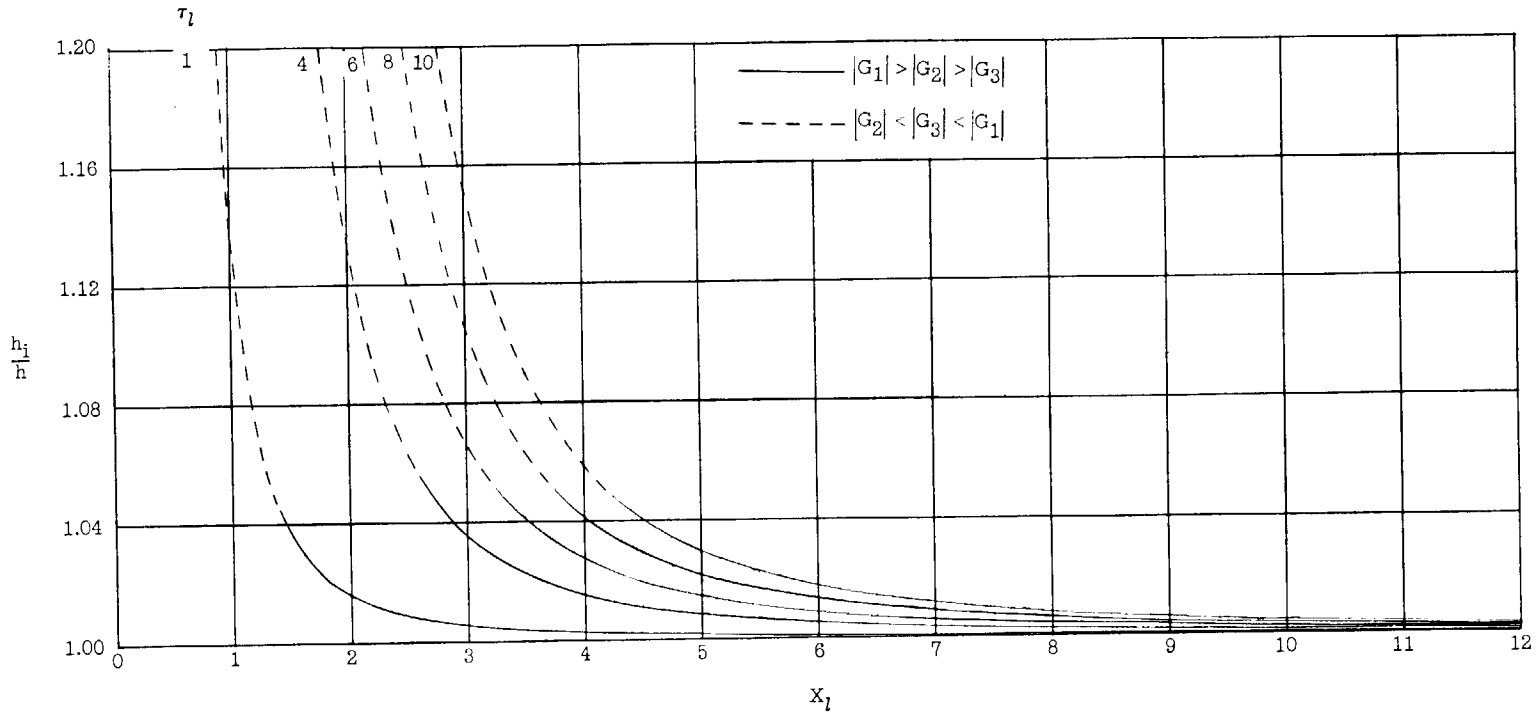

(b) Error distribution.

Figure 9.- Concluded.

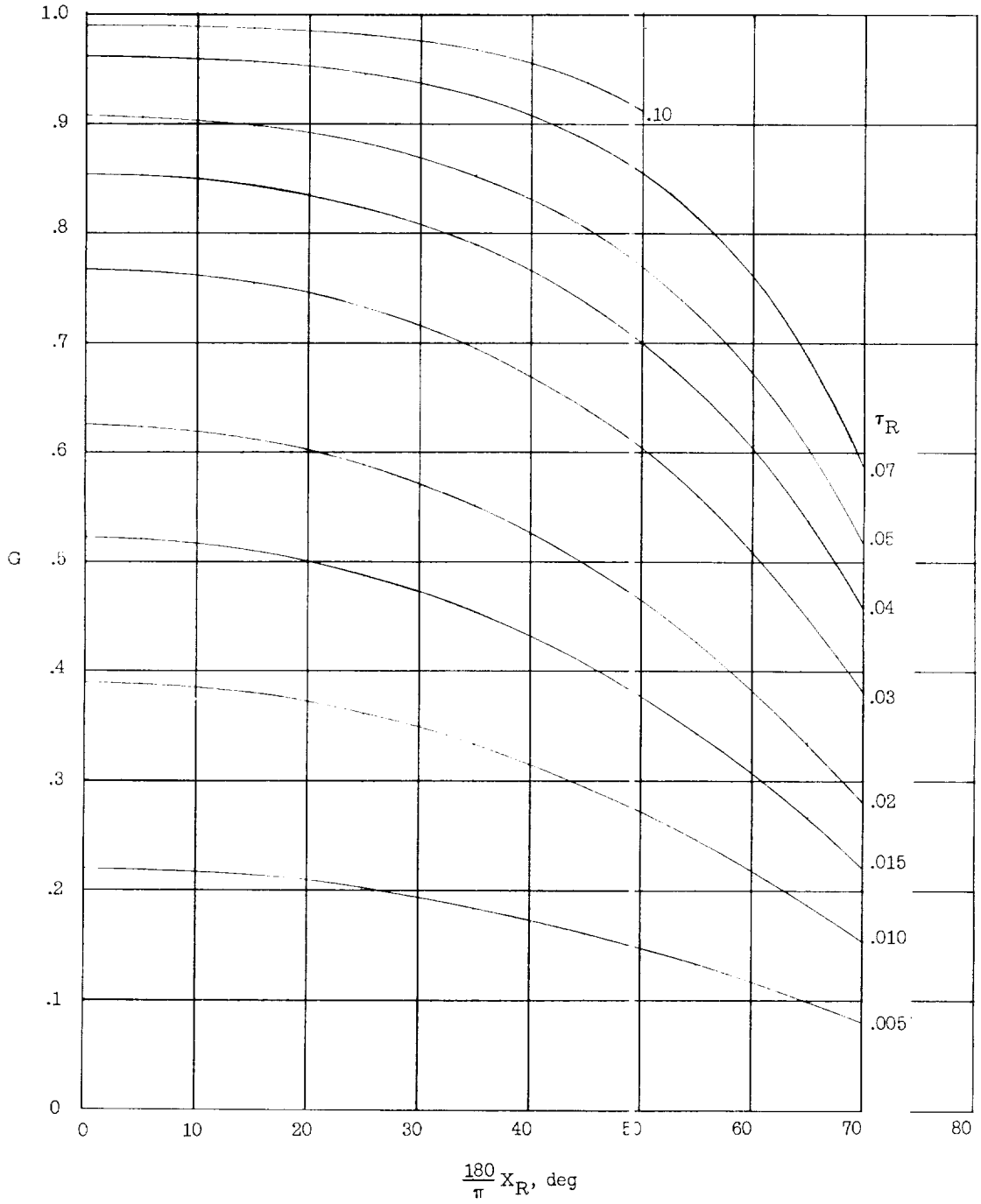

(a) Temperature distribution.

Figure 10.- Typical temperature and error distributions for hemispherical shell of constant thickness with laminar boundary layer. S = 50.

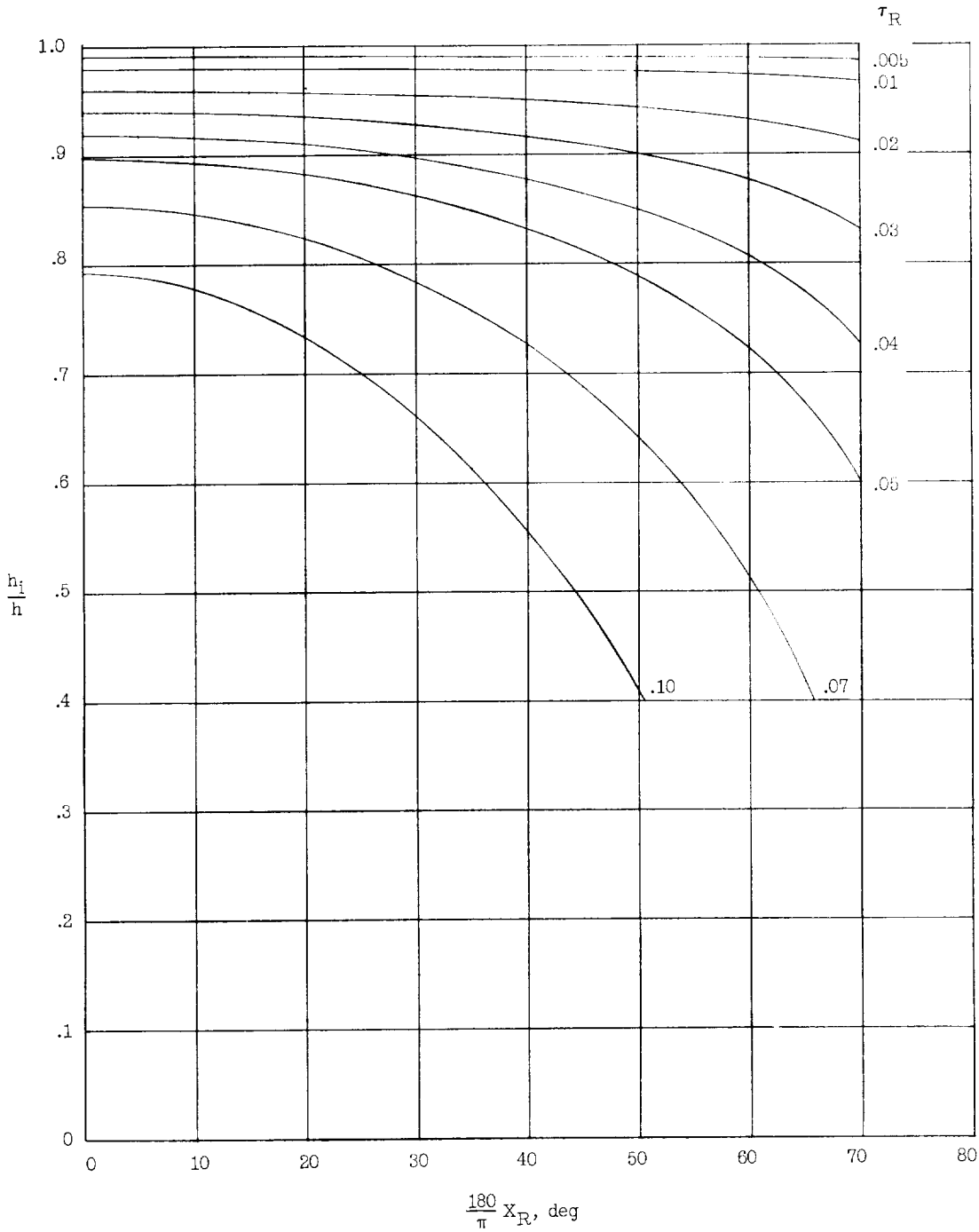

(b) Error distribution.

Figure 10.- Concluded.

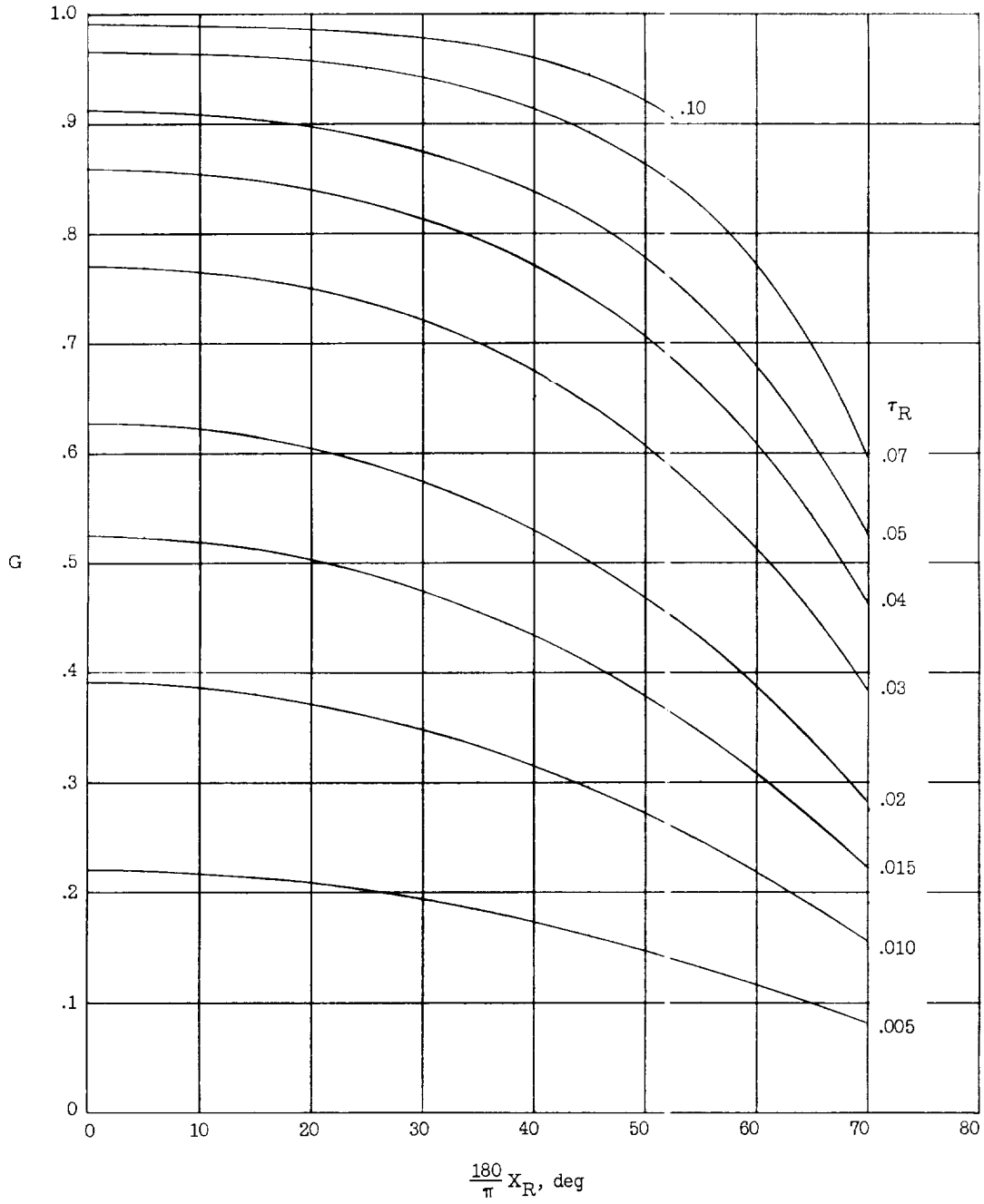

(a) Temperature distribution.

Figure 11.- Typical temperature and error distributions for hemicylindrical shell of constant thickness with laminar boundary layer. $C_Y = 50$.

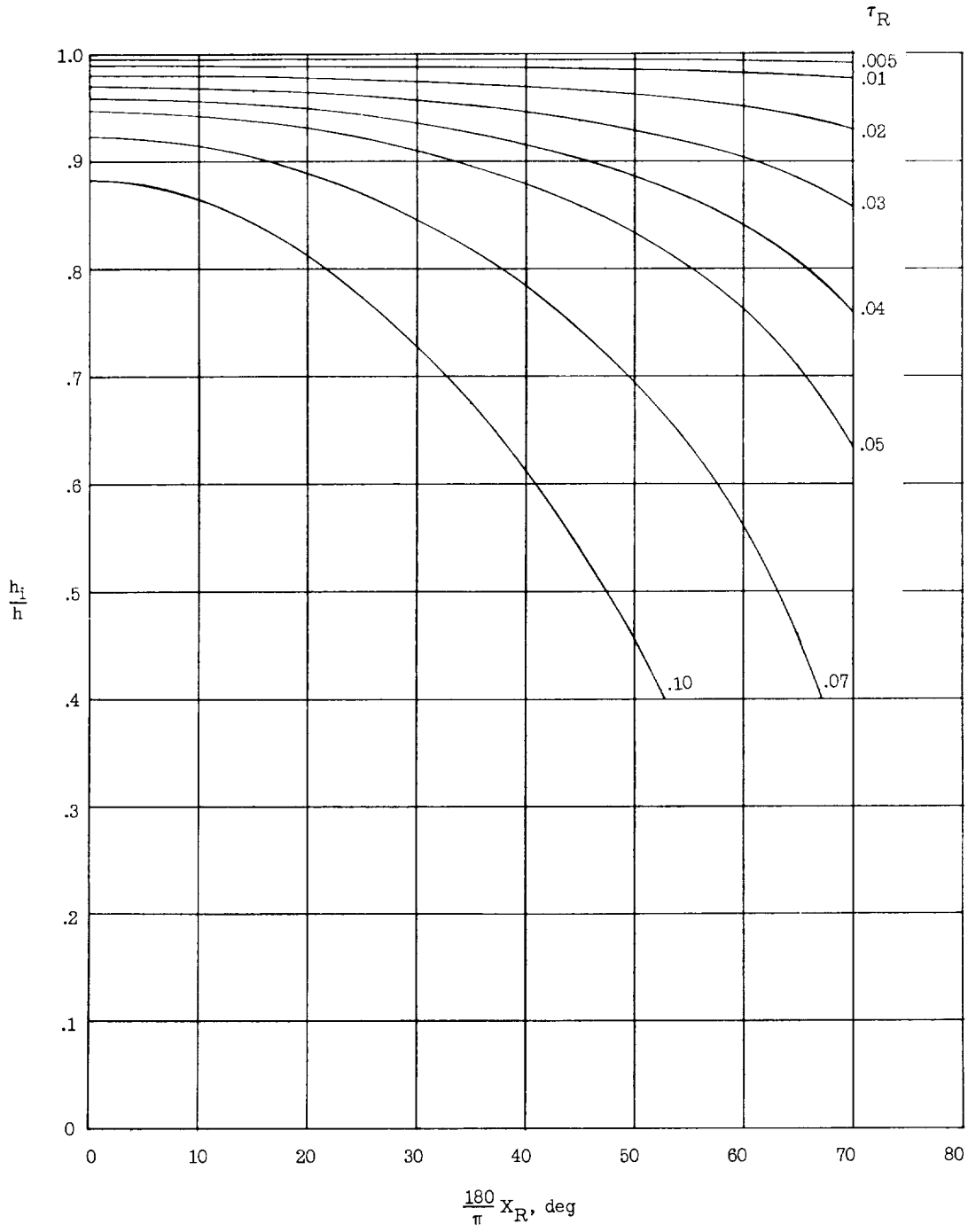

(b) Error distribution.

Figure 11.- Concluded.

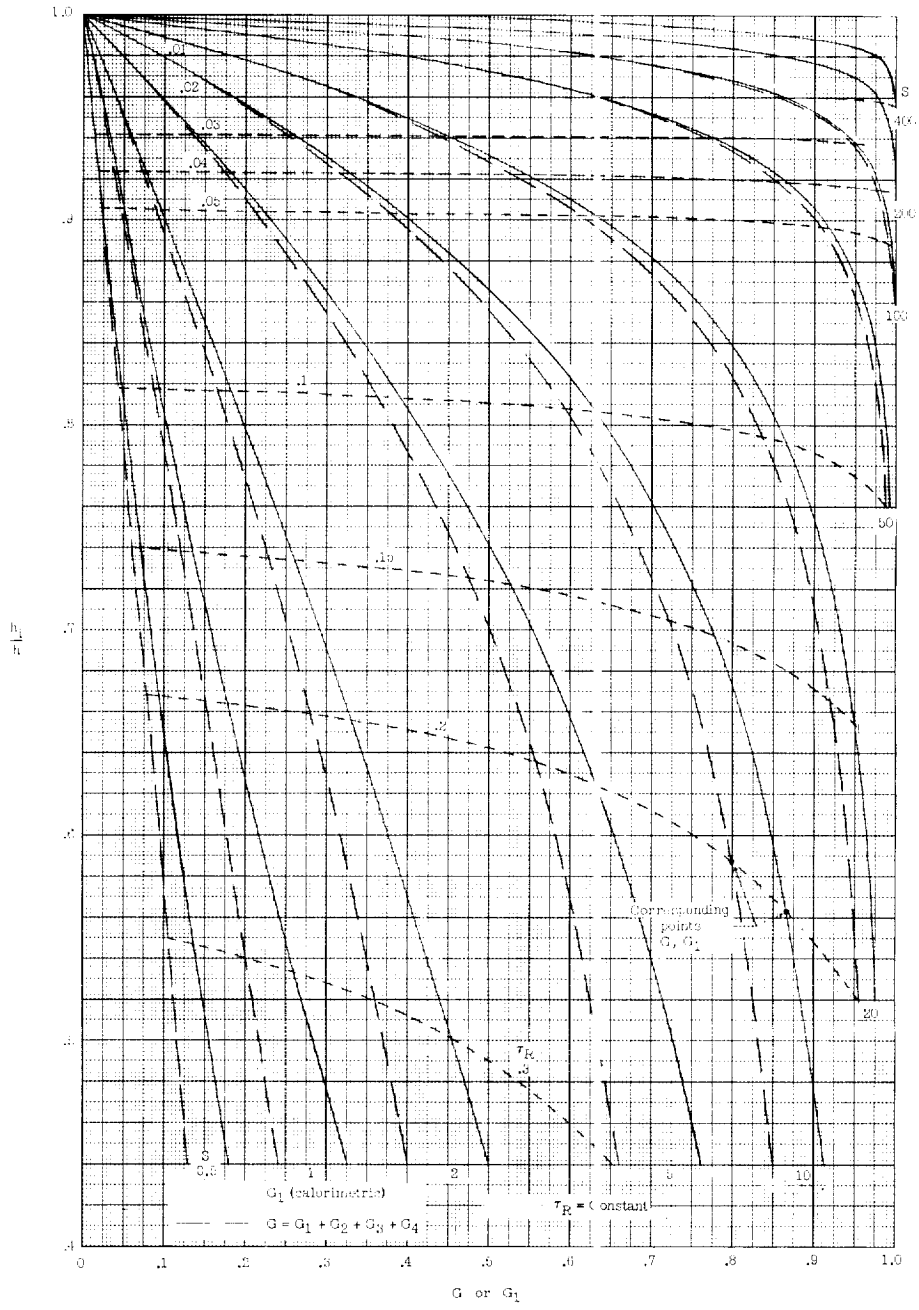

Figure 12.- Conduction error at stagnation point for hemispherical shell of constant thickness. The $\frac{h_i}{h}$ scale applies to broken lines (G and τ_R). To find corresponding G_1 proceed along τ_R curves to intersection with solid line.

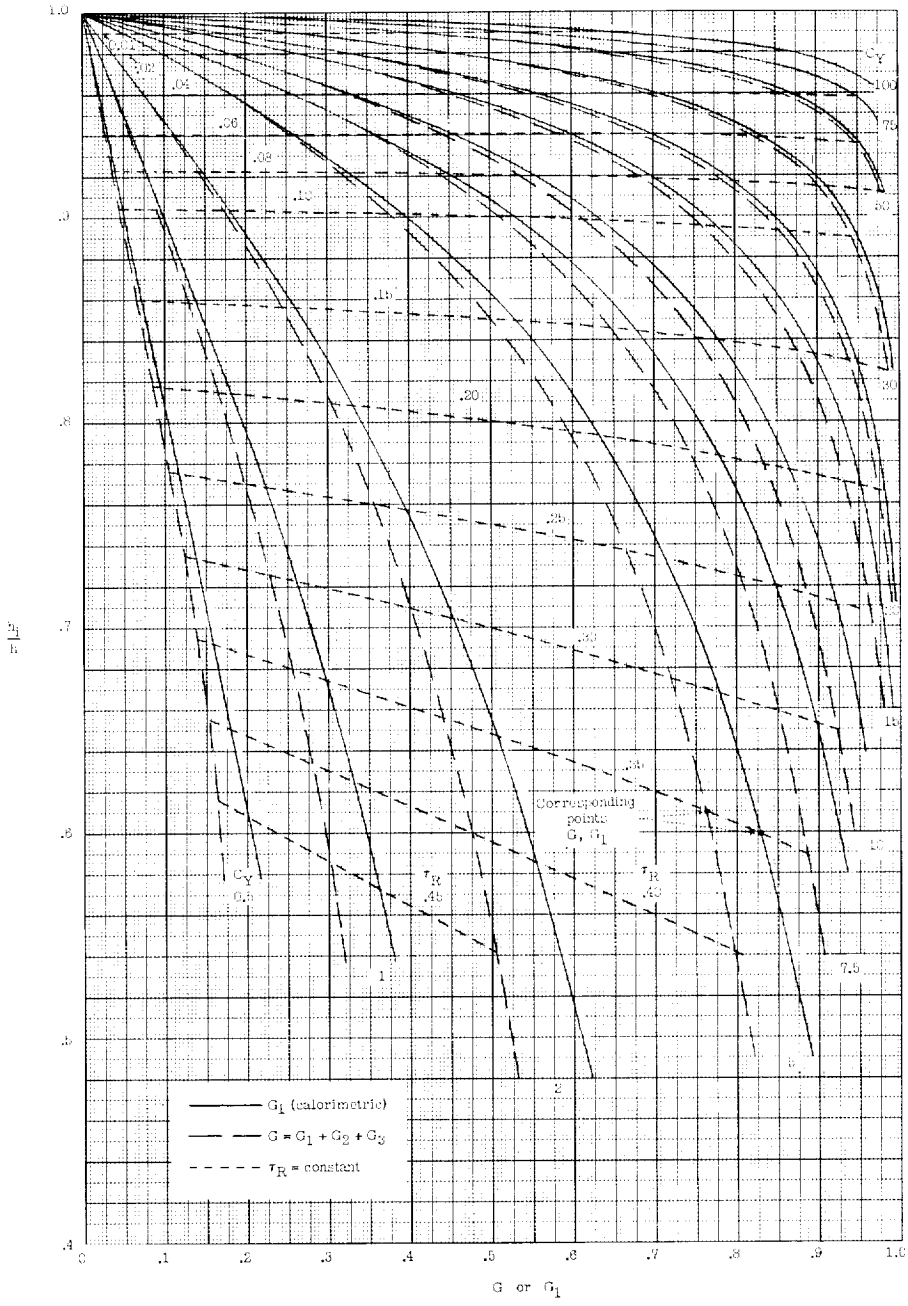

Figure 13.- Conduction error at stagnation point for hemicylindrical shell of constant thickness. The $\frac{h_i}{h}$ scale applies to broken lines (G and τ_R). To find corresponding G_1 proceed along τ_R curves to intersection with solid lines.

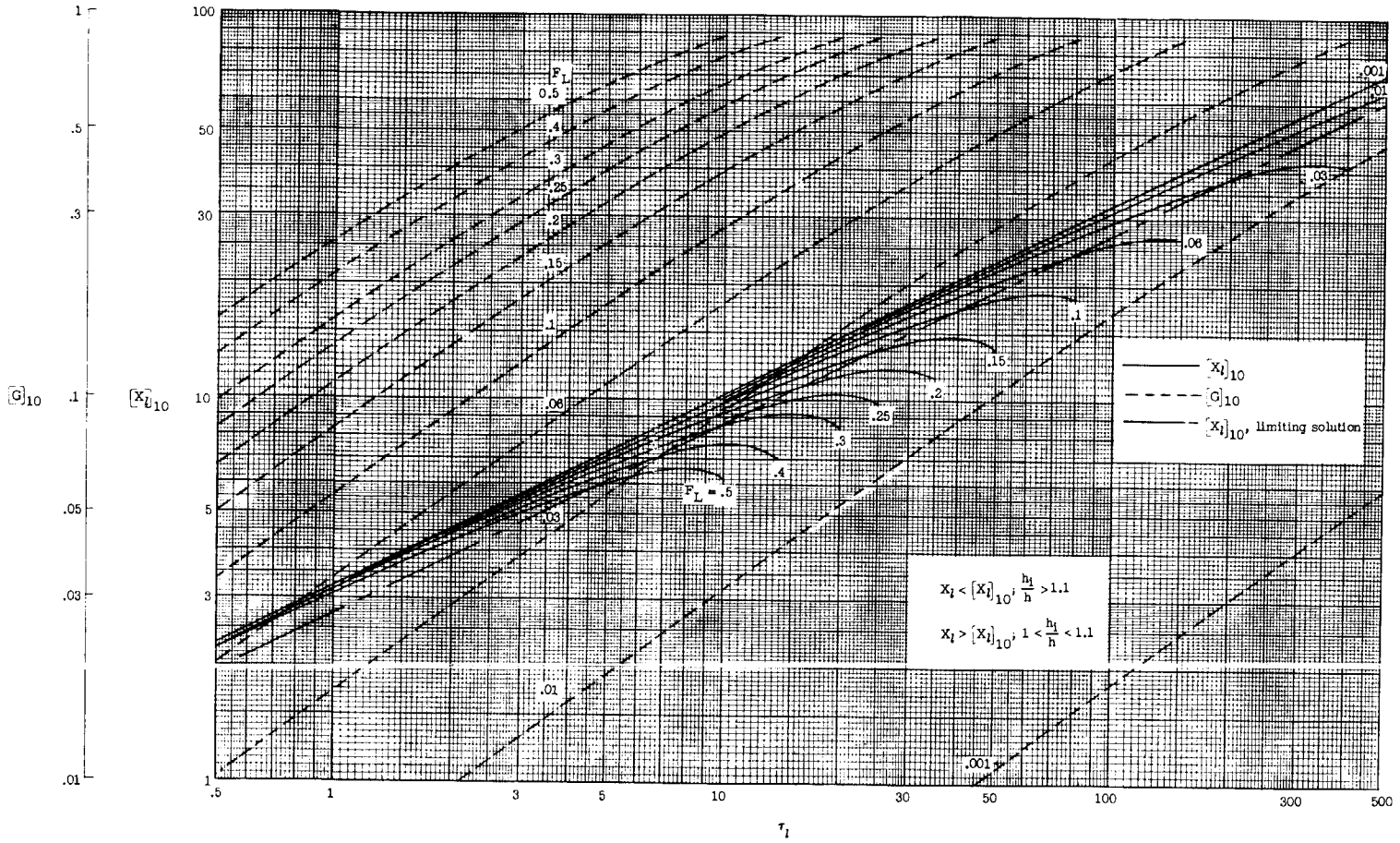

(a) Laminar boundary layer.

Figure 14.- Location and temperature of point having 10-percent conduction error for flat plate of constant thickness.

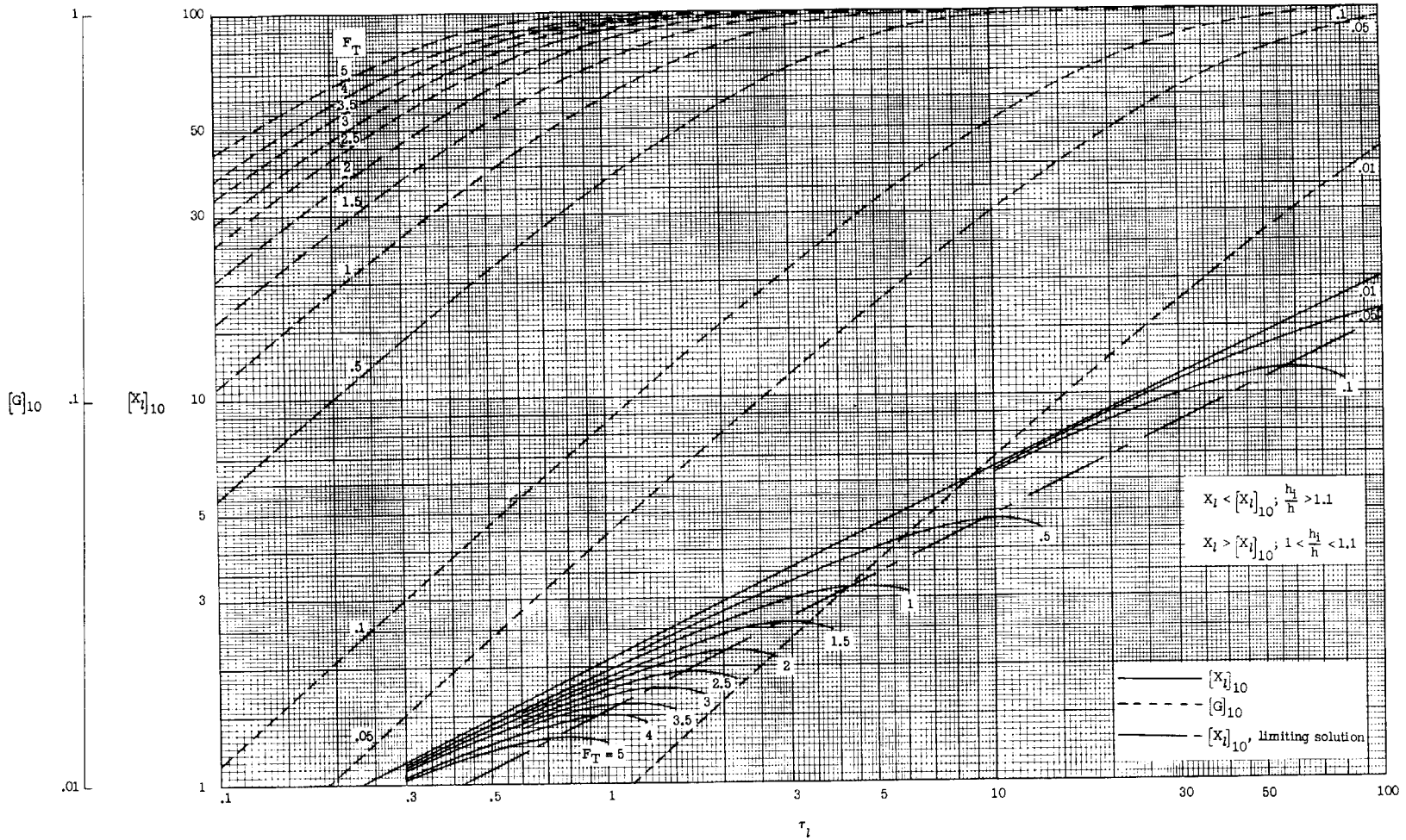

(b) Turbulent boundary layer.

Figure 14.- Concluded.

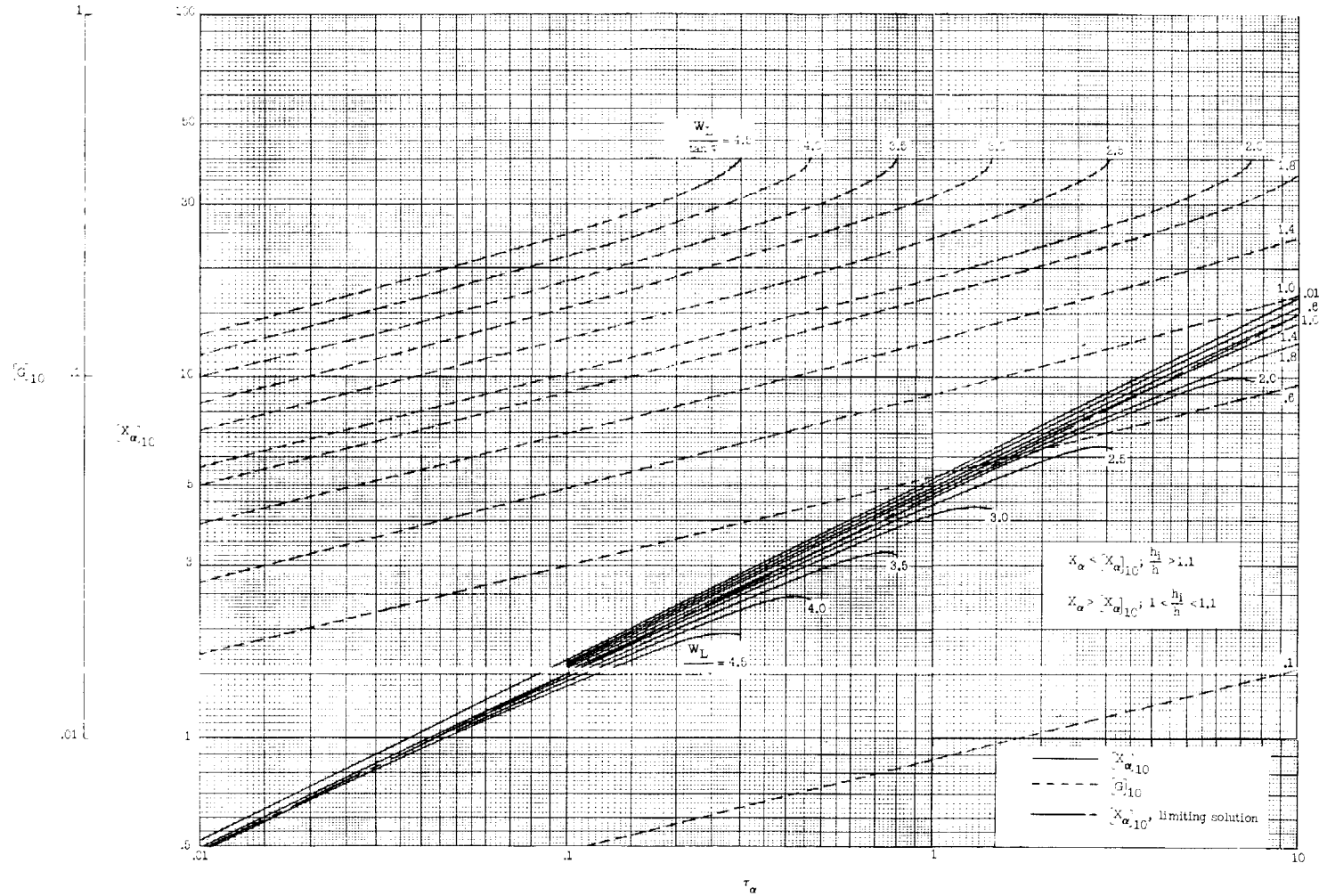

(a) Laminar boundary layer.

Figure 15.- Location and temperature of point having 10-percent conduction error for wedge.

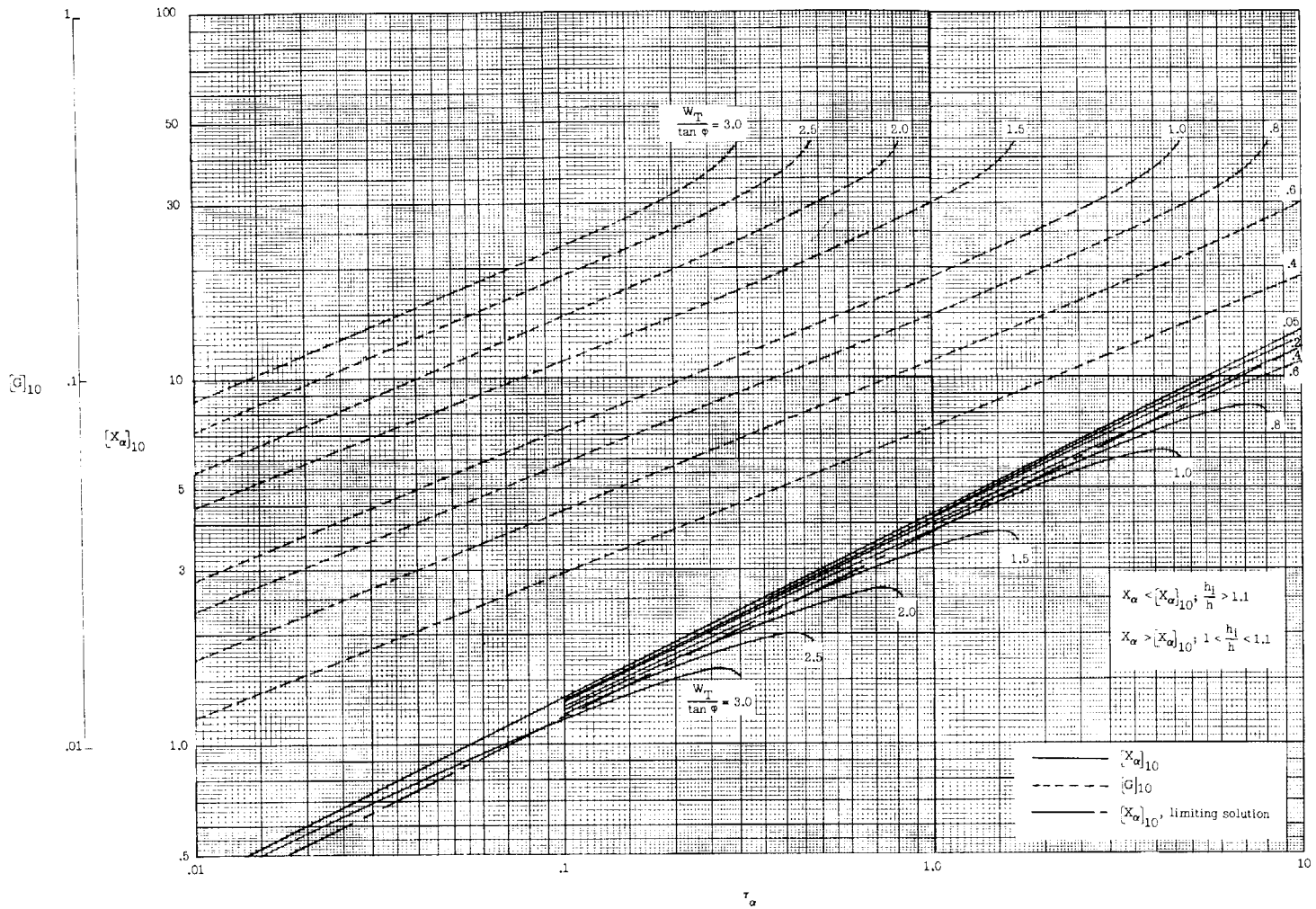

(b) Turbulent boundary layer.

Figure 15.- Concluded.

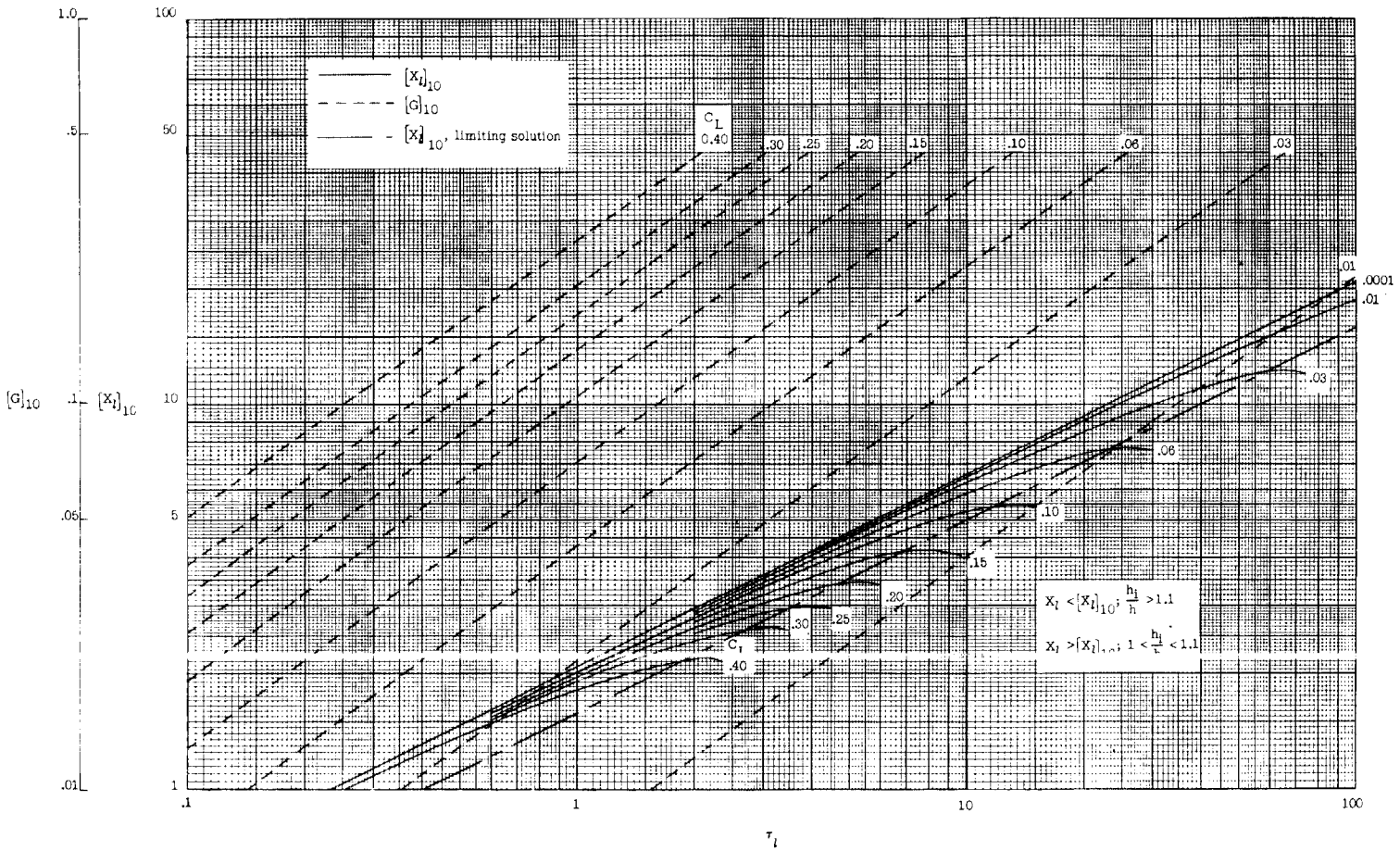

(a) Laminar boundary layer.

Figure 16.- Location and temperature of point having 10-percent conduction error for conical shell of constant thickness.

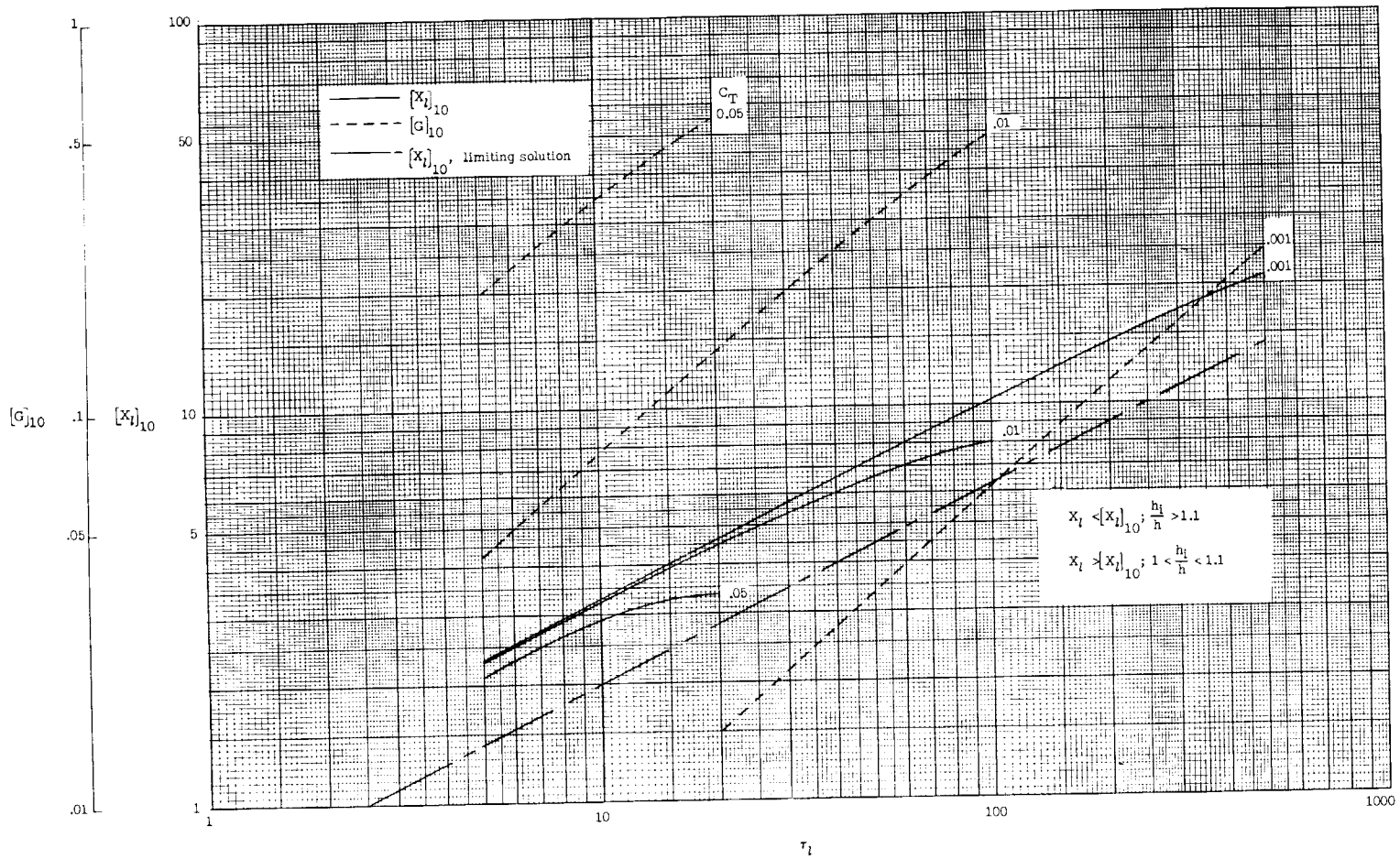

(b) Turbulent boundary layer. Extrapolated.

Figure 16.- Concluded.

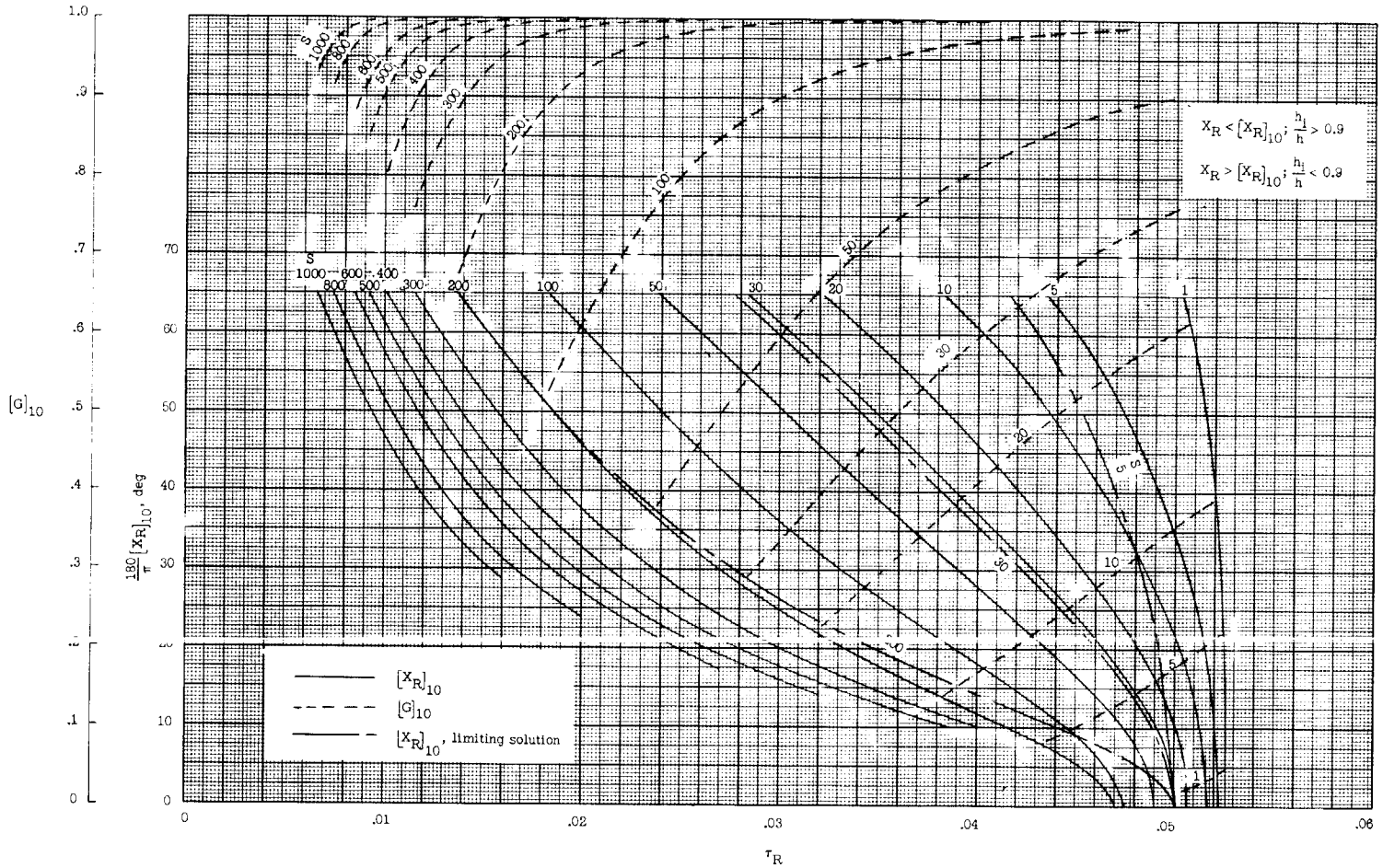

Figure 17.- Location and temperature of point having 10-percent conduction error for hemispherical shell of constant thickness with laminar boundary layer.

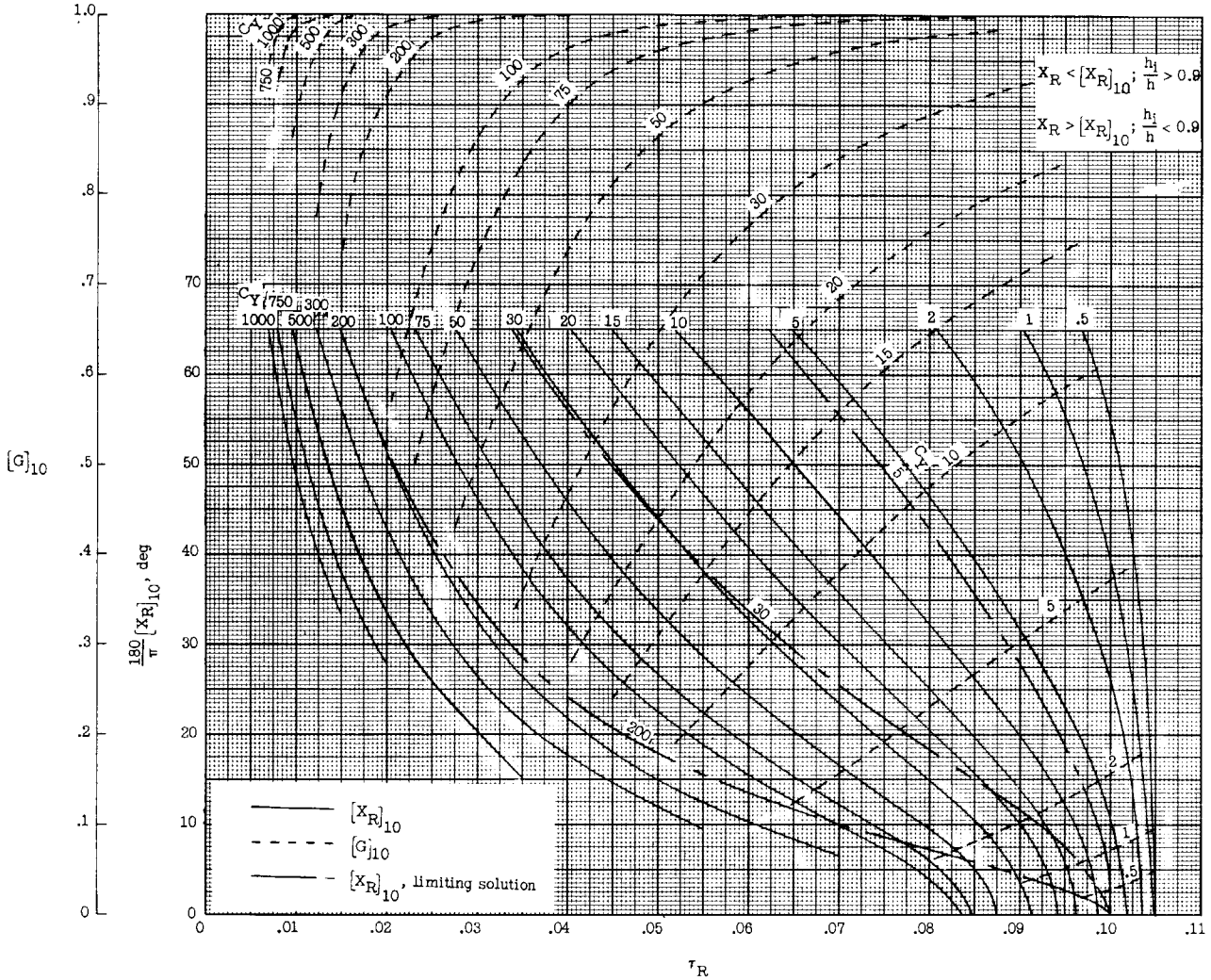

Figure 18.- Location and temperature of point having 10-percent conduction error for hemicylindrical shell of constant thickness with laminar boundary layer.

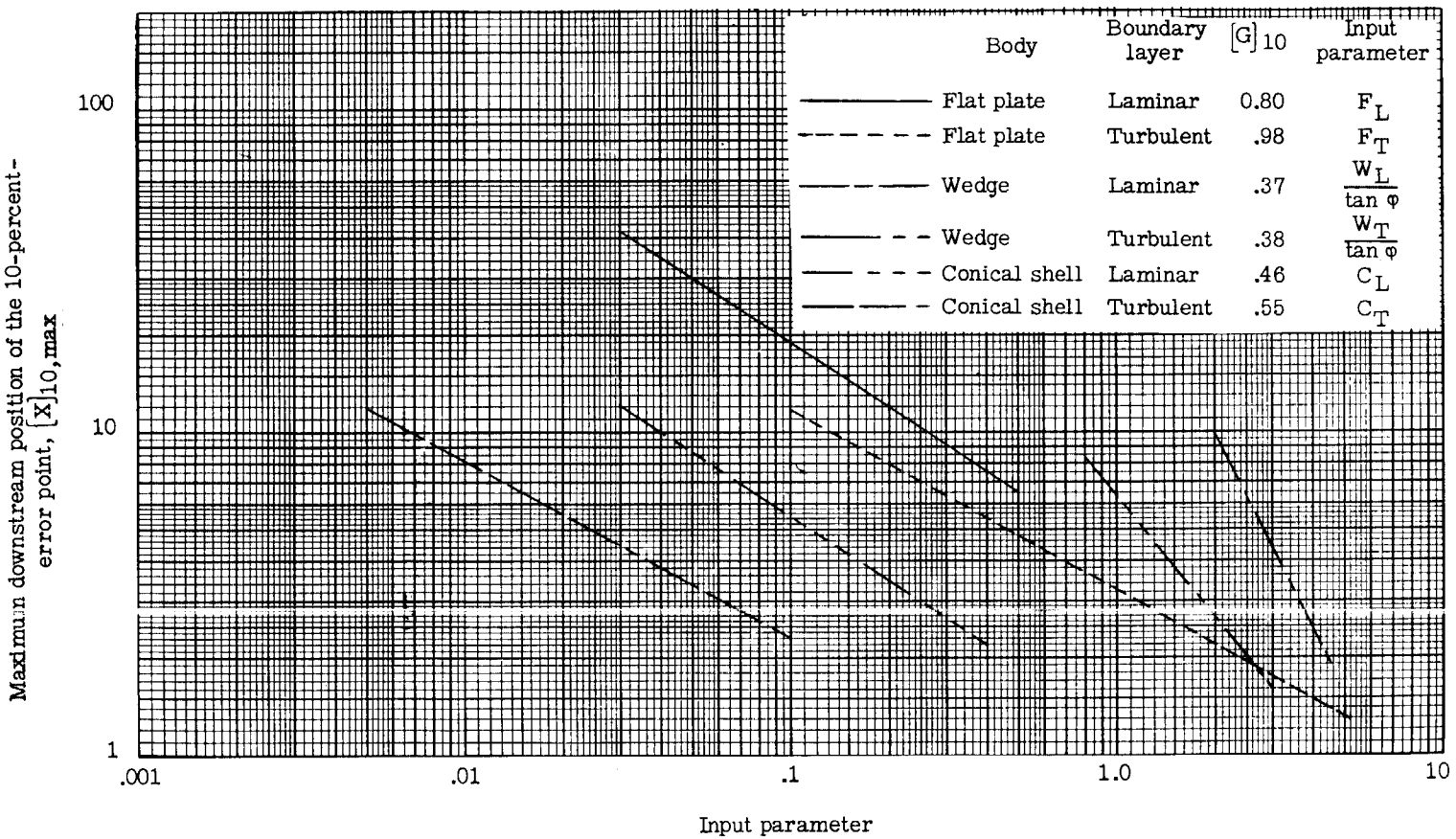

Figure 19.- Maximum downstream position of 10-percent-error point for flat plate, wedge, and conical shell.

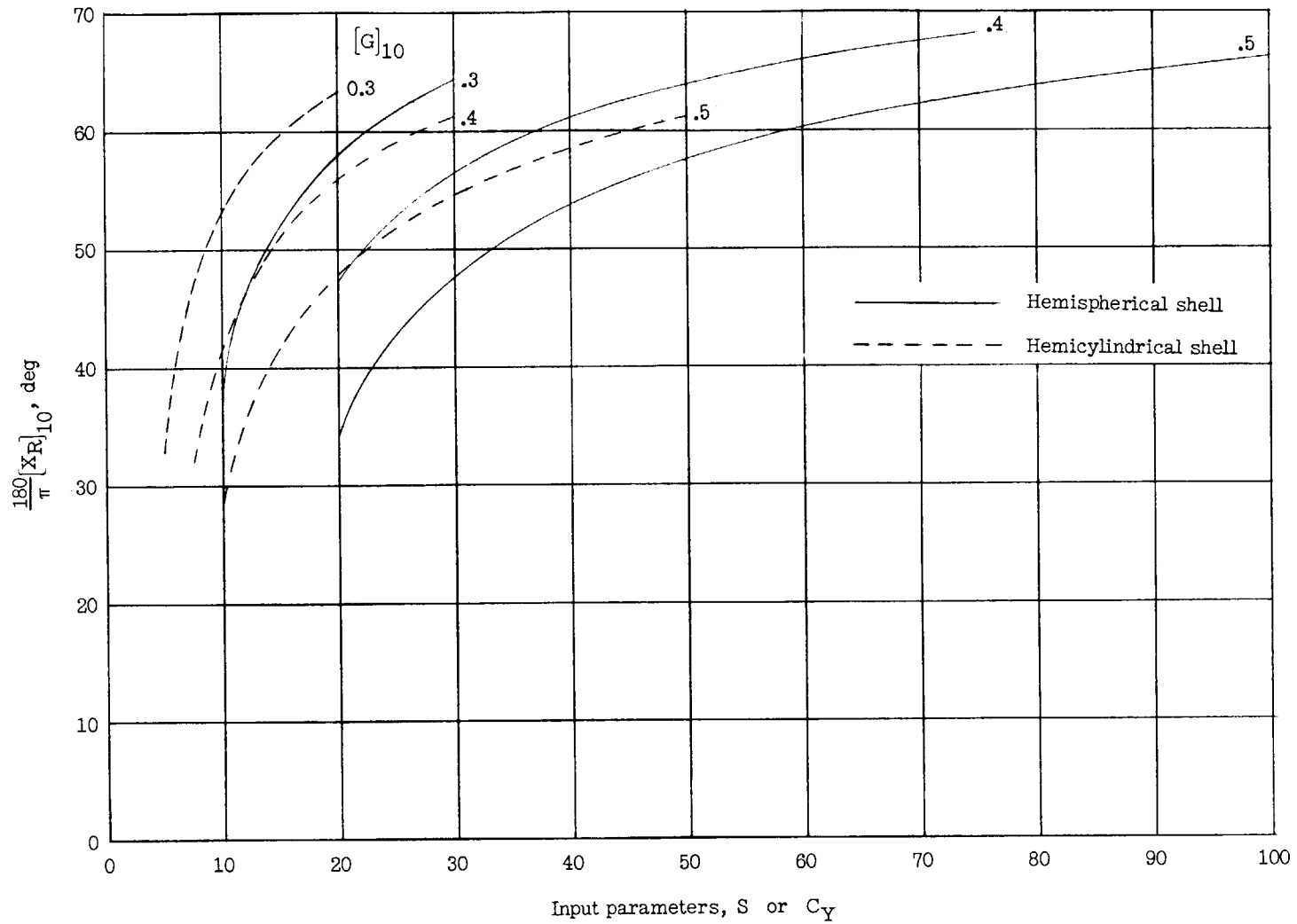

Figure 20.- Location of 10-percent-error point for given temperature for hemispherical and hemicylindrical shells.

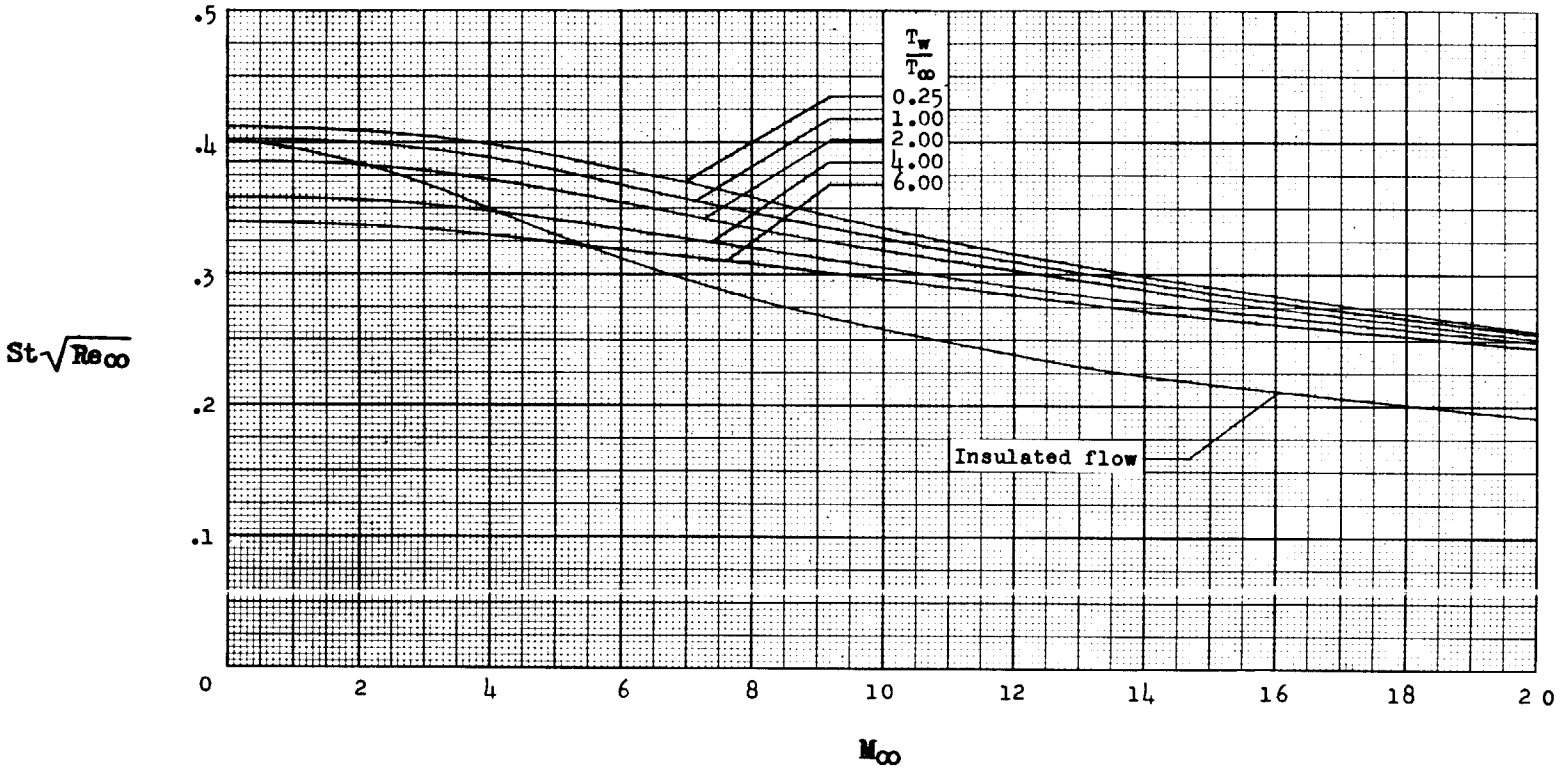

Figure 21.- Local heat-transfer coefficient for laminar boundary layer of a compressible fluid flowing along a flat plate (from ref. 6).

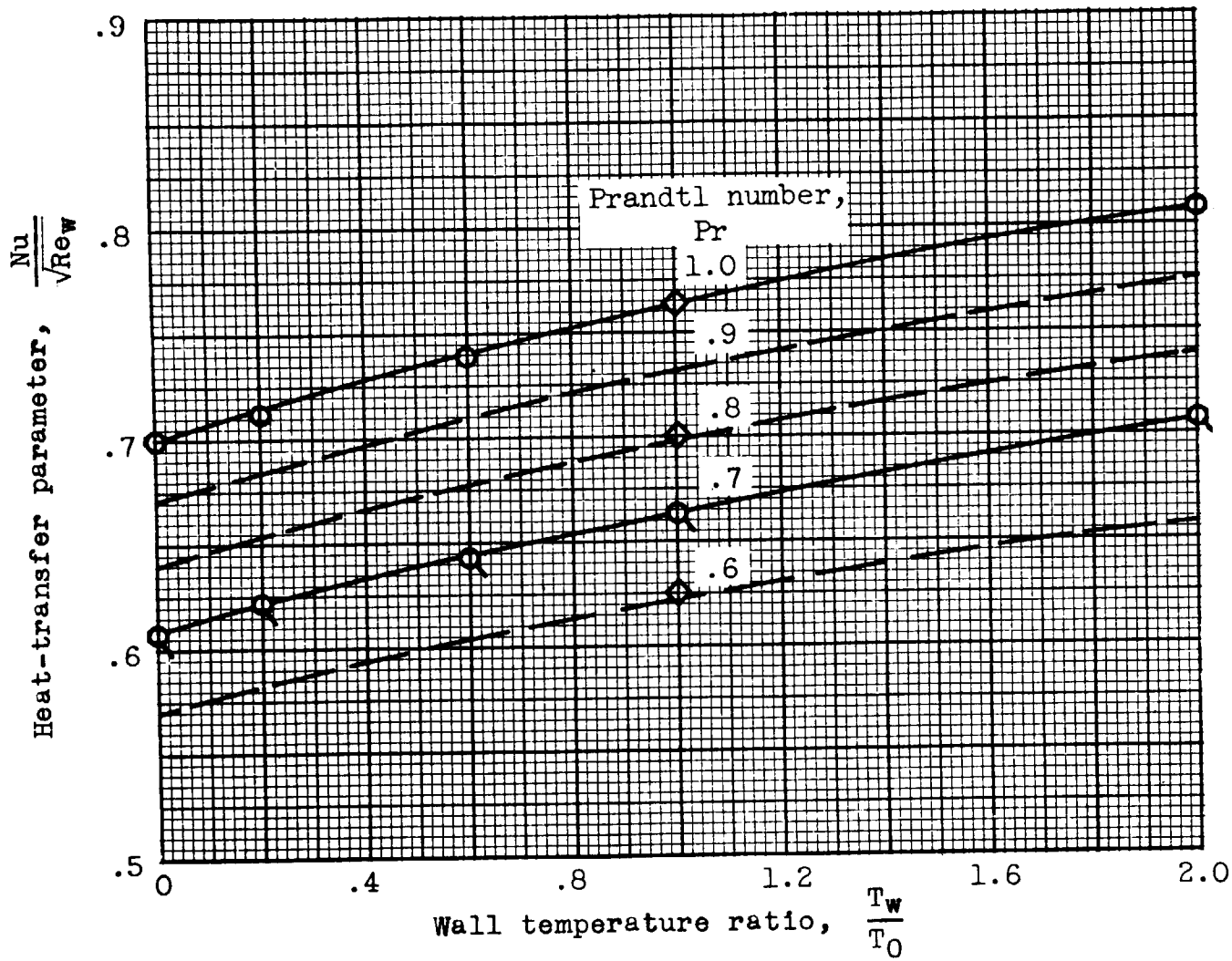

Figure 22.- Heat-transfer parameter at the stagnation point of three-dimensional blunt bodies (from ref. 9).

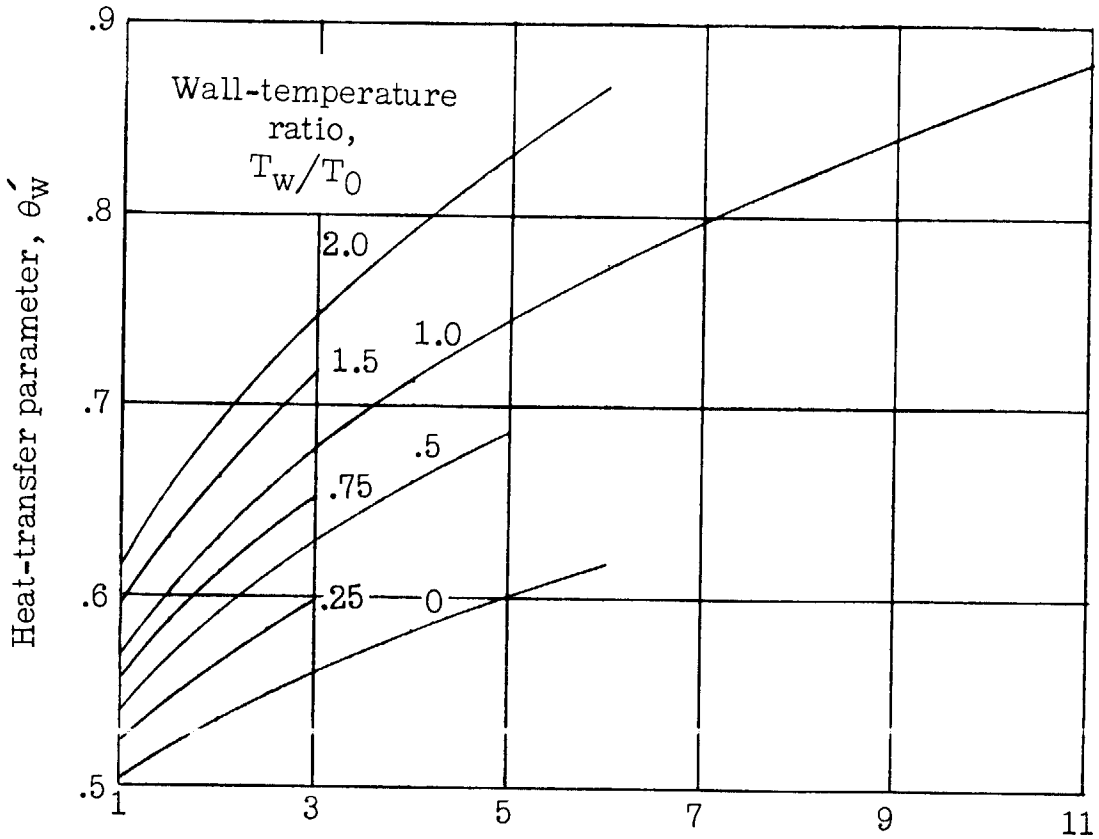

Figure 23.- Effect of yaw on heat-transfer parameter for stagnation-line flow in cylinder (from ref. 3).

NASA-Langley, 1961 L-1227